Investigation of Surface Rupture for Phuket Landslide Using Integrated Electrical Resistivity Imaging and Slope Modeling

NAUNG NAUNG HTWE

A Thesis Submitted in Fulfillment of the Requirements for the Degree of Master of Science in Earth System Science Prince of Songkla University 2019

Investigation of Surface Rupture for Phuket Landslide Using Integrated Electrical Resistivity Imaging and Slope Modeling

NAUNG NAUNG HTWE

A Thesis Submitted in Fulfillment of the Requirements for the Degree of Master of Science in Earth System Science Prince of Songkla University 2019

Thesis Title: Investigation of Surface Rupture for Phuket Landslide Using Electrical Resistivity Imaging and Slope Modeling

Author: Mr. NAUNG NAUNG HTWE

Major Program: Earth System Science

Major Advisor

………………………….

(Dr. Avirut Puttiwongrak)

Examining Committee:

……………………….…Chairperson

(Prof. Dr. Piti Sukontasukkul)

……………………….…Committee

(Dr. Rawee Rattanakom)

……………………….…Committee

(Dr. Kritana Prueksakorn)

……………………….…Committee

(Dr. Avirut Puttiwongrak)

The Graduate School, Prince of Songkla University, has approved this thesis as fulfillment of the requirements for the Master of Science Degree in Earth System Science

………………………………………

(Prof. Dr. Damrangsak Faroongsarng)

Dean of the Graduate School

This is to certify that the work here submitted is the result of the candidate's own investigations. Due acknowledgement has been made of any assistance received.

....Signature

(Dr. Avirut Puttiwongrak)

Major Advisor

....Signature

(Mr. Naung Naung Htwe)

Candidate

I hereby certify that this work has not been accepted in substance for any degree, and is not being currently submitted in candidature for any degree.

....Signature

(Mr. Naung Naung Htwe)

Candidate

Thesis Title   Investigation of Surface Rupture for Phuket Landslide Using Electrical Resistivity Imaging and Slope Modeling

Author   MR. NAUNG NAUNG HTWE

Major Program Earth System Science

Academic   2018

ABSTRACT

Landslides are worldwide natural disasters and they usually occur in the mountainside areas. In this phenomenon, the resistance force of the slope is decreased due to the side effects (geological condition, morphology, heavy and prolonged rainfall, and anthropogenic effect) then the slope is collapsed. Life losses and economic losses are occurred because of this hazard. The purpose of this paper is to delineate the structural deformation of the slope in Phuket, Thailand, using electrical resistivity imaging (ERI) and coupled slope modeling of SEEP/W-SLOPE/W under rainfall-induced conditions. The landslides' geometries are defined using ERI method then coupled slope modeling (using/without using ERI geometry reconstruction) under rainfall-induced condition are used to check the stability of the slope. Moreover, both methods can also estimate the maximum thickness of the surface rupture. Slope modeling results between using ERI geometry and without using ERI geometry are compared. Therefore, the thicknesses of the landslide body are compared and identified from these two results. ERI surveys (parallel to the slope) are done in three locations: Location 1 at Kamala, and Locations 2 and 3 at Chalong. Locations are selected based on the past event landslide area, and the landslide hazard high-risk areas of previous researches. Direct boreholes cannot make on the study locations. So, the secondary hydro-mechanical and geological parameters are applied in coupled modeling. The 24-hr rainfall data are used to simulate the transient seepage analyses. Slope geometries of SEEP/W-SLOPE/W modeling are constructed using the sharp evident near study areas for first modeling and ERI geometries for second modeling. Theoretically increasing the positive pore water pressure (PWP) makes the slope failure because of its degree of saturation increase. Both model simulations show in Location 1 for 16th –29th June,

2018 rainfall data, the peak PWP occurs on 26th June with the factor of safety 3.884 for "without using ERI geometry reconstruction" and 3.484 for "using ERI geometry reconstruction". However, the variations of PWP in Location 2 for 10th–29th May, 2018 rainfall data are different. The maximum PWP appears for "without using ERI geometry reconstruction" on 29th May with the factor of safety 1.554 and "using ERI geometry reconstruction" on 18th May with the factor of safety 1.175. The F.S. values for both locations do not reach under 1 which means the slopes are stable. But, Location 3 is governed by homogeneous fresh granite bedrock and SEEP/W-SLOPE/W coupled modeling is not considered because this place is already stabled with bedrock. However, its ERI result supports to determine the resistivity range of fresh granite bedrock. Location 1 shows the surface rupture is at the top layer of clayey gravel and Location 2 is in the fractured granite. As the final results, the maximum thickness of the sliding mass getting from ERI and using ERI geometry reconstruction are good in correlation at a slope distance. The factor of safety between using and without using ERI geometry are found quite different. Moreover, the disparity of the thickness of sliding mass given from without using ERI geometry for Location 2 is very large in comparing to those of ERI result and using ERI geometry reconstruction. Finally, it can confirm that the maximum thickness of surface rupture for Location 1 is about 5.5 m at a slope distance 13.5 m and Location 2 is about 2.5 m at a slope distance 5.5 m.

Keywords: landslide, surface rupture, thickness, electrical resistivity imaging (ERI), seepage modeling, slope stability modeling, pore water pressure (PWP), a factor of safety (F.S.)

ACKNOWLEDGEMENT

CONTENTS

CONTENTS (Continued)

CONTENTS (Continued)

LIST OF FIGURES

LIST OF FIGURES (Continued)

LIST OF FIGURES (Continued)

LIST OF FIGURES (Continued)

LIST OF FIGURES (Continued)

LIST OF FIGURES (Continued)

LIST OF TABLES

LIST OF ABBREVIATIONS

σ_n total normal stress on the failure plane

J_i' transport Jacobian matrix of partial derivatives or sensitivity

$[K]$ element characteristic matrix

$[M]$ element mass matrix

$\{H\}$ vector of nodal head

$\{Q\}$ applied element flux vector

Δq_i change in model resistivity

ΔV net potential difference

$\sum Fh$ the sum of all horizontal forces

$\sum Fv$ the sum of all vertical forces

$\sum M$ the sum of all moment

a the perpendicular distance from the resultant external water force to the center of moment

A the resultant external water forces

$C(h)$ correlation function which is ranging from 1 (low suction) to 0 (high suction)

c' effective cohesion

D an external point load

d the perpendicular distance from a point load to the center of rotation or to the center of moments

E electric field (Vm^{-1})

e the vertical distance from the centroid of each slice to the center of rotation or to the center of moments

E_L interslice normal force (left)

EP   Electrical Profiling

E_R interslice normal force (right)

ERI   Electrical Resistivity Imaging

f   the perpendicular offset of the normal force from the center of rotation or from the center of moments

F.S.   Factor of Safety

LIST OF ABBREVIATIONS (Continued)

g_i data misfit

GIS   Geographic Information Systems

h matric suction

H total hydraulic head

h_r matric suction harmonizing to the residual water content θ_r

I current (A)

J current density (A/m^2)

J_i Jacobian matrix of partial derivatives or sensitivity

k geometric factor

K_{min} minimum hydraulic conductivity

K_r relative hydraulic conductivity

K_s saturated hydraulic conductivity

kW horizontal seismic load applied through the centroid of each slice

K_w unsaturated hydraulic conductivity

K_x the coefficient of hydraulic conductivity in x direction

K_y the coefficient of hydraulic conductivity in y direction

LEM   Limit Equilibrium Method

M_v coefficient of volume compressibility

M_w the slope of water content curve

N normal force at the slice base

p power factor for adjusting the prediction of water content

PDE   partial differential equation

PWP   pore water pressure

q applied flux

R' radius for a circular slip surface or the moment arm associated with the mobilized shear force

R resistance (Ω)

r, r_1, r_2, r_3, r_4 distance between current electrodes and potential electrodes

LIST OF ABBREVIATIONS (Continued)

RMS   Root Mean Square

S_m mobilized shear force

SPC   soil permeability curve

SWCC soil-water characteristic curve

t time

u pore water pressure

V voltage (V)

VES   vertical electronic sounding

VWC   volumetric water content

W weight of the slice

x the horizontal distance from the centerline of each slice to the center of rotation or to the center of moments

X_L interslice shear force (left)

X_R interslice shear force (right)

z elevation head

α slice base inclination angle

β slice base length

θ volumetric water content (VWC)

θ_r residual water content

θ_s saturated water content

λ_i roughness filter damping factor

ρ resistivity

σ conductivity ($\Omega\ m^{-1}$)

τ' shear strength on the failure plane

Υ_w specific weight of water

ω the angle of the point load from the horizontal

ϕ friction angle

CHAPTER 1
INTRODUCTION

1.1 Background of the Study

Landslide is a type of geological phenomenon, in which a huge range of ground is moved in the various directions along the slope or on a plane surface. It is one of the most fearful natural disasters, which can destroy human properties, infrastructures and then it occasionally causes losses of life. It highly influences the socio-economic effects wherein the resettlement processes. Moreover, it can directly affect the quantity and quality of water available in some places causing water flooding.

Thailand locates in the tropical zone and so it occasionally affects natural disasters particularly in the southern part. Besides, Thailand has been suffering landslides and flooding yearly due to anthropogenic factors. The result directly impacts on the socio-economic status of the community and people. Soralump, 2010a stated that Thailand had been facing heavy landslides every 3-5 years due to heavy rainfall. The direct economic losses due to the landslide are equal to approximately 100 million Baht per year.

Phuket is an Andaman coastal province and mountainous island. It has a tropical climate, therefore, rainfall occurs every 8 months per year (Pantanahiran, 2005). According to the Asia Disaster Preparedness Center (ADPC), 2008 reports, Phuket Island is an active landslide area. Heavy rainfall and strong winds cause debris flows in some watershed areas and sliding occurs in the manmade undercuts. Therefore, the people living around the underlying areas are seriously endangered (Asia Disaster Preparedness Center, 2008). Table 1.1 shows some landslide events and their triggering mechanisms in Phuket occurred between 2007 and 2017 (Phuket Gazette, 2007-2017). By seeing the past landslide events around Phuket, heavy rainfall, prolonged rainfall, and man-made undercuts are major triggering mechanisms.

Table 1.1 Some landslide events and their triggering mechanisms in Phuket occurred between 2007 and 2017 (Phuket Gazette, 2007-2017)

Year	Place	Triggering Mechanism	Affected Things
2007	Patong	Heavy Rainfall	-
2008	Patong	Manmade Undercut	3 people died
2009	Kathu	Heavy Rainfall	Kathu-Patong road destroyed
2010	Patong	Heavy Rainfall	3 people injury
2011	Rasada	Heavy Rainfall	6 houses destroyed
	Kamala	Heavy Rainfall	1 house affected
2012	Patong	Heavy Rainfall	Phar Barami road destroyed
2013	Patong	Retaining Wall Collapse	1 people died, 1people injury
2014	Wichit	Heavy Rainfall	3 people died, 1 people injury
	Patong	Wall Collapse	6 vehicles destroyed
2015	Wichit	Manmade Undercut	Power Cable Line Collapse
2016	Phuket International Airport	Prolong Rain Fall and Manmade Undercut	-
2017	Rasada	Heavy Rainfall and Retaining wall Collapse	5-6 houses destroyed, 22 houses affected
	Patong	Heavy Rainfall	12 houses affected

Moreover, Phuket is a famous tourist destination in Thailand. Tourism produces the major income of the country. Therefore, the natural disaster, e.g., landslide, becomes a considerable special challenge case of Phuket. Chotikasathien and Soralump, 2007 had mentioned that most of the landslide in Phuket occurred by heavy rainfall and manmade undercut.

1.2 Problem Statement

The earlier researchers studied the landslide events of Phuket by using geotechnical methods and GIS techniques. However, no one has studied the detailed geometry of the landslide-prone areas yet. The thickness and the sliding surface of the landslide body are very important to studying landslide in order to use for mitigation techniques and warning systems. Therefore, this study selected on the previous research landslides of the high-risk areas to give an answer to "How are the thickness and the sliding surface of the investigated landslides? Why are the thickness and the surface rupture necessary for studying landslides?" The integrated between Electrical Resistivity Imaging (ERI) and slope modeling (coupled simulation of SEEP/W-SLOPE/W) techniques are used to estimate the failure thickness and the sliding surface of the landslide body.

1.3 Research Objective

- To investigate the thickness and the surface rupture of the landslide mass in the study areas.
- To simulate the landslide modeling in the study areas triggered by heavy and prolonged rainfall.
- To propose the model geometry reconstruction using ERI for enhancing the simulation results of the slope modeling.

1.4 Research Scope

Area: This research is done in the landslide high-risk areas of Kamala and Chalong Districts, Phuket.

Method: Two-dimensional Electrical Resistivity Imaging (2-D ERI) is used to research and verify with coupled slope modeling of SEEP/W-SLOPE/W for estimating the landslide thickness and the sliding surface.

Time: This research is executed within the M.Sc. (Earth System Science) Programme in a timeframe of 20 months.

CHAPTER 2
LITERATURE REVIEW

2.1 Introduction to Phuket

Phuket is the biggest island in Thailand. It is situated latitude between 7°45'-8°15' and longitude between 98°15'-98°40'. The area of Phuket is about 570.03 km^2 (including the other islands). The most area is the mountainous area (the mountains are 70% of the total area), and it is lying from North to South. Therefore, the flat area can be seen mainly in the middle and eastern part of the island. Besides, most of the mountains have a slope angle ranging from 0-50° as shown in Figure 2.1. (DMR, 2011b).

The island does not have the main river, and it has only nine brooks and creeks. Mai-Sip-Song is the highest mountain on this island, and it has an elevation of about 529 m above sea level. Phuket is situated in the Andaman Sea. Therefore, it has a tropical climate. The dry season is from December to March. Furthermore, June to October is the monsoon season. The average annual rainfall is approximately 1000 mm as shown in Figure 2.2. (World Weather & Climate Information).

2.1.1 Geological Setting of Phuket

In Phuket, metamorphic, igneous, and sedimentary rocks occupied as the bedrock and alluvial deposits (Brown *et al.,* 1951). The geological condition of Phuket has two formations, including the lower and the upper formations. Besides, it is composed of eight major rock groups, i.e., 1) Carboniferous-Permian granite, 2) Jurassic granite, 3) Jurassic-cretaceous granite, 4) volcanic rock and other intrusive rock, 5) sedimentary rock (calcium, clay, and lime), 6) metamorphic rock, 7) quaternary sediment and 8) limestone (Mitchell *et al.,* 1970; Soralump, 2010b and DMR, 2011a) (Figure 2.3). The metasedimentary rocks outcropped in the North of the East side, black slate or shale containing scattered pebbles is exposed. The pebbles are of quartzite, siliceous slate, and medium-grained biotite granite.
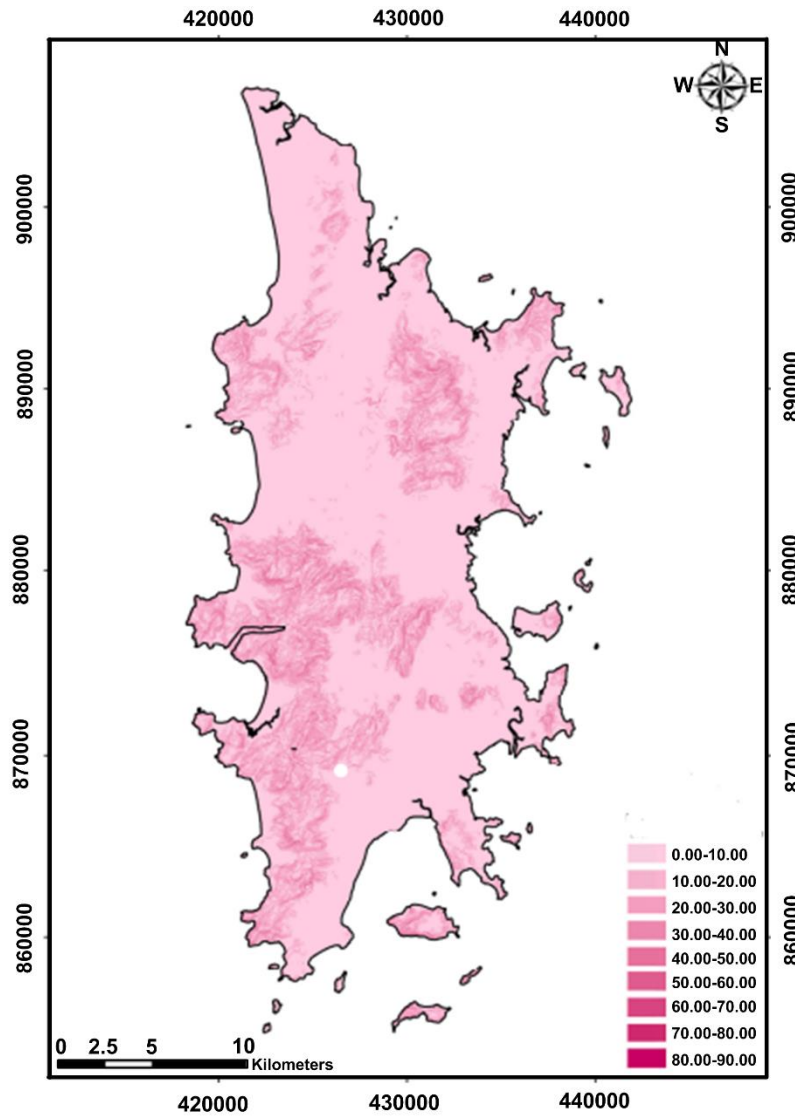
Figure 2.1 Slope angle map of Phuket (DMR, 2011b)
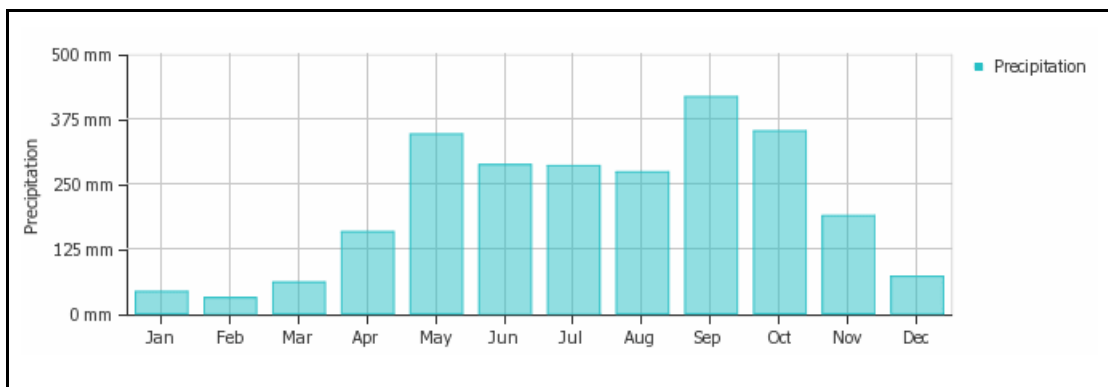
Figure 2.2 Average monthly rainfall data of Phuket (Source: 2016 www.weather- and-climate.com)
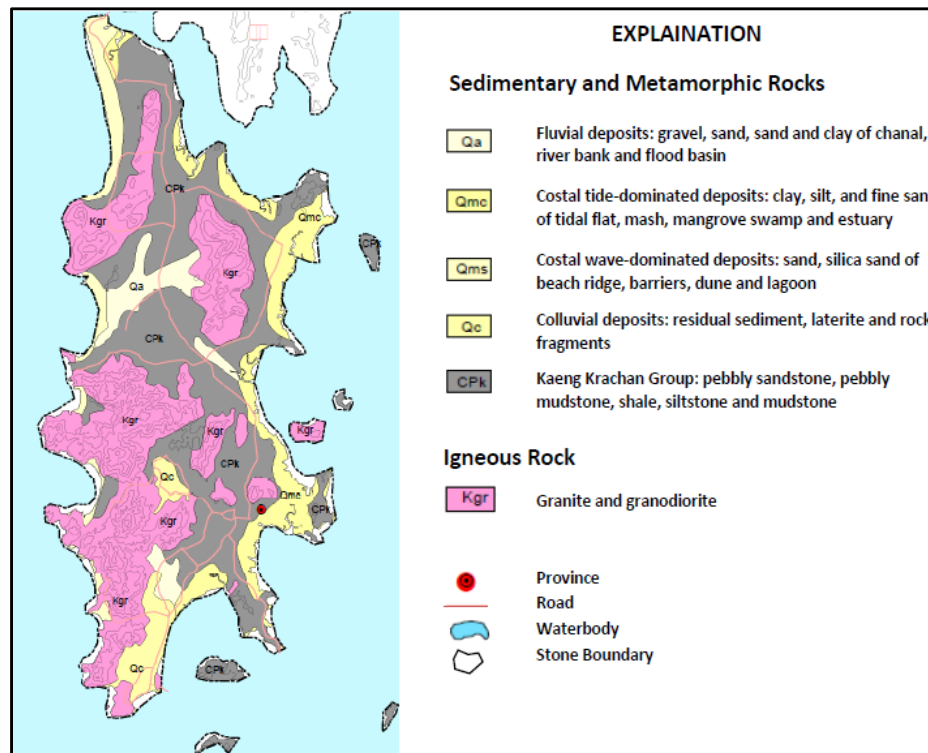
Figure 2.3 The complete geological map of Phuket (DMR, 2011a)

2.1.2 Soil Properties of Phuket

Soralump, 2007 had created the landslide hazard map of Phuket based on three geotechnical data (grain size distribution, strength reduction due to increasing of moisture content, and soil plasticity) in cooperated with rainfall data. Geotechnical properties of soils were studied and found that the most risk landslide areas of Phuket are governed by the weathered rock, i.e., weathered granite and residual granitic soil, where strength reduction is 50% (soaked condition) as shown in Figure 2.4.

2.1.3 Hydrogeology of Phuket

Charoenpong, *et al*., 2012 stated that the hydrological condition of Phuket can be divided into highland and lowland. In Phuket, the hydrogeological aquifers grouped into unconsolidated aquifers and consolidated aquifer. Beach aquifer, floodplain deposit aquifer, and colluvium aquifer are the unconsolidated aquifer, whereas the meta-sedimentary aquifer and granitic aquifer are the consolidated aquifer (DGR, 2010 and 2012). In the report of ISET, *et al.,* 2013, they have stated there were around 1290 wells in Phuket Province. Kong, 2016 studied the groundwater wells distribution in Phuket as Kathu (168 wells), Muang (363 wells), and Talang (759 wells).

Then he created a fence diagram to show the subsurface layers of Phuket using a total of 43 wells data. Finally, he mentioned the groundwater wells distribution of subsurface layer around Phuket as shown in Table 2.1.
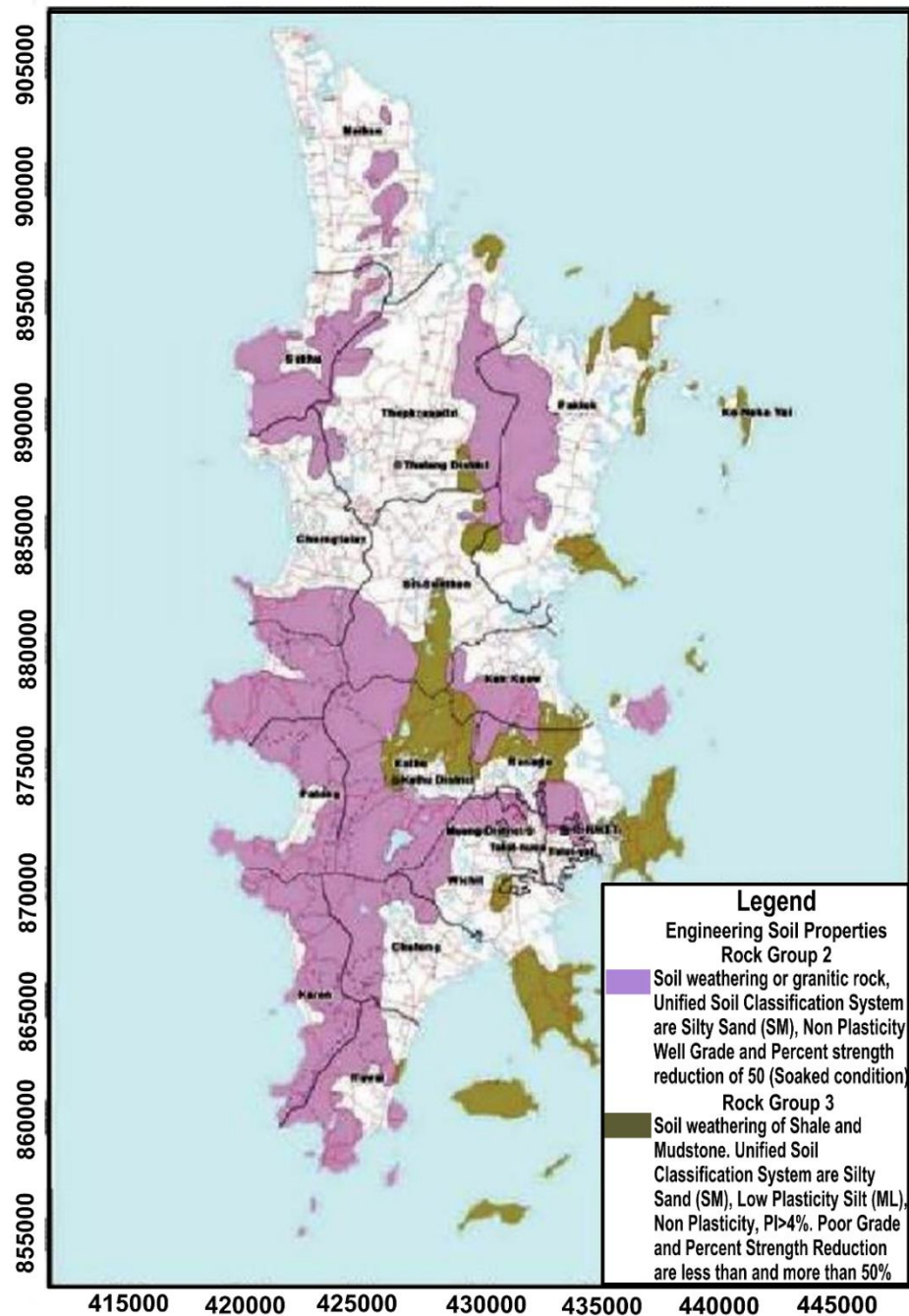
Figure 2.4 Geologic map of Phuket (Soralump, 2007)

Table 2.1 Groundwater wells distribution of subsurface layer around Phuket (Kong, 2016)

District	Layer	Layer Average Thickness (m)	Notes
Kathu	1. Fine grain sediments (soil, clayey sand and clay)	13.52	The aquifers of Kathu district are unconfined aquifers type. It is called
	2. Weathered and fractured rock	40.04	Rayong-Satoon aquifers and the average aquifer
	3. Base rock (mixed with granite and some shales)	81.76	thickness is 53.56 m.
Meung	1. Fine grain sediments (soil, clayey sand and clay)	18.41	The aquifers of Meung district are unconfined aquifers type. It is called
	2. Weathered and fractured rock	35.22	Rayong-Satoon aquifers and the average aquifer
	3. Base rock (mixed with granite and some shales)	69.90	thickness is 53.63 m.
Thalang	1. Fine grain sediments (soil, clayey sand, clay, silt, sand and gravel)	22.88	The aquifers of Thalang district are unconfined aquifers type. It is called
	2. Weathered and fractured rock	34.38	Rayong-Satoon aquifers and the average aquifer
	3. Base rock (mixed with granite and some shales)	69.47	thickness is 57.26 m.

2.2 Landslides

Soralump & Kulsuwan, 2004 studied 220 potential landslide locations in six provinces of the southern part of Thailand (Phan-Nga, Satun, Phuket, Krabi, Ranong, and Trang) to map the landslide hazard zone. They used a weighing factor method on the F-N chart and carried out a soil test to get information about Strength Reduction Index (SRI) on all study locations. Classes and scores on life loss, economic loss, landslide area, past events, geography, and geology then F-N charts were generated base on the scores of living loss and economic loss. One hundred and eighteen numbers of undisturbed soil samples were collected in different locations with the conventional direct shear machine to get SRI. According to their studies, 20 landslide high-risk areas were found in Phuket. The granitic rock and pebbly mudstone are very tendency to occur landslide because it can reduce the strength by 40% in saturated condition according to the SRI test results. High-risk locations of the landslide in Phuket is pointed out in Figure 2.5.
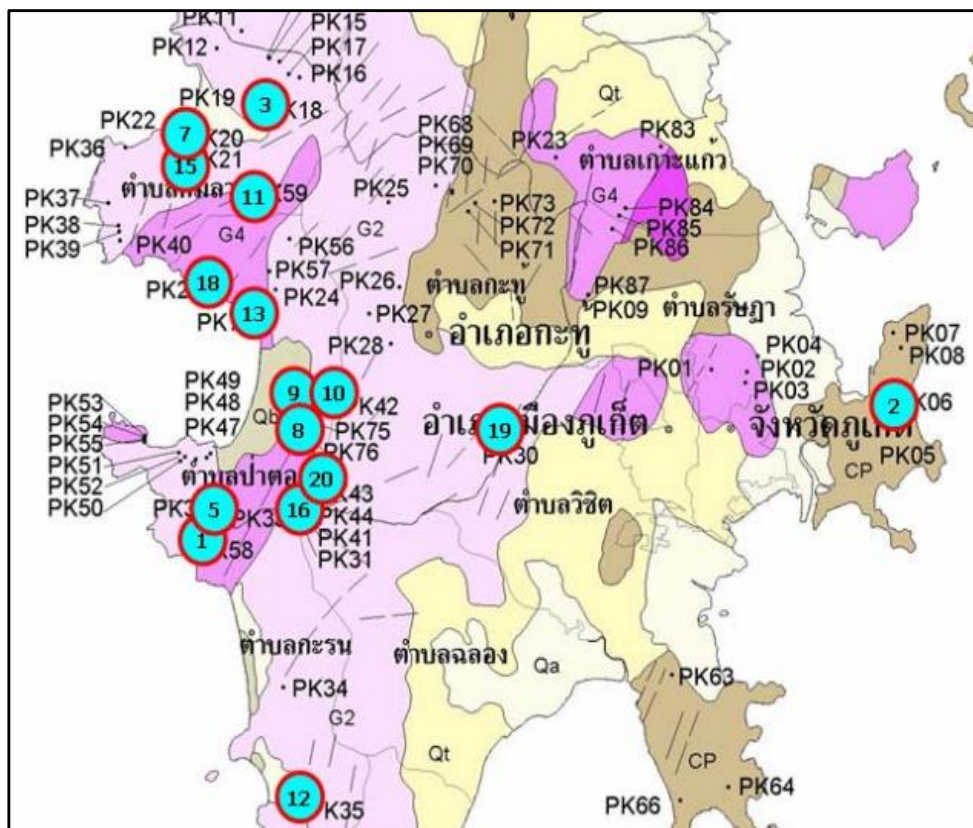
Figure 2.5 High-risk locations of landslide in Phuket (Soralump & Kulsuwan, 2004)

Similarly, Soralump, 2007 had created the landslide hazard map of Phuket based on the factors of the landform (slope and elevation), land-use, soil characteristics, geologic condition (rock type and lineament zone), rainfall intensity, distance from surface water, and geotechnical engineering properties of residual soil. The map had done using GIS technique to classify the hazard area using the 50×50 m grid size for each layer of information. All factors were used as input factors and generated in GIS software using a weighing factor method. Landslide hazard map was established using one-year return period in 3-days accumulations of rainfall data combined with other factors as shown in Figure 2.6. Using weighting and rating values of Phuket and other six provinces preparing landslide hazard table are mentioned in Table 2.2.
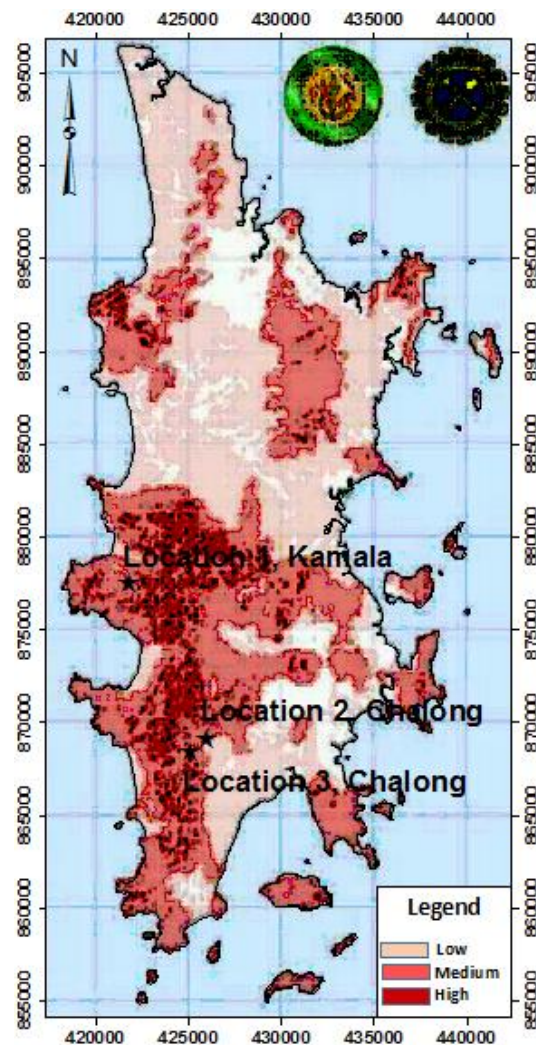
Figure 2.6 Landslide hazard map of Phuket (Soralump, 2007)

Table 2.2 Weighting and rating values of Phuket and other 6 provinces (Soralump, 2007)

Parameter	Weight Value		Rating Value	
	Parameter	**Sub-parameter**	**Decription**	**Rating (1-5)**
1.Geology 1.1 Rock Type	5	3	A. Granite Rock	5
			B. Shale/Mudstone	4
			C. Sandstone/Siltstone	3
			D. Quartizite, Sandstone and Siltstone	2
			E. Limestone/Dolomite	1
1.2 Lineament		2	A. Area inside lineament zone	5
			B. Area outside lineament zone	1
2. Landform 2.1 Slope (%)	4	3	A. > 70%	5
			B. 50-70%	4
			C. 30-50%	3
			D. 15-30%	2
			E. 0-15%	1
2.2 Elevation (meter)		1	A. >400 m	5
			B. 300-400 m	4
			C. 200-300 m	3
			D. 100-200 m	2
			E. 0-100 m	1
3. Surface drainage	2		A. Area inside surface drainage zone	4
			B. Area outside surface drainage zone	1
4. Soil characteristics	2		A. Gravel loam/Gravelly sand	5
			B. Sand	4
			C. Sandy loam	3
			D. Clayey loam/loam	2
			E. Clay, Mud	1

Table 2.2 Weighting and rating values of Phuket and other 6 provinces (Soralump, 2007) (Continued)

Parameter	Weight Value		Rating Value		
	Parameter	Sub-parameter	Decription		Rating (1-5)
5. Land use and land cover	3		A. Agriculture area		4
			B. Urban and built-up area		3
			C. Other deforestation		2
			D. Forest area		1
6. Rainfall intensity	5		Return Period 1	Return Period 1, 5, 20, 50, 100 years	
			A. >203mm	>857 mm	5
			B. 161-203 mm	651-827 mm	4
			C. 119-161 mm	446-651 mm	3
			D. 77-119 mm	240-446 mm	2
			E. 35-77 mm	35-240 mm	1
7. Engineering Soil Properties (in term of parent rock)	4		A. Weathered Sandstone/Siltstone		5
			B. Weathered Granite Rock		4
			C. Weathered Shale/ Mudstone		3
			D. Weathered Quartzite, Sandstone and Siltstone		2
			E. Weathered Limestone/ Dolomite		1

In addition, Pantanahiran, 2005 studied Tsunami and landslide-probable areas in Phuket Island. Slope, elevation, flow direction, flow accumulation, adjusted aspect, LANDSAT TM-band 4, brightness, and wetness parameters were applied to prepare for landslide and Tsunami risk map for Phuket Island using GIS technique (Figure 2.7).
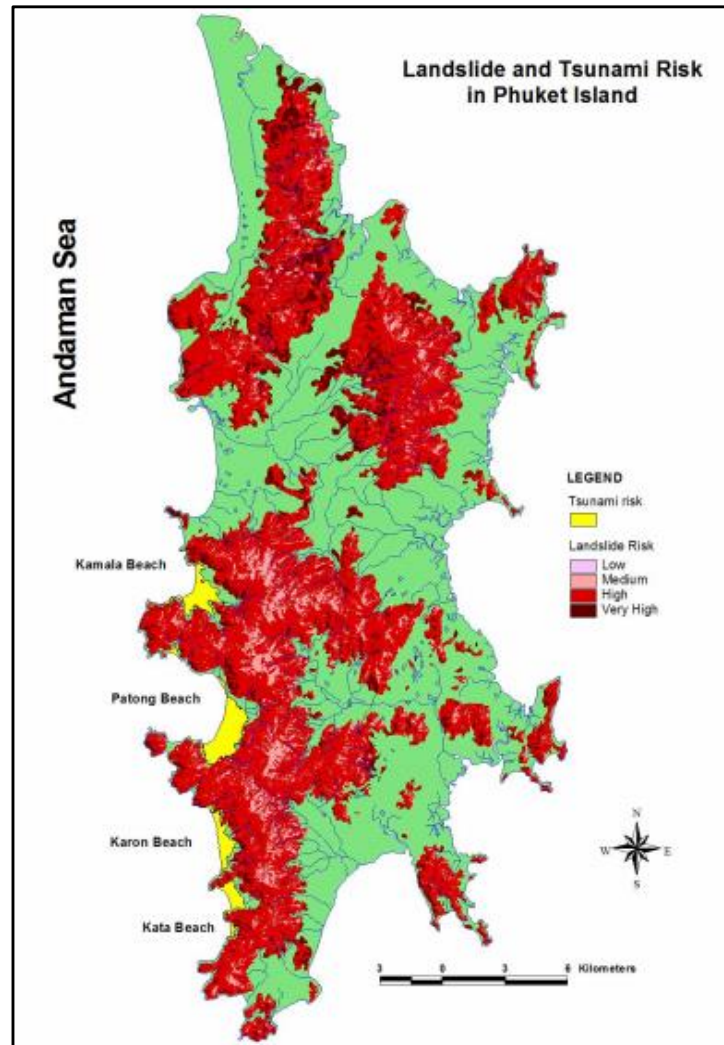
Figure 2.7 Landslide and tsunami risk map of Phuket (Pantanahiran, 2005)

2.2.1 Definition of Landslide

A geological phenomenon, in which a huge range of the ground is moved in the various direction along the slope or on a plane surface, is called a landslide (Highland & Bobrowsky, 2008). Theoretically, the driving force or mobilized force of a slope is greater than the resistance force of a slope is said to be slope failure or landslide and it is denoted as a factor of safety (F.S.) as follows:

$$F.S. = \frac{resistance\ force}{driving\ force\ (or)\ mobilized\ force} \tag{2.1}$$

Hence, it can simply denote that landslides start when the stability of the slope alters from a stable state to an unstable state. Herein, soils are failed deeply or shallowly along the slopes and rock cliff (Figure 2.8).
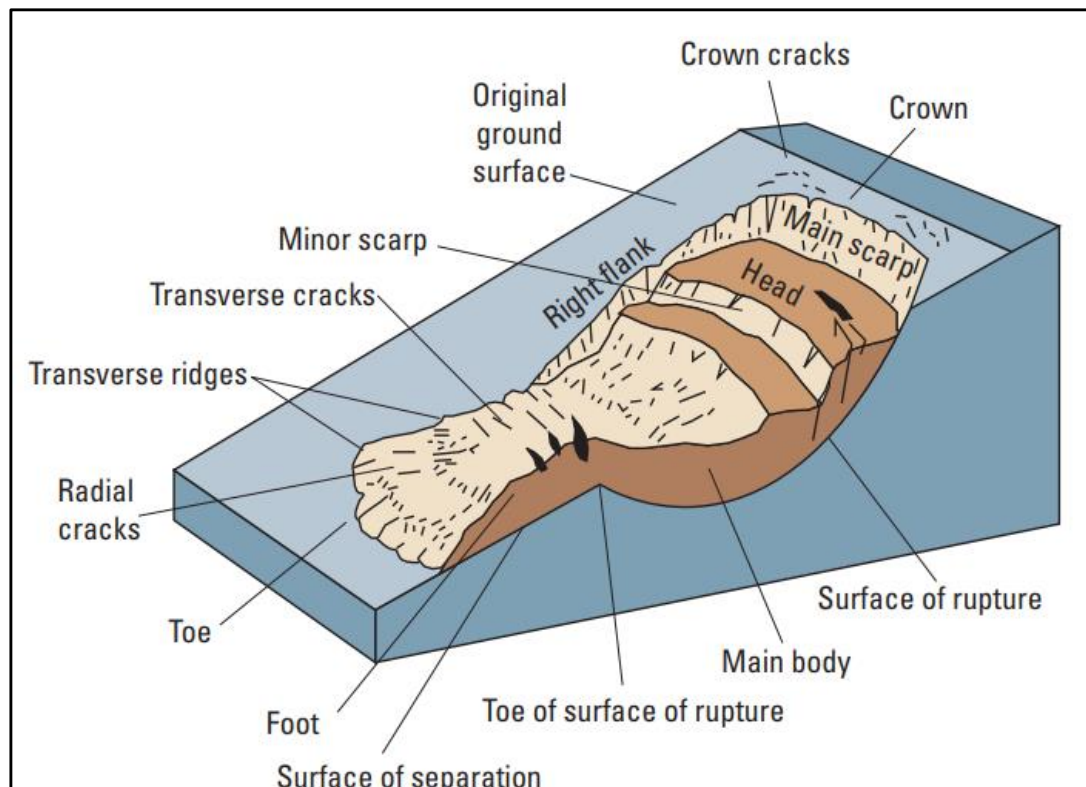
Figure 2.8 Landslide terminology (Highland & Bobrowsky, 2008)

2.2.2 Influenced Factors

Causes of landslide depend on two main factors: (i) natural factors and (ii) anthropogenic factors (USGS, 2004).

(i) Natural Factors

(a) Geological factors: If the geological conditions of a slope are weak-sensitive materials, weathered materials, fractured materials, and permeable materials, they are prone to saturate by glaciers and snow melting or heavy rainfall, then the slope becomes a destabilization.

(b) Heavy and prolonged rainfall: It relates an increasing of underground water pressure, and resulting in the destabilizing slope. It is considered a primary factor in various landslide problems.

(c) Morphology: The slopes are destabilized, if the morphological conditions have a sharp tectonic or volcanic and glacial rebound. Besides the lack of vegetation, loading on the slope or its crest, erosion, freezing, thawing, shrinking or swelling weathers can also destabilize the slope.

(ii)   Anthropogenic Factors (Factors by Human Actions)

(a) Informal drainage system

(b) Deep excavations and cutting the ground

(c) Land use

(d) Artificial vibration

(e) Water leakage from utilities

2.2.3 Types of Landslide and Triggering Mechanisms

Landslides are categorized into two fundamental types: shallow types and deep-seated types (Natural Resources, 2017). Shallow landslides are initialized from the topsoil layer or regolith zone. Most shallow landslides are triggered by heavy and prolonged rainfall that critically increase pore water pressure or accelerated ground due to earthquakes at tectonic fault nearby. Therefore, these types of landslide usually slump along roadways or fast-moving debris flows downward valleys.

However, deep-seated landslides are initialized from the bedrock. Their major triggering mechanisms are accumulated rainfall over a long period (e.g. weeks to years) and large magnitude of earthquakes. Normally, these types of landslide take a long time to develop with higher depth and they move slowly in large areas.

Moreover, Highland and Bobrowsky, 2008 classified various types of landslide depend on the movement and material involved (Figure 2.9) and stated their triggering mechanisms (Table 2.3).

(i) Falls (Rockfalls)

The materials movement are suddenly occurred in the form of free-falling, bouncing, and rolling from steep slopes or cliffs.

(ii) Flows

They are a mass movement of materials. Creep, lahar, debris flow, debris avalanche, mudflow, and earthflow are flow types.

(a) Creep: The soils or rocks are moved steadily. They can easily notice by seeing the curved tree trunks, walls, fences, and lamp- posts.

(b) Debris Flow: This is a fast movement landslide. They include liquefied materials of mixed unconsolidated soil, debris materials, and water.

(c) Debris Avalanche: The debris flows with high momentum are called debris avalanche.

(d) Lahar: This is a kind of mudflow or debris flow. It usually occurs in the slope of the volcano.

(e) Mudflow: This is the rapid flow of wet mass materials. It contains 50% of sand, clay, and silt.

(f) Earthflow: It is initial on the gentle or moderate slopes. These slopes may contain clay, silt, fine-grained soil, and clay-bearing bedrock.

(iii) Spreads (Lateral Spread)

Due to the earthquake, the saturated sediments change from the solid state into the liquefied state due to breaking out of a shallow unconfined groundwater layer. It occurs on very gentle slopes with near horizontal movement of earth material.

(iv) Slides

Slides include two types of mass movement such as rotational landslide and translational landslide. These kinds of sliding can occur along the beaches, on the steep slopes, along with the improper drains, where geological conditions exist.

(a) Rotational Landslide: The movement is spoon shape (concave upward) and it has more or less rotation (e.g. Slump).

(b) Translational Landslide: The materials are moved to the downslope with little tilt backward rotation that occurs along a distinctive weakness surface of joint, fault, or bedding plane. Its ruptured surface is straight.

(v) Topple

It is a free-falling, bouncing and rolling of a block of rock downward the slope.
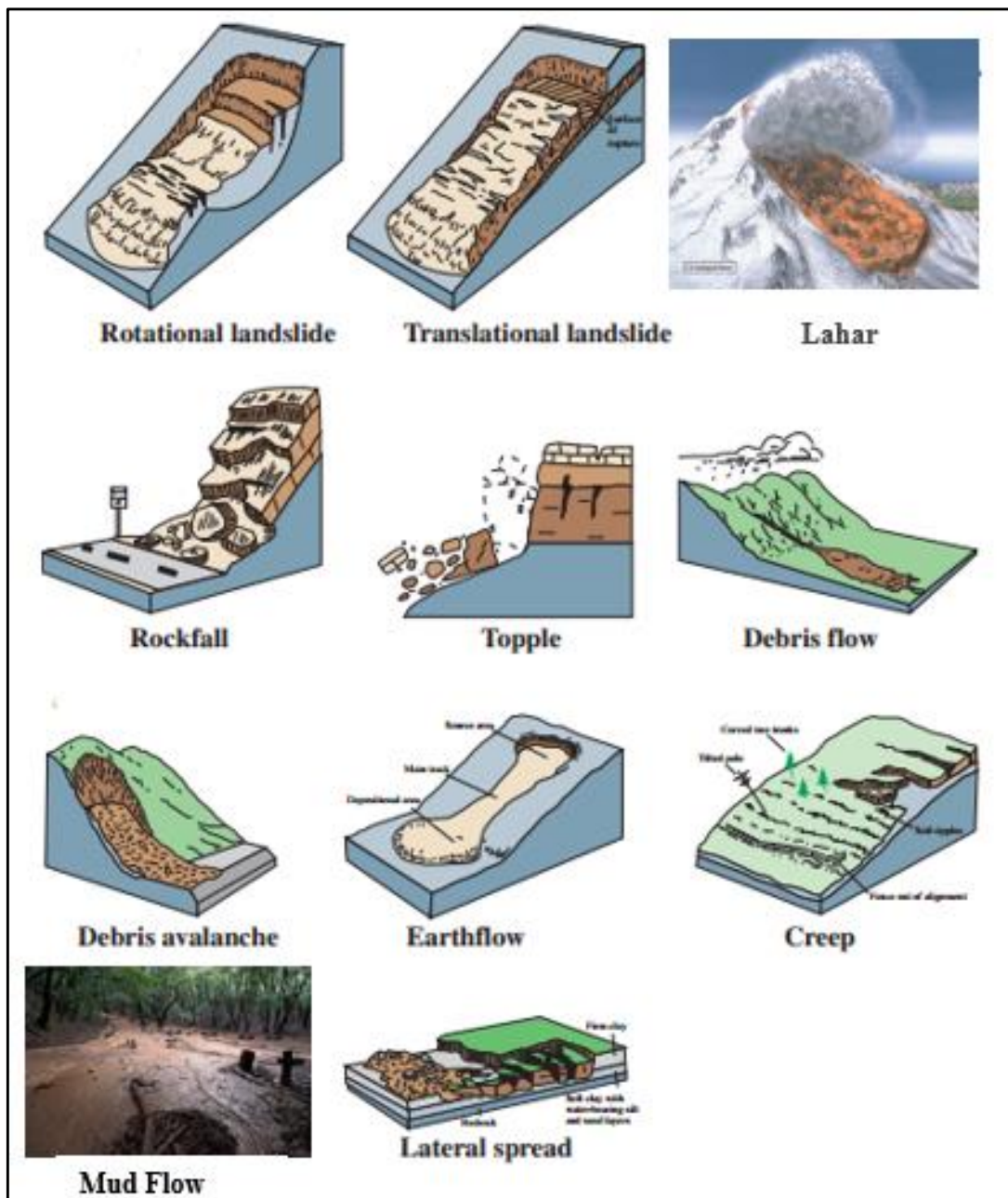
Figure 2.9 Types of landslide (USGS, 2004)

Table 2.3 Types of landslide and its triggering mechanisms

Landslide Types		Triggering Mechanism
Flow	Earth Flow	excavation, excessive loading on a slope and induced vibration by human, groundwater table drawdown rapidly, erosion, earthquakes
	Debris Flow	heavy and prolong rainfall, rapid snowmelt
	Debris Avalanche	unstable terrain affected by weather (hot avalanche occurs due to volcanic earthquake)
	Lahar	water, falling down the melting snow or ice from the top of high volcanoes, eruption the volcano
	Mud Flow	Heavy rainfall, snowmelt, or high levels of groundwater
Slide	Rotational Landslide	intense or heavy rainfall, raising up groundwater, earthquake
	Translational Landslide	intense rainfall, raising up groundwater table, cutting the slope, earthquake
Spread	Lateral Spread	plastic deformation of weak material at depth due to liquefaction by the earthquake, groundwater change, anthropogenic overload, liquefaction of basement sensitive marine clay
Fall	Rock-fall	human activities, naturally undercutting slope, differential weathering
Topple	Topple	undercutting, excavation, and vibration by human, differential weathering, stream erosion, gravity

2.3 Electrical Resistivity Imaging (ERI)

Loke, 2004 recommended that ERI method can easily resolve the subsurface information by injecting the direct electric current beneath the ground and it can collect vertically and laterally variation of the subsurface materials. Normally,

the combination of vertical electrical sounding (VES) and electrical profiling (EP) is called electrical resistivity imaging (ERI). ERI has to perform with different electrode configurations and it gives very effectively for illustrating with higher resolution near-surface of resistivity anomalies for various environmental problems. This technique is widely used in the observation of mineral exploration, engineering studies, geothermal exploration, archaeological investigation, and geological mapping. Moreover, it is very helpful in studying landslides because it gives the information of specific geo-electrical heterogeneity zone and lithological variations of the study location (Yilmaz, 2011).

2.3.1 Concept of Electrical Resistivity Imaging (ERI) Method

The purpose of the ERI survey is to delineate the electrical distribution into the subsoil. Therefore, artificially generated electric currents are injected into the subsoil then voltages are measured. These voltages provide the heterogeneous sub-soil layers (Kearey *et al.,* 2002 cited in Samouëlian *et al.*, 2005). Ohm's Law is used to solve this assumption. Ohm's law stated the electrical property of a medium that the voltage of a circuit is equal to the product of the current and the resistance of that material. However, Ohm's law cannot consider the material constant directly.

$$V = IR \tag{2.2}$$

where *V* is the voltage, *I* is the current, and *R* is the resistance of the material. However, Ohm's Law cannot directly consider the material resistivity constant.

On the other hand, Ohm's law expressed current density (*J*) for a resistivity material is the product of conductivity (σ) and electric field (*E*).

$$J = \sigma E \tag{2.3}$$

Therefore, the current density (*J*) can be express as:

$$J = \frac{1}{\rho} \times \frac{V}{r} \tag{2.4}$$

where ρ is resistivity and *r* is the distance between the current electrode and the potential electrode.

In a real condition, ERI survey is done on the ground surface. Therefore, the electrical equipotential is considered as hemispherical shape and the current density for all the radial directions can be calculated with:

$$J = \frac{I}{\frac{1}{2}(4\pi r^2)} = \frac{I}{2\pi r^2} \tag{2.5}$$

According to equations (2.4) and (2.5), the potential V becomes as follow:

$$V = \frac{\rho I}{2\pi r} \tag{2.6}$$

In principle, the ERI measurement is based on four-points geometries: two electrodes, i.e., A and B are used as injected current electrodes while the other electrodes (M and N) are used for voltage measurement. However, modern instruments use multiple channels to yield for multi-electrode arrays using multiple voltage electrodes M and N for one injection between A and B. The injected direct current (DC) is a type of low frequencies current. Therefore, the resistivity of a homogeneous half-space can be calculated as:

$$\Delta V = \frac{I\rho}{2\pi}\left[\left(\frac{1}{r_1} - \frac{1}{r_2}\right) - \left(\frac{1}{r_3} - \frac{1}{r_4}\right)\right] \tag{2.7}$$

$$\rho = 2\pi\left[\frac{1}{\left(\frac{1}{r_1} - \frac{1}{r_2}\right) - \left(\frac{1}{r_3} - \frac{1}{r_4}\right)}\right]\frac{\Delta V}{I} = (k)\frac{\Delta V}{I} \tag{2.8}$$

where r_1, r_2, r_3, and r_4 are the distances from the current electrodes (A and B) to the voltage electrodes (M and N) which are shown in Figure (2.10), k is the geometric factor that depends on the settlement of the electrodes A, B, M, and N.
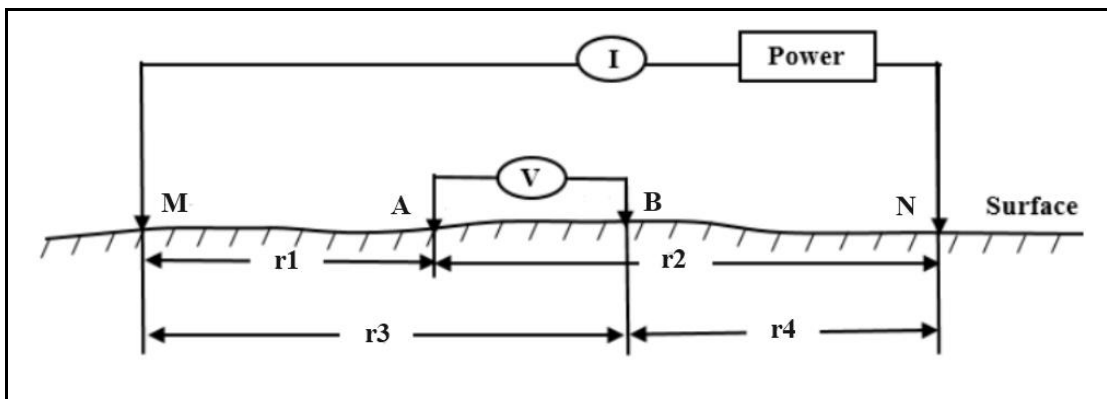
Figure 2.10 Geo-electric survey with current and potential electrodes (Modified from Telford *et al.,* 1990)

The collected data is plotted as a pseudo-section as shown in Figure 2.11. This pseudo-section cannot interpret as an image of the measured subsoil because

the measured resistivity data cannot create directly a depth section. Therefore, an inversion model is needed to convert the pseudo-section to a true image of the subsoil.
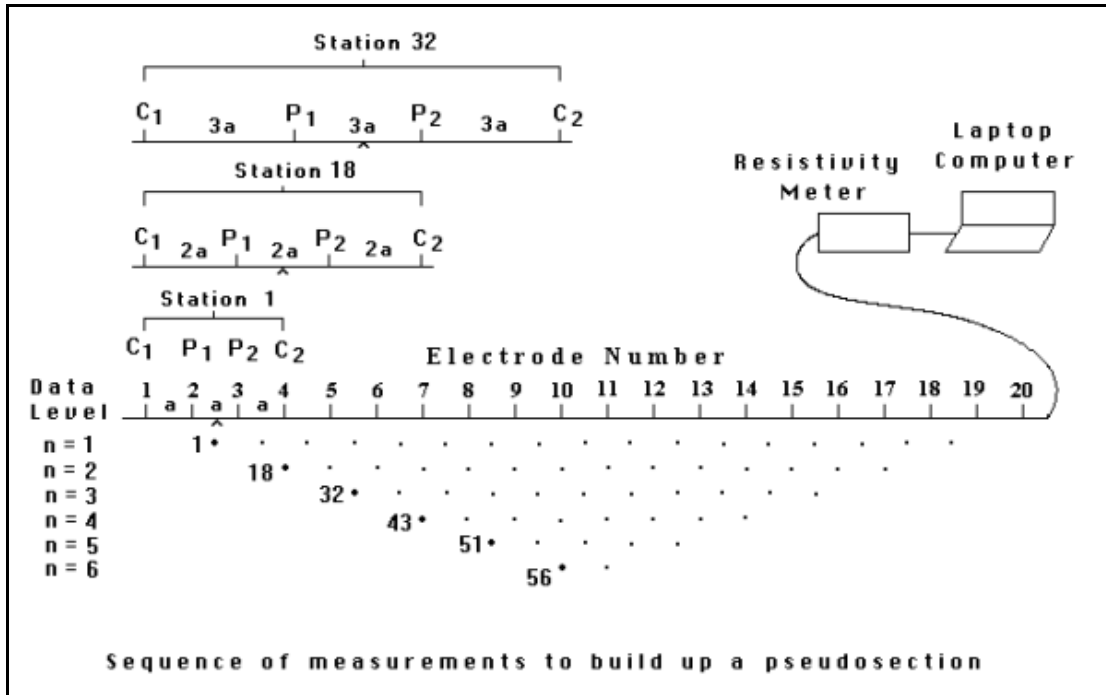
Figure 2.11 Schematic of 2-D field survey Wenner array (Loke, 2015)

2.3.2 Investigation of Landslide by Electrical Resistivity Imaging (ERI)

Some geophysical methods cannot use to survey on the landslide areas, if the topography is very rough. The direct geotechnical investigation methods can approach to study the landslide characteristics (Mukhlisin *et al.,* 2011). In some cases, a detail structural interpretation of the landslide body is not easy and impossible (Jomard *et al.,* 2007). Electrical Resistivity Imaging (ERI) is the most popular and useful method to investigate in the shallow areas and then the topographic inversion software is used to produce the advancements in computer technology (Bichler *et al.,* 2004).

Recently, the ERI technique has been widely applied in landslide survey. ERI is a vigorous geophysical method and it can fully provide 2-D or 3-D images by injecting current to ground. Besides, it can give not only the lateral but also vertical resistivity variation of the subsoil. ERI can investigate the geometry, fluid movement, and the water content of the subsurface leading to the stability of the slope and the

sliding surface. Therefore, ERI can perform electrical profiling (2-D or 3-D resistivity measurements) on the slope (Lapenna *et al.,* 2003).

Jomard *et al.*, 2010 carried out on a deep-seated landslide body to investigate the depth and the geometry of the sliding surface using ERI method. They used the IRIS instrument, pole-pole arrays with 48 electrodes, and 10 m electrode spacing on a landslide body. RES2DINV software was used to obtain the vertical resistivity true section. They have found that the deep-seated landslide results of the ERI on the gravitational deformation by morphological were correlated with the fluid content in the sub-horizontal structure (Figure 2.12).
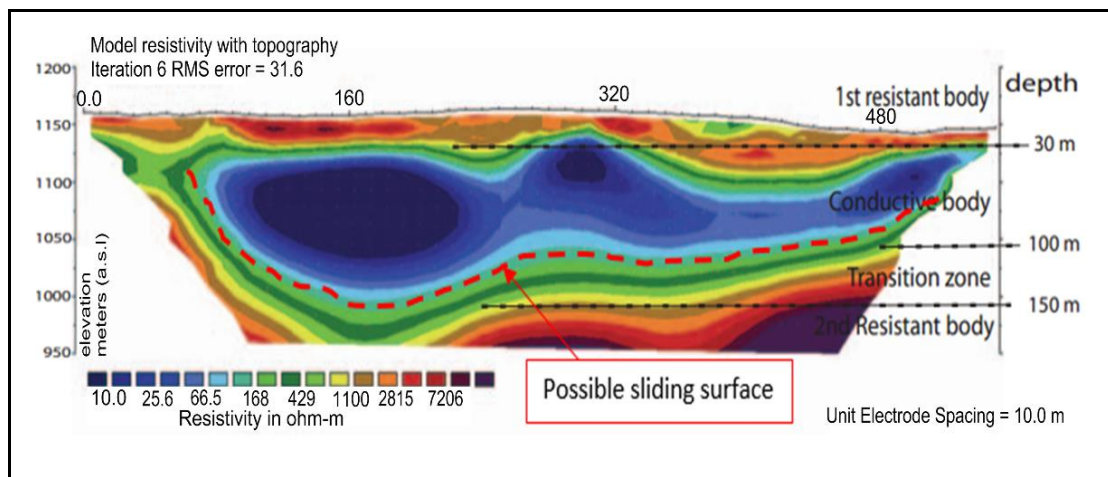
Figure 2.12 ERI result of a deep-seated landslide on a conductive body (Jomard *et al.,* 2010)

In addition, Grandjean *et al.*, 2011 significantly proved that the combined methods of electromagnetic, seismic, electrical, drilling, and inclinometer interpretations of the morphological structure of the sliding mass were very useful for studying complex landslides. They applied Syscal Pro 10 resistivity meter, pole-dipole array, a multi-gradient array with 96 electrodes, and 3 and 5 m electrode spacing for the electrical surveys. They used RES2DINV software to do the inversion model. As a result, they have found that the resistivity value less than 150 Ωm was the clayey layer and it was a possible landslide layer (Figure 2.13).
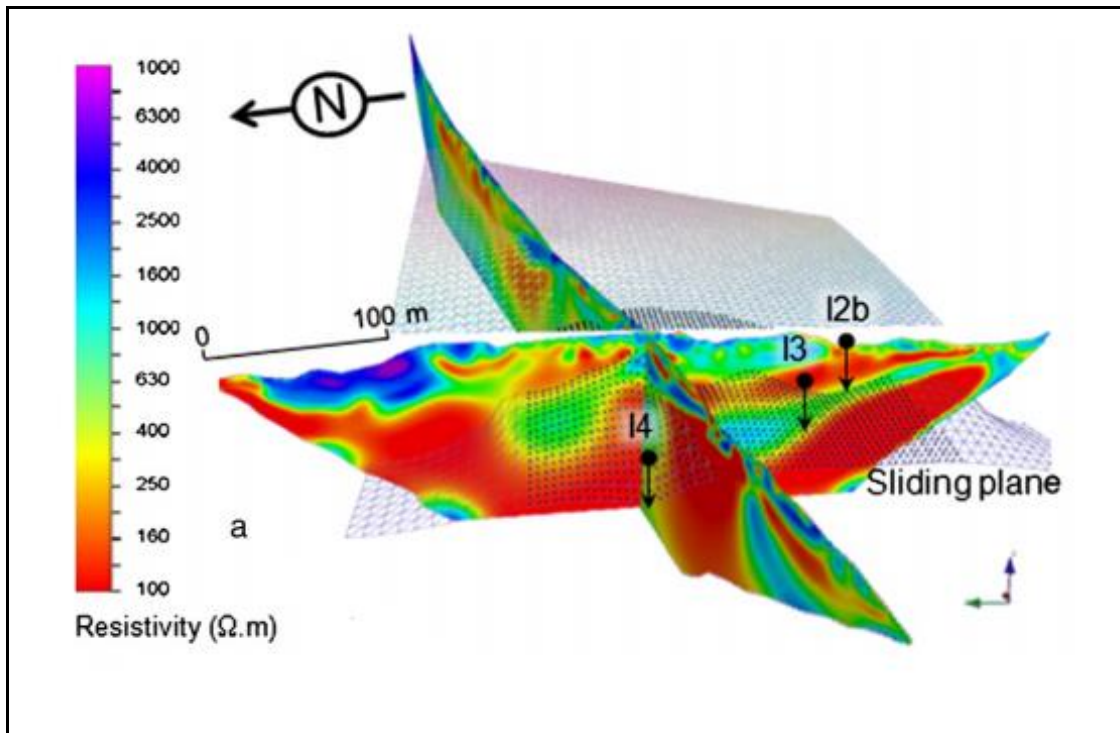
Figure 2.13 ERI result shows the sliding plane (Grandjean *et al.,* 2011)

Moreover, ERI surveys were carried out by Lapenna *et al.*, 2003 to investigate the thickness of the sliding surface and formation on the main pattern of the underground water movement at Giarrossa landslide in Southern Italy. They studied five ERI lines on an active trans-rotational earthflow slide. They applied the electrode configuration of Dipole-Dipole with the spacing of 10-30 m to delineate the sliding surface. After that, the Quasi-Newton method was used to make inversion processes. Seven times of an iteration process got an RMS value of 7.1%. The low resistivity values of about 5-30 Ωm indicated landslide body which was composed of water and clayey material. The resistivity values 60-100 Ωm represented in-situ rock head. Boreholes data were used to interpret and found that the estimated thickness of the slipped mass varied from 25-35m (Figure 2.14).
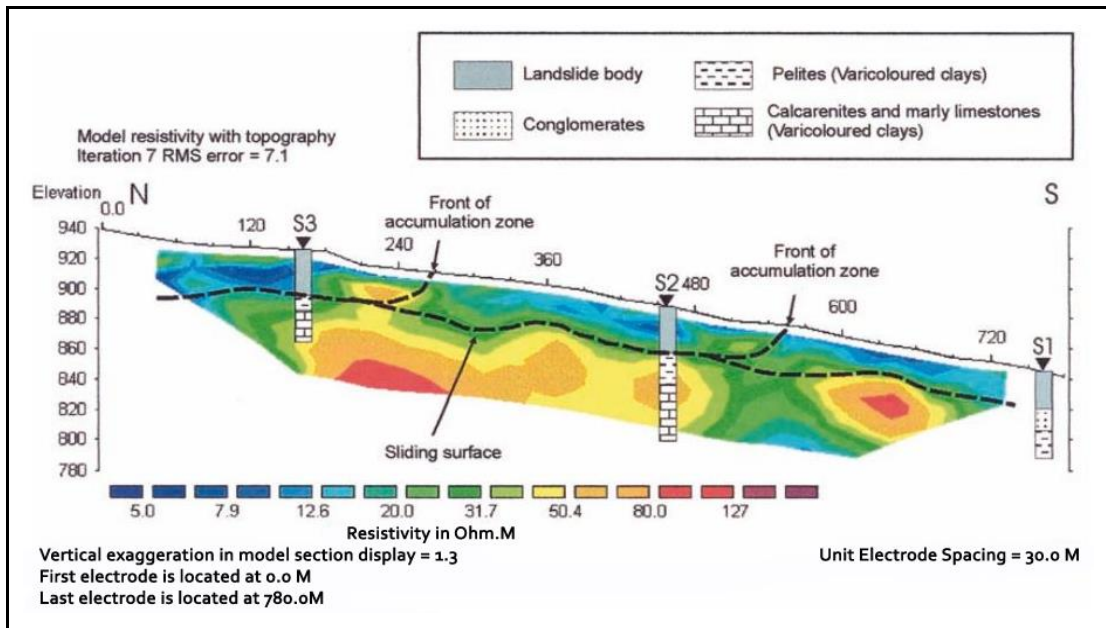
Figure 2.14 ERI longitudinal profile with boreholes data in an accumulation zone of the landslide body (Lapenna *et al.,* 2003)

Furthermore, Drahor *et al.*, 2006 investigated the landslide event in Turkey using ERI survey. They carried out three ERI survey lines on a rotational landslide. Wenner configuration, 30-electrode cable with 5 m electrode spacing were used to collect resistivity data. RES2DINV was used to do an inversion model. Line 1 and Line 2 were 60 m long and situated on the landslide body while Line 3 was 110 m long and it was laid across the landslide mass. They interpreted the geometry using boreholes data. The inversion of the resistivity data and borehole data were quite similar, thus they concluded that the landslide material, sand, silt and clay, water saturated zone were a possible sliding surface. (Figure 2.15).
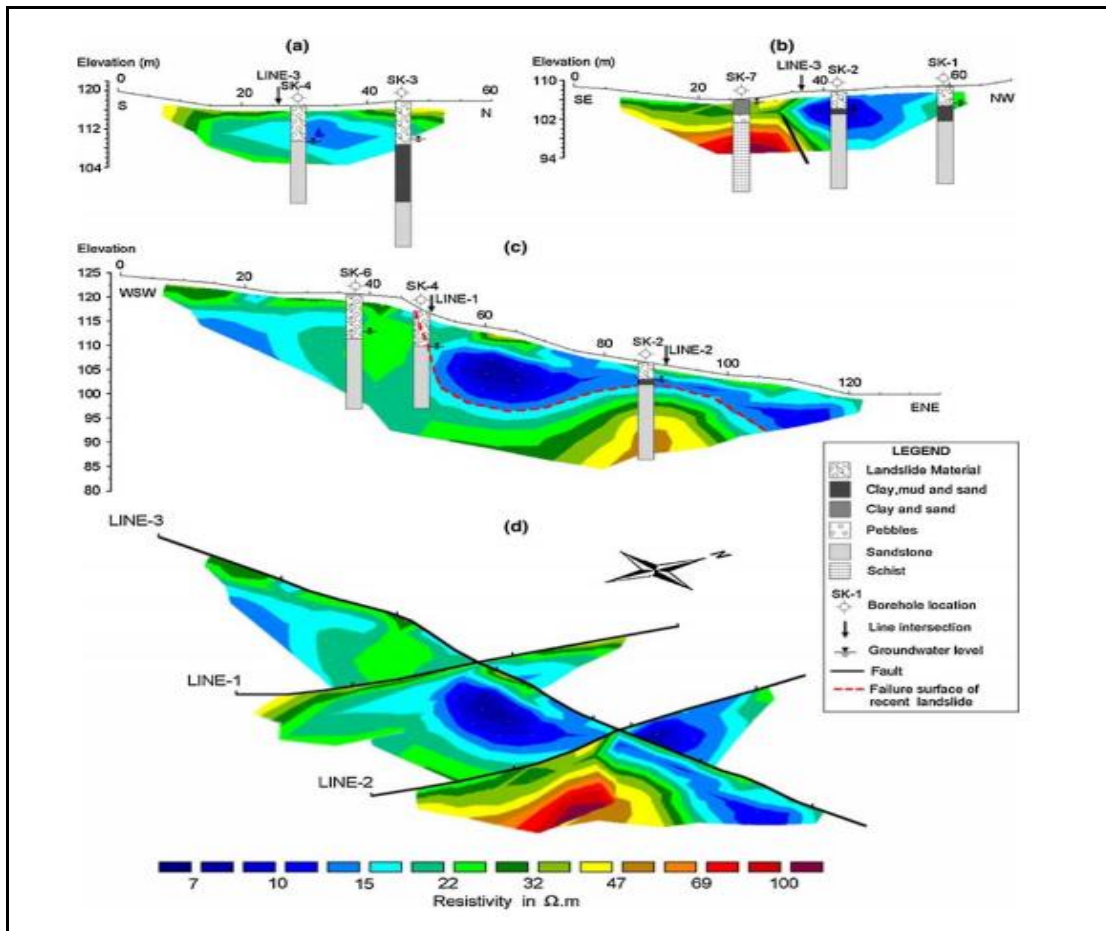
Figure 2.15 ERI result combined with boreholes data and 3-D fence diagram of resistivity section (Drahor *et al.,* 2006)

Most of the authors were applied 2-D ERI in various fields for the purpose of

● defining the geological structure of the subsoil

● reconstructing the landslide geometry

● estimating the depth of sliding mass

● locating the possible surface rupture

● characterizing fractures or tectonic elements and

● evaluating the groundwater conditions.

Table 2.4 mentions some authors successfully studied some landslide events using ERI method.

Table 2.4 The application of ERI method in some landslide events

Case Study, Authors, Year	Objective	Methodology	Result
Electrical resistivity tomography technique for landslide investigation: A review, Perrone *et al.*, 2014	(i) to reconstruct the landslide bodies geometrically (ii) to identify the slide surface (iii) to study the case to landslide relating to the groundwater flows	- Dipole-Dipole array - 32 electrodes - 10-30 m electrode spacing - RES2DINV inversion software	The shape of the sliding surface and its limits in the accumulation zone has a resistivity value of about less than 16 Ωm and it was composed of landslide material.
Application of electrical resistivity tomography (ERT) in the study of various types of slope deformations in anisotropic bedrock: case studies from the flysch carpathians, Pánek *et al.,* 2008	(i) to show ERT advantages and limitations when studying the structure of various types of slope deformations (ii) to study the landform assemblages	- Schlumberger arrays - 3 & 5m electrode spacing - RES2DINV inversion software	The increased water saturation of the rock environment represented a critical sliding case.
Three-dimensional geophysical anatomy of an active landslide in Lias Group mudrocks, Cleveland Basin, UK, Chambers *et al.*, 2011	To know the efficacy of the 3-D survey with respect to the geological setting of the study area	- AGI Supersting R8 IP instrument - Dipole-Dipole and Wenner arrays - 96 electrodes - 3,6,9,12 & 15m electrode spacing for 2D and na= 1a to 8a for 3-D	They have found that the sliding surface is located at the junction of mudstone and sandstone.

Table 2.4 The application of ERI method in some landslide events (Continued)

A case study of the application of electrical resistivity imaging for investigation of a landslide along the highway, Yilmaz, 2011	To predict the sliding surface and the thickness of the mobilized material.	-Dipole-Dipole arrays -56 electrodes -5m electrode spacing -AGI EarthImager inversion software	The landslide mass, siltstone, and clay-stone had high moisture content and these made landslide. The depth of sliding mass has 15-50 m.
2-D Electrical resistivity tomography (ERT) assessment of ground failure in an urban area, Nordiana *et al.,* 2017	To assess the foundation defects around an urban area in Selangor, Malaysia using 2-D electrical resistivity tomography (ERT)	-ES10-64C -Pole-Dipole arrays -41 electrodes -5m electrode spacing -RES2DINV inversion software	Silt, sand and clay (<100 Ωm) and highly weathered granite (100-1000 Ωm) at the depth 20-70 m may lead to the ground movement.

2.4 Hydraulic Model of Seepage Analysis

The movement of water under the ground is a major concerned case for geo-environment and geotechnical engineering. If the water is gained in various ways on a slope such as runoff water, rainfall induces and seepage, that slope will suffer the increasing the PWP and the changing the behavior of soil (GEO-SLOPE International Ltd., 2012a). Hydrological models become an essential role to predict PWP concerning rainfall infiltration (Brooks & Richards, 1994; Ekanayake & Phillips, 1999; Iverson, 2000; Frattini *et al.,* 2009). Although the simulation of numerical modeling for the water flow through the soil is very complex, the Geostudio (2018) product of SEEP/W is very useful and powerful 2-D finite element method (FEM) based program to analyze the PWP distribution, seepage and groundwater flow along the slope.

2.4.1 Conceptual Theory of Seepage Modeling

SEEP/W numerical model simulation performs mathematically on the water movement through a particular medium. It can be formulated with Darcy's Law. But vaporization process on the ground surface is not considered in SEEP/W modeling.

Darcy's Law 2-D differential equation (Richards, 1931; Papagianakis & Fredlund, 1984; GEO-SLOPE International Ltd., 2012a) can be expressed as:

$$\frac{\partial}{\partial x}\left[K_x \frac{\partial H}{\partial x}\right] + \frac{\partial}{\partial y}\left[K_y \frac{\partial H}{\partial y}\right] + q = \frac{\partial \theta}{\partial t} \tag{2.9}$$

where K_x and K_y are the coefficient of the hydraulic conductivities in x-direction and y-direction respectively, H is the total hydraulic head, q is applied flux, θ is the volumetric water content (VWC) and t is the time.

The above equation can describe as the summation of the entry flow (q) and exist flow ($\left[K_x \frac{\partial H}{\partial x}\right], \left[K_y \frac{\partial H}{\partial y}\right]$) is equal to the rate of change of the water storage amount in the soil element over time $\frac{\partial \theta}{\partial t}$.

If any change does not have in the storage of the soil, this state is called steady state and equation (2.11) becomes:

$$\frac{\partial}{\partial x}\left[K_x \frac{\partial H}{\partial x}\right] + \frac{\partial}{\partial y}\left[K_y \frac{\partial H}{\partial y}\right] + q = 0 \tag{2.10}$$

The changes of VWC and PWP of the soil are related to each other and which can be expressed as:

$$\partial \theta = M_w\, \partial u_w \tag{2.11}$$

where, M_w is the slope of VWC and u_w is the pore water pressure.

Equation (2.11) can be expressed in the form of total head and elevation head of water as:

$$\partial \theta = M_w\, \gamma_w \partial (H - z) \tag{2.12}$$

where γ_w is the specific weight of water and z is the elevation head.

For the flow condition of saturated and unsaturated, the differential equation given from equation (2.9) in each time step (elevation is a constant, therefore, the change in elevation with respect to time is considered as zero) becomes:

$$\frac{\partial}{\partial x}\left[K_x \frac{\partial H}{\partial x}\right] + \frac{\partial}{\partial y}\left[K_y \frac{\partial H}{\partial y}\right] + q = M_w \gamma_w \frac{\partial H}{\partial t} \tag{2.13}$$

Actually, in the FEM of seepage modeling, the main domain is created many small elements. Then the main domain is characterized by connecting each

individual element equations. Therefore, Galerkin's weight residual method is used in the finite element seepage general differential equation and it can be expressed as:

$$[K]\{H\} + [M]\{H\}, t = \{Q\} \tag{2.14}$$

in which $[K]$ is the element characteristics matrix, $\{H\}$ is the vector of nodal heads, $[M]$ the element mass matrix, $\{Q\}$ is the applied element flux vector. The detailed finite element formulation can be found in GEO-SLOPE International Ltd., 2012a.

2.4.2 Hydraulic Function Analysis

SEEP/W is used to simulate the nonlinear differential equation of the seepage mentioned in equation (2.15). The convergence of the main domain seepage condition is obtained from the iterative procedures of the size of the seepage or hydraulic conductivity of the element nodes using PWP exerted nodes. There are two main functions to estimate the hydraulic conductivity: (i) van Genuchten function and (ii) Fredlund & Xing function.

van Genuchten, 1980 proposed three-parameter equation to estimate a closed form of dimensionless VWC (Θ) function as follows:

$$\Theta = \frac{1}{(1 + (ah)^n)^m} \tag{2.15}$$

where *a, m, n* are the shape factors related to the air-entry value of the soil (kPa), *h* is the matric suction. The parameter *m* is can be shown:

$$m = \frac{1}{(1 - n)} \tag{2.16}$$

But, VWC of soil generally can express in terms of saturated and residual water content values. This dimensionless water content function is

$$\Theta = \frac{\theta - \theta_r}{\theta_s - \theta_r} \tag{2.17}$$

where θ is the volumetric water content, θ_s is the saturated water content and θ_r is the residual water content. A typical soil-water characteristic curve (SWCC) is displayed in Figure 2.16.
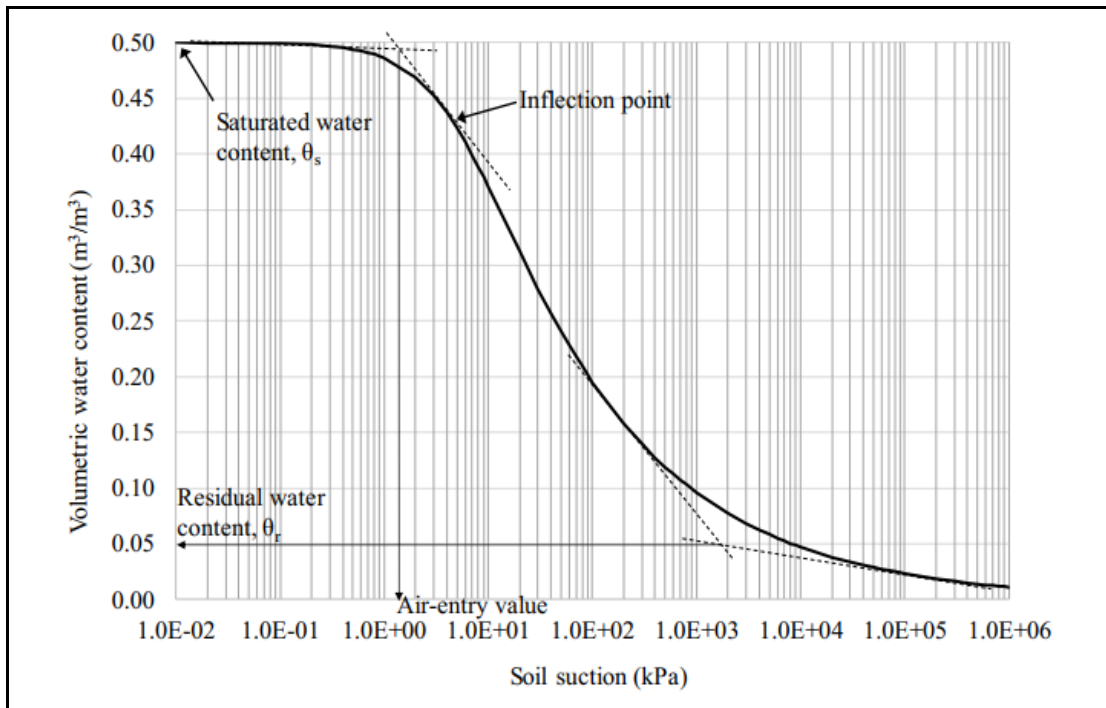
Figure 2.16 A typical soil-water characteristic curve (GEO-SLOPE International Ltd., 2012a)

Therefore, SWCC can be represented from the equations (2.15), (2.16) and (2.17).

$$\frac{\theta - \theta_r}{\theta_s - \theta_r} = \left[\frac{1}{(1 + (ah)^n)}\right]^m \tag{2.18}$$

In considering unsaturated hydraulic conductivity, the relative hydraulic conductivity (K_r) is used to normalize the equation from the unsaturated hydraulic conductivity (K) and saturated hydraulic conductivity(K_s):

$$K_r = \frac{K}{K_s} \tag{2.19}$$

But Mualem, 1976 proposed the following equation to predict the unsaturated hydraulic conductivity:

$$K_r = \Theta^{1/2} \left[\frac{\int_0^\theta \frac{1}{h(x)} dx}{\int_0^1 \frac{1}{h(x)} dx}\right]^2 \tag{2.20}$$

After that, van Genuchten, 1980 modified the relative hydraulic conductivity equation from the equations (2.19), (2.20), (2.21) and (2.22):

$$\frac{K(\Theta)}{K_s} = \left[\frac{\theta - \theta_r}{\theta_s - \theta_r}\right]^{1/2} \left\{1 - \left[1 - \left[\frac{\theta - \theta_r}{\theta_s - \theta_r}\right]^{1/m}\right]^m\right\}^2 \qquad (2.21)$$

Fredlund and Xing, 1994 recommended to estimate a closed form of dimensionless VWC (Θ) function as follows:

$$\Theta = C(h) \frac{\theta_s}{\left[ln\left[e + \left(\frac{h}{a}\right)^n\right]\right]^m} \qquad (2.22)$$

$$C(h) = 1 - \frac{ln\left(1 + \frac{h}{h_r}\right)}{ln\left(1 + \frac{10^6}{h_r}\right)} \qquad (2.23)$$

Where $C(h)$ is the correction function which is ranging from 1(low suction) to 0 (high suction, h= 10^6 kPa), e = the natural number (2.71828), h_r = matric suction harmonizing to the residual water content θ_r.

The hydraulic conductivity (K_w) of unsaturated soil is used as proposed by Campbell, 1974 and which can be explicated as follows:

$$K_w = (K_s - K_{min})\theta^p + K_{min} \qquad (2.24)$$

where K_w is the unsaturated hydraulic conductivity, K_{min} is the minimum hydraulic conductivity, p is the power factor for adjusting the prediction.

2.4.3 The Under-relaxation Criteria Setting in Seepage Modeling

GeoStudio supports the general parameters of under-relaxation criteria that satisfy for all types of soil (Figure 2.17). But, in some cases, if the material properties are highly non-linear, the default parameters cannot support to approach under-relaxation condition. In this condition, there are two ways to minimize the divergence state (Geo-Slope International Ltd ,2012a). The first matching is reducing the initial rate and minimum rate (e.g., initial rate = 0.65, minimum rate = 0.01). The second matching is reducing the minimum rate and reduction frequency (e.g., minimum rate = 0.01, reduction frequency = 5). More details mathematical expressions relating to convergence solution can be seen in Geo-Slope International Ltd ,2012a.
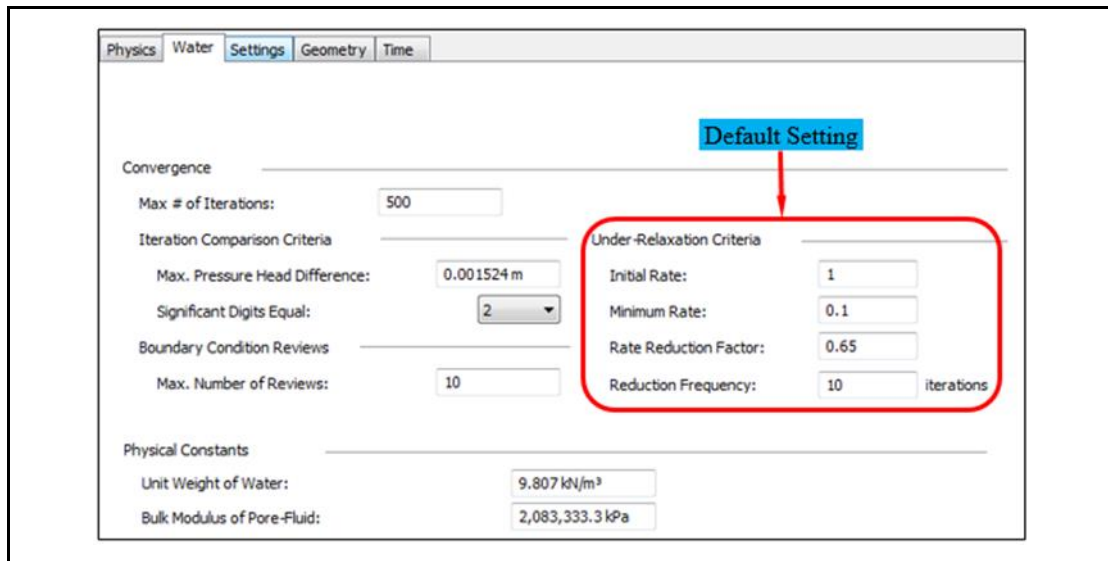
Figure 2.17 The default setting of convergence criteria in SEEP/W modeling

2.4.4 Evaluating the Convergence and Under-relaxation Criteria in Seepage Modeling

The computed result is required to check whether the result reaches the acceptable convergence condition. Figure 2.18 (a) shows the iterative procedure is fully solved condition whereas (b) does not have. In such case of Figure 2.18 (b), the nodes are painting red cross and circle dot and which indicate the domain areas do not reach the convergence criteria. At the time, the above mention procedures are coming necessary using trial and error method to judge the convergence criteria. If all the nodes are fully solved, the result will show convergence and the solution is will achieve under-relaxation condition. Figure 2.19 (a) and (b) mention examples of non-convergence and convergence results. Here, if the input conductivity function and the computed conductivity are coincided, this solution is said to be convergence condition. Figure 2.20 indicates the iterative procedure reach under-relaxation condition. The graph means all the pressure head nodes in a starting condition cannot convergence and then convergence in suitable iteration numbers. The pressure head nodes value zero means the iterative procedure reaches the under-relaxation condition.
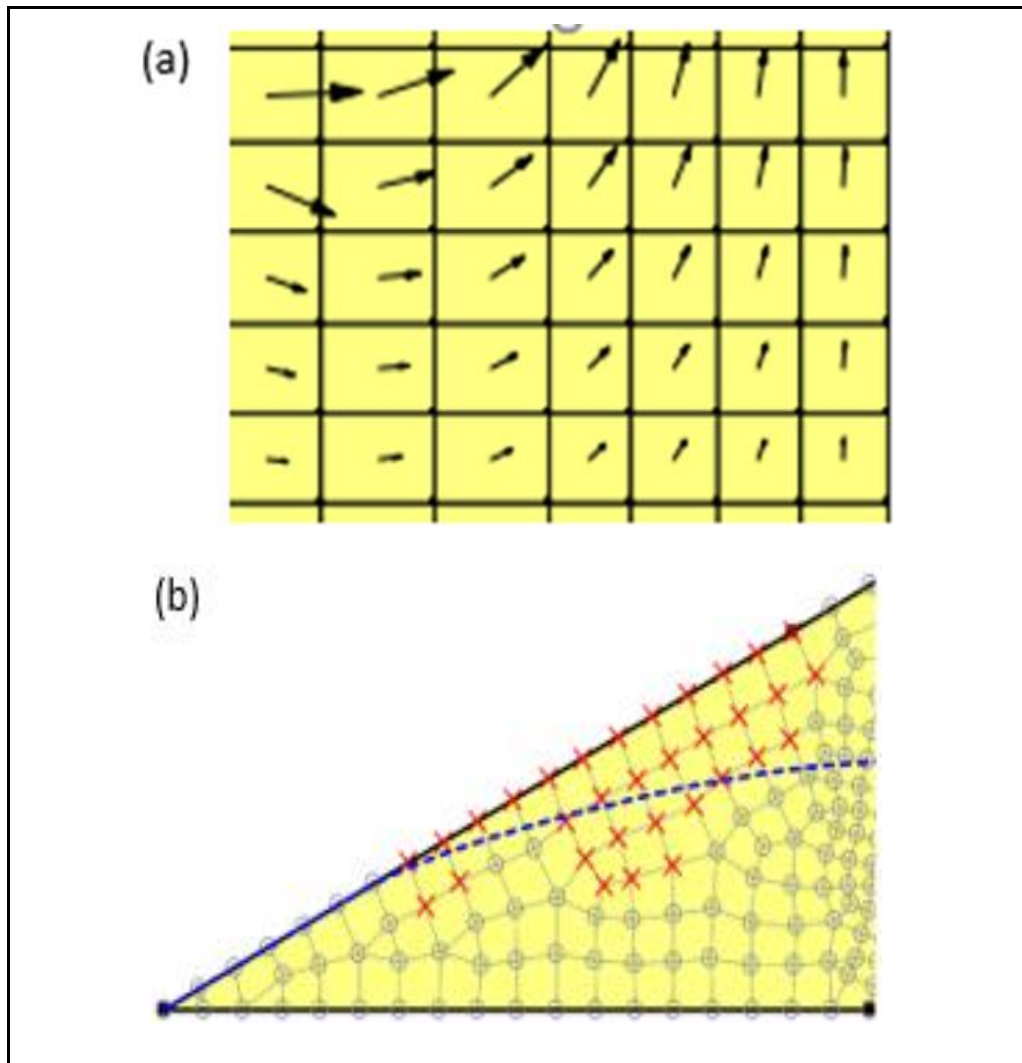
Figure 2.18 (a) Nodes that have reached the convergence state (b) Nodes that have   not reached the convergence state (Geo-Slope International Ltd., 2012a)
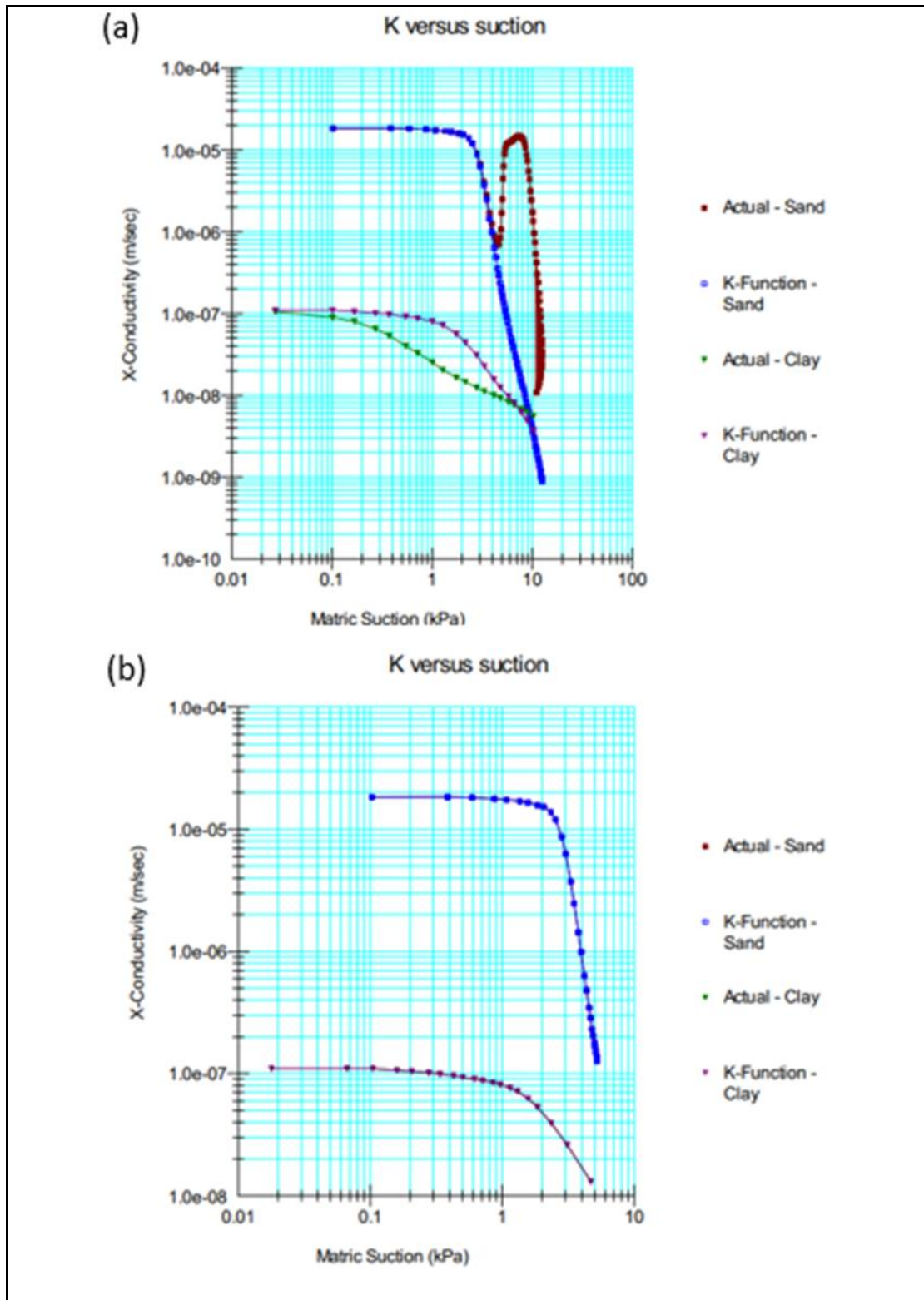
Figure 2.19 Illustrating on Conductivity versus suction (a) non-convergence state (b) convergence state (Geo-Slope International Ltd., 2012a)
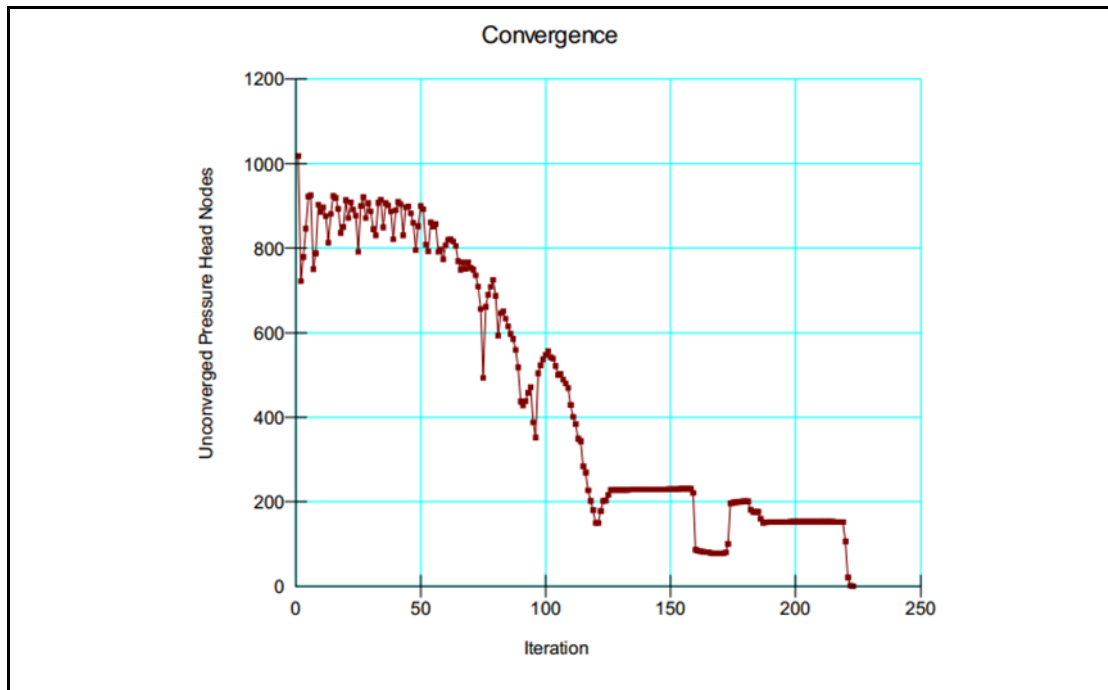
Figure 2.20 Non-converged nodes versus number of iterations (Geo-Slope

       International Ltd., 2012a)

2.5 Slope Stability Analysis

Slope stability analysis is widely used on the various types of the slopes such as natural slopes and manmade undercuts (cutting and filling processes, embankments, open-pit mining sites, etc.) to simulate the slopes failures (GEO-SLOPE International Ltd., 2012b). This analysis can determine the potential failure surface with different triggering mechanisms and factor of safety (F.S.) of the slope. The geometry, hydrogeological condition, topology, groundwater condition, and geotechnical parameters are essential factors to construct the perfect design of the slope. Although the stability analysis was done with hand calculation in the past, computer-based slope stability software can apply in the present moment.

2.5.1 Concept of SLOPE/W

All the slope stability analysis methods are purposed to find the F.S. of the desired slope. Therefore, all methods consider F.S. to know the structural capacity is exceeded the actual or expected load. The SLOPE/W software (Geostudio software) is one of the computer program, which performs the limit equilibrium method (LEM)

of the man-made slope, natural slope, and soil reinforcement on the geotechnical survey sites. It can simulate the composite, circular and non-circular slip surfaces. This software based on many methods to check the stability of the slope. Besides, it can estimate the possible sliding surface of the slope. The geometry, hydrogeological condition, topology, and geotechnical parameters are required to simulate F.S. along the failure surfaces.

2.5.2 Limit Equilibrium Method (LEM) for Slope Stability Analysis

LEM of SLOPE/W is based on the method of the slice. In this method, several vertical slices are created on a mass of soil over the failure surface to study the equilibrium conditions of each slice. Hence, the sums of the exerted forces on a free body slice, i.e., the sum of all moments ($\sum M$), the sum of all vertical forces ($\sum F_v$) and the sum of horizontal forces ($\sum F_h$) are equal to zero and this condition is called limit equilibrium. Engineers are conducting various types of slope stability analysis using LEM. It can perform on a complex stratigraphy section and high content of irregular PWP conditions. Ordinary method (Fellenius's Method), Bishop's simplified method, Janbu's simplified method, Spencer's Method, and Morgenstern-Price's method are the most common methods of LEM. All methods are solved base on the distribution of internal forces statically Mohr-Coulomb (Perfect elastoplastic Model) analytical method with internal friction. The general equation of the Mohr-Coulomb failure criterion expressed as follows:

$$\tau' = c' + (\sigma_n - u)tan\phi \qquad (2.25)$$

where τ' is the shear strength on the failure plane, c' is effective cohesion, σ_n is total normal stress on the failure plane, u is pore water pressure and ϕ is friction angle.

Figure 2.21 shows the force acting on horizontal and vertical plane surfaces representing a slice of the slope potential in rupture. The magnitude of the shear force mobilized to satisfy conditions of limiting equilibrium is:

$$S_m = \frac{\tau'\beta}{F.S.} = \frac{c'\beta + (\sigma_n - u)\beta tan\phi}{F.S.} \qquad (2.26)$$

where S_m is the mobilized shear force, β is the slice base length.

According to Figure 2.21, the solution procedures for the LEM are considered as follows:

- The summation of all vertical direction acting forces at the base of each slice is called normal forces (N) as:

$$(X_L - X_R) - W + Ncos\alpha + S_m sin\alpha - Dcos\omega = 0 \qquad (2.27)$$

where X_L is the interslice shear force (left), X_R is the interslice shear force (right), W is the weight of the slice, α is the slice base inclination angle, D is the external point load, and ω is the angle of the point load from the horizontal (always measure counter-clockwise from the positive X-axis.)

Figure 2.21 Exerted forces on a slice of a sliding mass with a circular slip surface (Modified from GEO-SLOPE International Ltd., 2012b)

- By substituting S_m value in equation (2.11), the equation of the normal force N value becomes:

$$N = \frac{W + (X_L - X_R) - \left[\dfrac{c'\beta sin\alpha - u\beta tan\phi sin\alpha}{F.S.}\right]}{cos\alpha + \dfrac{sin\alpha tan\phi}{F.S.}} \qquad (2.28)$$

The summation of all horizontal directions of interslice forces ($\sum F_h$) is considered as:

$$\sum F_h = \sum E_L - E_R - \sum(Nsin\alpha) + \sum S_m cos\alpha - \sum kW + \sum Dcos\omega \pm \sum A = 0 \quad (2.29)$$

where E_L is the interslice normal force (left), E_R is the interslice normal force (right), kW is the horizontal seismic load applied through the centroid of each slice, and A is the resultant external water forces.

In addition, integral manner equation across the slice from left to right is used to solve the equation. $\sum F_h$ is applied to solve the force equilibrium F.S.

- The summation of all the possible moments ($\sum M$) of each slice that can appear from a slip surface circle's center is considered as:

$$\sum M = \sum Wx - \sum S_m R' - \sum Nf + \sum kWe \pm \sum Dd \pm \sum Aa = 0 \qquad (2.30)$$

where x is the horizontal distance from the centerline of each slice to the center of rotation or to the center of moments, R' is the radius for a circular slip surface or the moment arm associated with the mobilized shear force, f is the perpendicular offset of the normal force from the center of rotation or from the center of moments, d is the perpendicular distance from a point load to the center of rotation or to the center of moments, a is the perpendicular distance from the resultant external water force to the center of moment.

By assuming the direction of resultant interslice forces, F.S. due to moment and force equilibrium is calculated. A unique F.S., which satisfy both moment and force equilibrium are defined as General Limit Equilibrium (GLE) F.S.

Fellenius's method (1936) considers that the resultant of the inter-slice forces in each vertical slice is parallel to its base. This method can satisfy only the moment equilibrium and its F.S. on a circular slip is:

$$\text{F.S.} = \frac{\sum[c'\beta + N\tan\emptyset]}{\sum W\sin\alpha} \qquad (2.31)$$

General Limit Equilibrium Method was developed by Fredlund (1981) at the University of Saskatchewan, and it has two basic equations to solve F.S. of the slope.

- F.S. with respect to moment equilibrium:

$$\text{F.S.} = \frac{\sum[c'\beta R' + (N - u\beta)R\tan\emptyset]}{\sum Wx - \sum Nf \pm \sum Dd} \qquad (2.32)$$

- F.S. with respect to horizontal force equilibrium:

$$\mathrm{F. S.} = \frac{\sum[c'\beta cos\alpha + (N - u\beta)tan\emptyset\ cos\alpha]}{\sum Nsin\alpha - \sum Dcos\omega} \tag{2.33}$$

Bishop, 1960 simplified F.S. in the absence of pore water pressure was as follows:

$$\mathrm{F. S.} = \frac{1}{\sum Wsin\alpha} \sum \left[\frac{c'\beta + W\ tan\emptyset - \frac{c\beta}{\mathrm{F.S.}}sin\alpha\ tan\emptyset}{m_\alpha}\right] \tag{2.34}$$

$$m_\alpha = cos\alpha + \frac{sin\alpha\ tan\emptyset}{\mathrm{F. S.}} \tag{2.35}$$

The estimated F.S. is required to calculate a new F.S. in Bishop's method. Bishop's simplified method considers only normal inter-slice forces, it neglects the inter-slice shear force. Therefore, as a result, it reconciles only overall moment equilibrium, it does not satisfy the overall horizontal force equilibrium.

Janbu's simplified method (1954) is identical to Bishop's method. This method considers the inter-slice normal forces and neglects the shear forces. Therefore, it only satisfies the horizontal force equilibrium.

Morgenstern-Price method (1965) considers both normal inter-slice force and shear force to satisfy both force and moment equilibriums. Limit equilibrium formulation is the basic assumption of this method and it needs to make an assumption the direction of the resultant of the inter-slice shear and normal forces, as follows:

- F.S. for moment equilibrium:

$$\mathrm{F. S_M.} = \frac{\sum[c'\beta R' + (N - u\beta)Rtan\emptyset]}{\sum Wx - \sum Nf + \sum kWe \pm \sum Dd \pm \sum Aa} \tag{2.36}$$

- F.S. for horizontal force equilibrium:

$$\mathrm{F. S_F.} = \frac{\sum c'\beta cos\alpha + (N - u\beta)tan\emptyset\ cos\alpha]}{\sum Nsin\alpha + \sum kW - \sum Dcos\omega \pm \sum A} \tag{2.37}$$

Besides, this method provides the variable connection between the inter-slice normal and shear forces (GEO-SLOPE International Ltd., 2012b). Moreover, in the composite slip surface, the rigorous method normally produces a good accurate result. Figure 2.22 illustrates a perfect closure result of a slice force polygon.
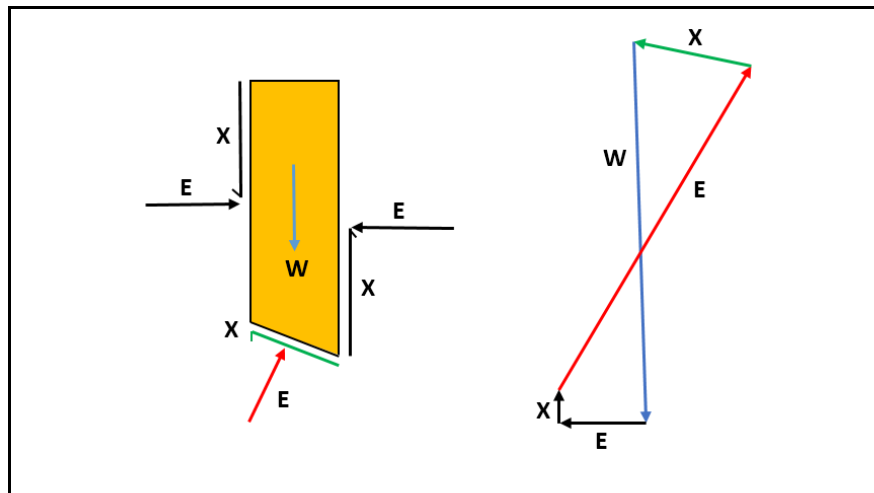
Figure 2.22 A free body diagram of a slice and, to the right, the corresponding force polygon (modified from GEO-SLOPE International Ltd., 2012)

When considering F.S. of a slope with various LEMs, it is noticeable that the geological parameters of friction angle (ϕ) and effective cohesion (c') are resistance forces and they are directly proportional to F.S. while unit weight (γ) is a driving force, and it is inversely proportional to F.S. Therefore, In SLOPE/W modeling, the effective cohesion (c'), the friction angle (ϕ), the unit weight (γ) are important geotechnical parameters. Besides, the slope angle of the study areas and the pore water pressures are also essential parameters because they are affected to the safety factor and the sliding thickness.

Naderi, 2013 stated that the influence of geological parameters and slope angle in SLOPE/W modeling as follows:

● Increasing the value of effective cohesion (c') causes increasing the surface rupture length and factor of safety.

● Increasing the value of friction angle (ϕ) causes decreasing the surface rupture length and increasing the factor of safety.

● The higher the unit weight of soil (γ) value causes the greater the surface rupture length and which will decrease the factor of safety.

● Decreasing slope angle causes increasing the surface rupture length and which will make the factor of safety increase due to high resisting force.

Moreover, the other parameters also affect F.S. Hence, the amount of added soil to the top part will act as an overburden load increasing the driving force and

it causes F.S. decreases. Then, if the slope angle decreases, the length of the arc (circular surface) will increase and this will lead to a more resisting force, which means F.S. increases (Naderi, 2013).

2.5.3 Investigation of Landslide Using Coupled Modeling of SEEP/W-SLOPE/W

Rainfall-induced slope failure is the common case around the world. Heavy and prolonged rainfalls can be directly related to the unsaturated soil slope stability (Brand *et al.,* 1981). The combined modeling SEEP/W-SLOPE/W (GEO-SLOPE International Ltd., 2012a) are widely used to study seepage and slope failure processes along mountain sides (Lee *et al.,* 2009; Rahimi *et al.,* 2010). In the coupled SEEP/W-SLOPE/W modeling, the finite element method based on SEEP/W performs as parent function and then directly linked a function of SLOPE/W. The changes of PWP under the subsoil and the stability of the slope condition are the major functions in this coupled modeling (GEO-SLOPE International Ltd., 2012c).

Acharya *et al.*, 2016 successfully studied the slope failure cases to investigate the hydrological and mechanical influenced slope failure due to an extreme rainfall event. The combined modeling was used to study seven locations (A, B, C, D, E, Fand G) of slope failure areas on the catchment in Shikoku, Japan. Detailed field observations such as the dimensions of the slope failures and soil laboratory tests were done for all locations (Table 2.5). In their studies, they assumed for implementing 2-D analysis of seepage and slope stability modeling as assumptions of 1) the failure slope mass exist on an upper single layer, 2) circular failure mode, 3) the entire soil depth and the maximum soil failure depth is equal, 4) the bedrock under the soil is impervious, 5) the failure soil mass is homogeneous material, 6) unit weight is the same in saturated and unsaturated condition 7) transient state with Fredlund and Xing method is considered as for rain infiltration, and 8) the maximum infiltration rate is the same as the soil permeability. In the seepage simulation with 283-time steps within 47 hours, they have found that the peak positive pore water pressure for all locations were reached at time step 223 (Figure 2.23).

Table 2.5 Field and soil laboratory test results of seven sites (Acharya *et al.,* 2016)

Slope failure spot	L (m)	B (m)	θ (°)	D (m)	*c' (kN/m²)	*Υ (kN/m³)	*φ' (°)	K (m/s)	n
A	38.02	10.45	33.38	0.60-1.10	0.49	16.92	34.86	1.20 ×10⁻⁶	0.50
B	20.13	9.11	27.46	0.26-1.03	0.62	15.83	33.72	5.80 ×10⁻⁸	0.45
C	19.33	12.92	33.00	0.11-1.42	1.44	16.92	34.14	6.08 ×10⁻⁸	0.46
D	15.32	13.51	32.90	0.16-0.80	0.78	17.08	36.76	8.03 ×10⁻⁸	0.48
E	25.02	12.26	38.86	0.12-1.18	0.86	17.22	33.01	1.70 ×10⁻⁸	0.43
F	13.81	8.67	21.78	0.55-1.78	0.13	15.83	34.21	2.35 ×10⁻⁸	0.50
G	22.32	13.41	29.70	0.33-0.99	1.33	16.79	33.85	3.10 ×10⁻⁷	0.49

Note: In this table, L= slope failure length; B=slope failure breadth; θ=average slope angle; D=soil thickness; c'= effective cohesion; Υ=unit weight of soil; ϕ'=effective angle of shearing resistance; k=soil permeability; and n=saturated volumetric water content. c' and ϕ' were determined from direct shear tests. Υ and n were obtained from laboratory experiments. k was measured by field experiment.

The Morgenstern-Price method with half-sine function was applied in slope stabilities analysis and their results shown that the F.S. decreases with an increase in precipitation under constant soil permeability and volumetric water content values. At the time step 223, the F.S. reduced to less than 1 in all sites because the groundwater table rises up to the crest of the slope. Finally, they concluded that rapid transient PWP made the slope instability in the study area and the instability range of PWP at the upper part of the slope was smaller than the lower part of the slope. The relationship among rainfall intensity, F.S. and time span are presented in Figure 2.24 and the optimized critical slip surfaces and the respective F.S. on the date of failure are exhibited in Figure 2.25.
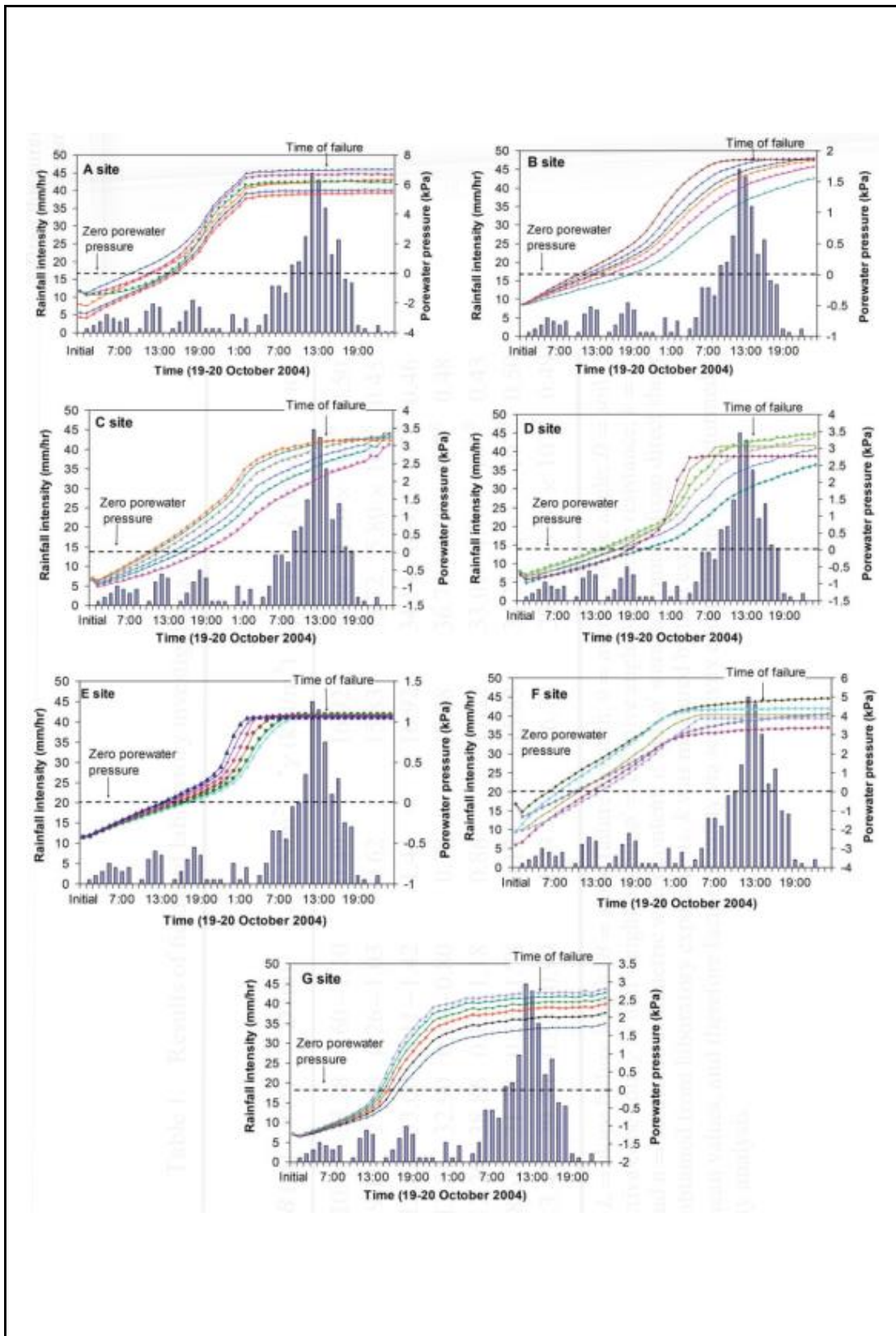
Figure 2.23 Transient pore water pressure distribution in slip surface of seven slope failure sites A, B, C, D, E, F, and G (Acharya *et al.,* 2016)
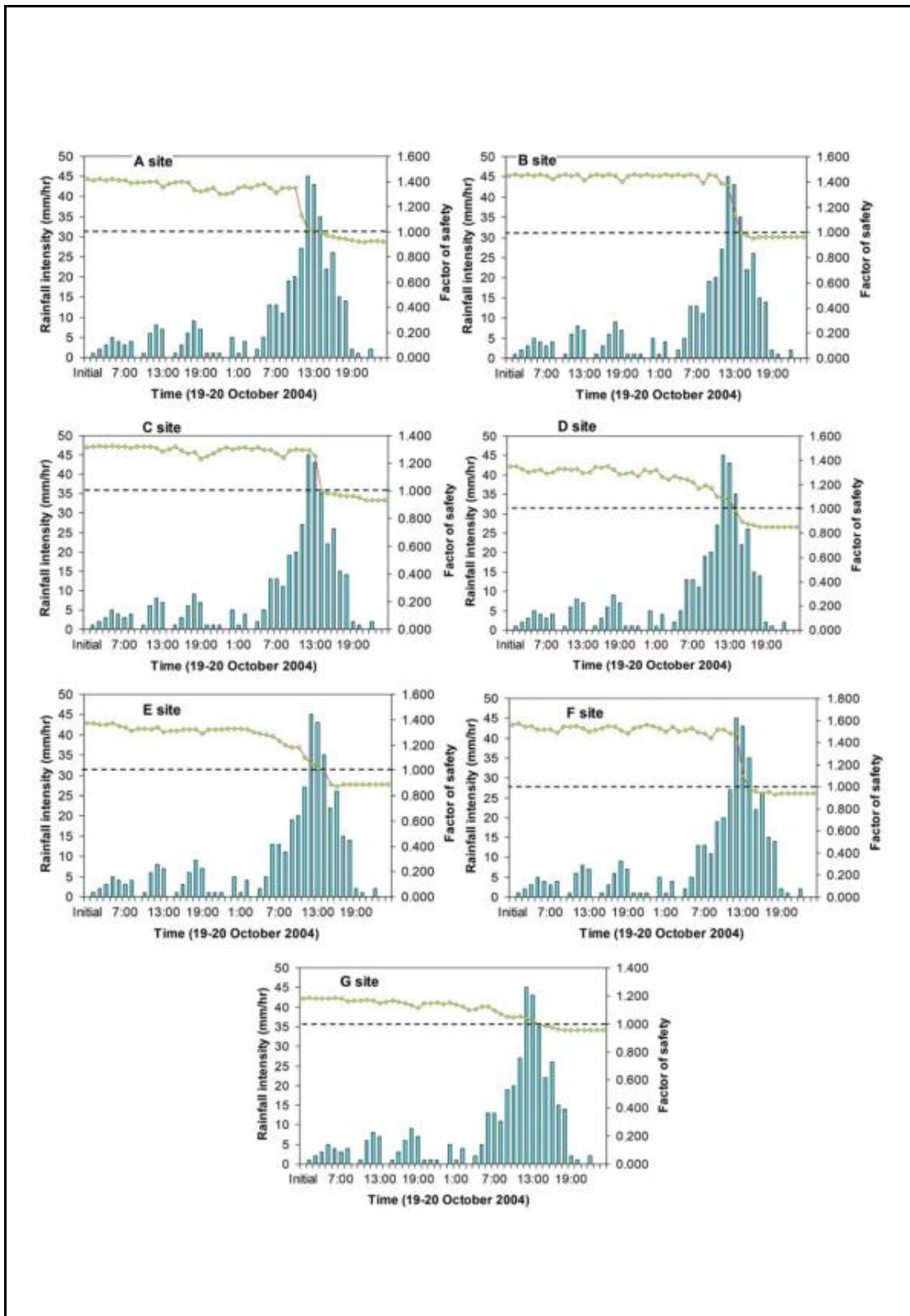
Figure 2.24 The relation between rainfall intensity, the factor of safety and time span
(Acharya *et al.,* 2016)
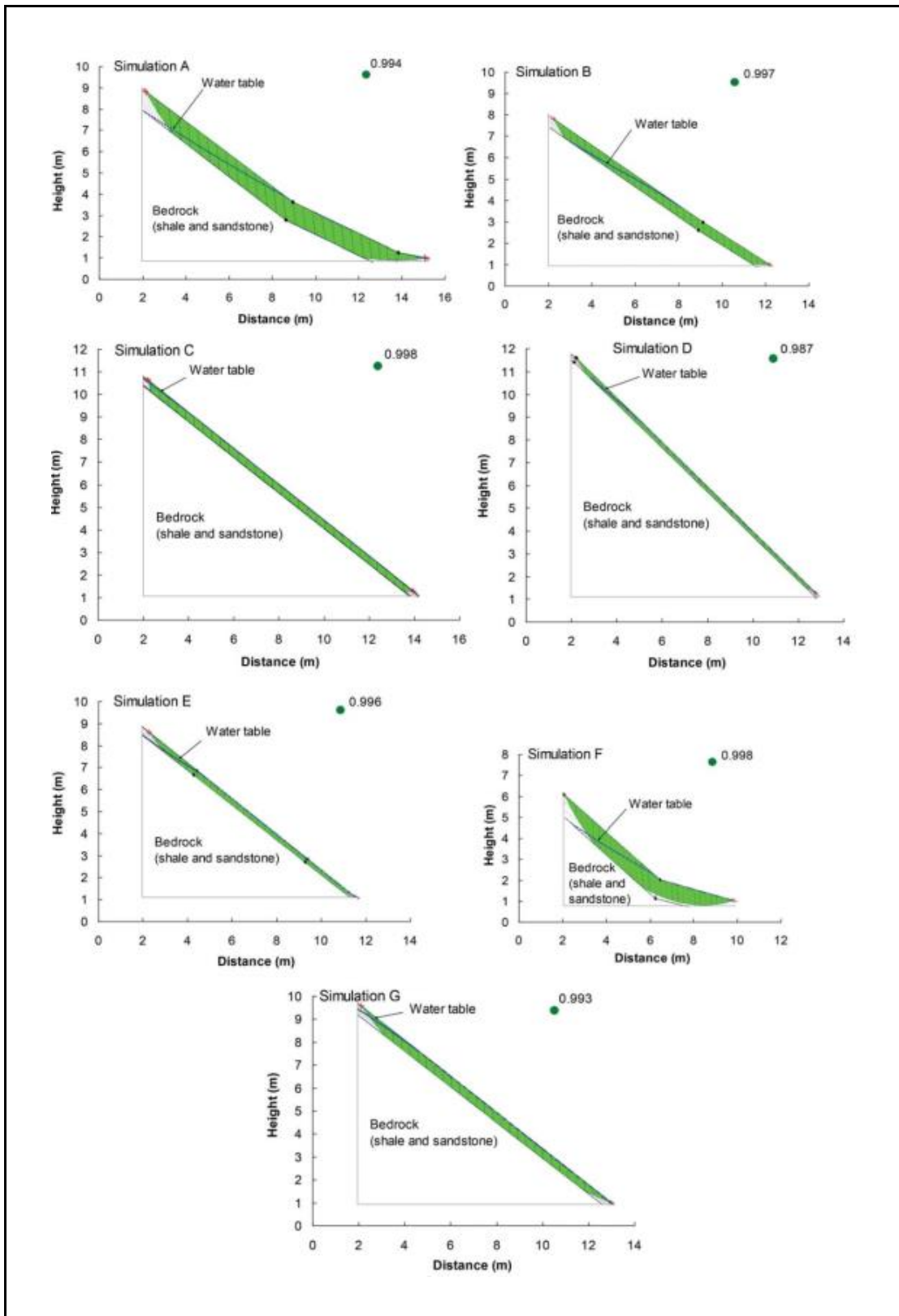
Figure 2.25 The optimized critical slip surfaces and the respective factor of safety on the date of failure (Acharya *et al.,* 2016)

Muntohar *et al.,* 2013 studied the landslides cases in Kulonprogo, Indonesia for the purpose of studying the rainfalls' mechanism induces landslide depend on time of instability. They used both seepage and slope stability analysis for their study. In this case landslide was occurred due to five days accumulated rainfall. The parameter they used in this study is mentioned in Table 2.6. The transient seepage analysis for 10-days and Bishop's method for slope stability analysis were used in this investigation and they have found that pore water pressure and stability were totally changed 4-days after the rainfall, slope failure occurred during 8-days precipitation and F.S. reached 0.88. Then, they concluded that the destabilization of the slope was controlled by rainfall infiltration due to increasing of pore water pressure, perched groundwater table and residual shear strength of the residual soils. Figure 2.26 shown (a) estimated rain-water infiltration, (b) pore water pressure on surface, (c) pore water pressure at failure surface, (d) change of slope stability with elapsed time.

Table 2.6 Hydrological and geological parameters (Muntohar *et al.,* 2013)

Parameter	Residual Soil	Weathered Breccia	Massive Breccia (bedrock)
Natural moisture content, W_N (%)	33.2	39.4	40.2
Bulk unit weight, Υ_b (kN/m3)	17.7	15.1	14.8
Unit weight above water table, Υ_d (kN/m3)	13.4	12.1	11.7
Degree of saturation, S_r (%)	90.1	64.8	41.9
Saturated volumetric water content, θ_s	0.48	0.53	0.50
Saturated permeability coefficient, k_{sat} (m/s)	1.19×10^{-4}	1.74×10^{-8}	-
Cohesion at failure (peak), c' (kPa)	16	48	-
Residual cohesion, c'_r (kPa)	12	36	-
Internal friction angle at peak, ϕ' (°)	24	10	-
Internal friction angle at residual, ϕ_r (°)	18	9	-
Unsaturated friction angle, ϕ^b (°)	15	8	-
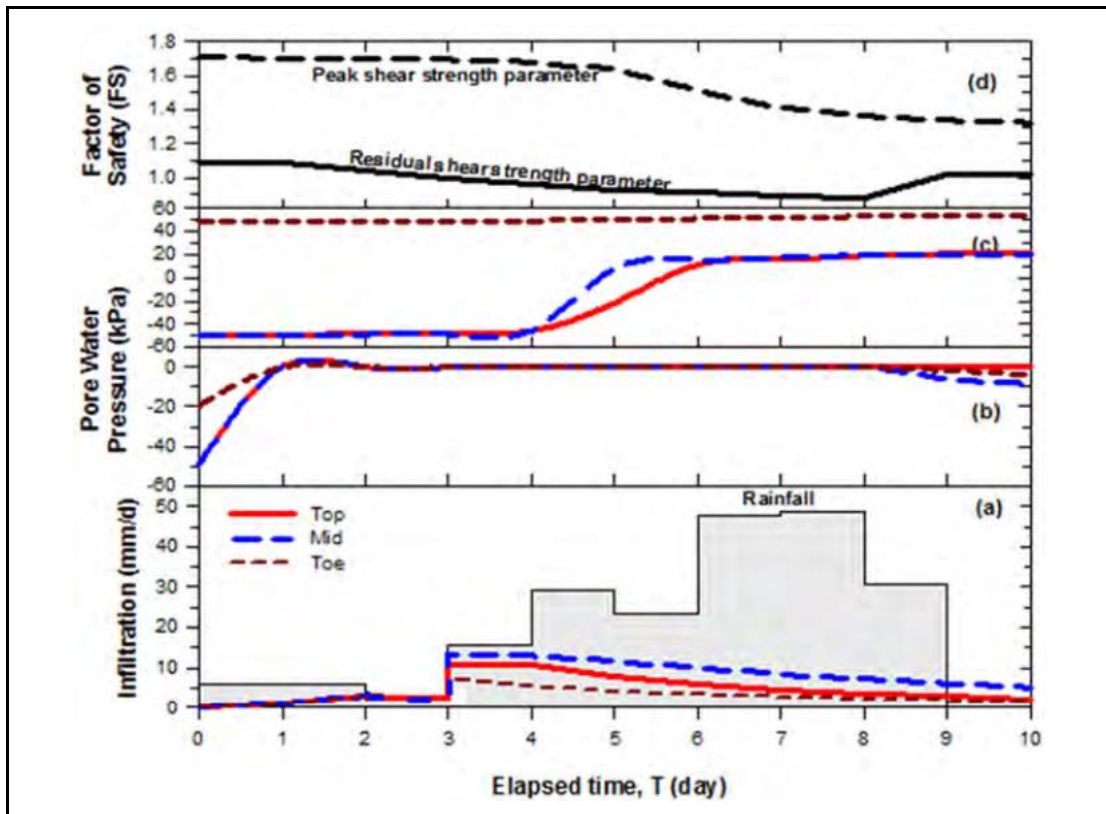
Figure 2.26 (a) estimated rain-water infiltration, (b) pore water pressure on surface, (c) pore water pressure at failure surface, (d) change of slope stability with elapsed time (Muntohar *et al.,* 2013)

Gofar *et al.,* 2006 also successfully studied a rainfall-induced landslide case occurred in an opened coal mining site in Indonesia. Secondary field data were used for their studies (Table 2.7). Three seepage models (before developed tension crack at the first layer, when tension crack developed at first layer and tension crack extended from the first layer to the second layer) with transient analysis (with the daily time step 589) were considered between April 21, 2001, and December 1, 2002. After seepage analysis had done, VADOSE/W was used as an inter-transferred modeling to get seepage pattern and forces for slope stability analysis. In the three cases of hydrological conditions analysis, the highest water table was found due to infiltration into the soils when tension crack extended from the first layer to the second layer at the time step 585 (Figure 2.27). Morgenstern-Price's method was applied for slope stability analysis. Failure process was found in day 585 (November 27, 2002) because deep tension crack allowed water infiltration directly to the soil and it caused increasing in

seepage force and moisture content. This effect made the soil cohesion reducing from 42 kN/m^2 to 12 kN/m^2. Figure 2.28 shows the factor of safety relating to the monthly rainfall during the period concerned. Finally, they can conclude that the formation of tension cracks made increasing of moisture content then the reduction in shear strength of the slope occurred landslide.

Table 2.7 Soil properties for each soil layers (Gofar *et al.,* 2006)

		Layer 1	**Layer 2**	**Layer 3**
Composition	Silt (%)	32.71	46.15	28.50
	Clay (%)	44.17	49.50	35.45
	Υ_b (kN/m3)	18.94	17.30	18.33
	Υ_d (kN/m3)	15.00	13.30	14.10
	LL (%)	66.41	58.50	60.60
	PI	36.44	23.00	24.83
	Gs	2.66	2.64	2.66
	e	0.73	0.90	0.80
	ω (%)	26.86	33.80	30.40
UU Test	c_u (kPa)	36.27	12.00	453.00
CU Test	*c* (kPa)	23.67	42.73	73.7
	ϕ(°)	16.6	5.8	26.3
DS Test	*c′* (kPa)	14.69	9.07	44.52
	ϕ' (°)	17.6	21.0	37.6
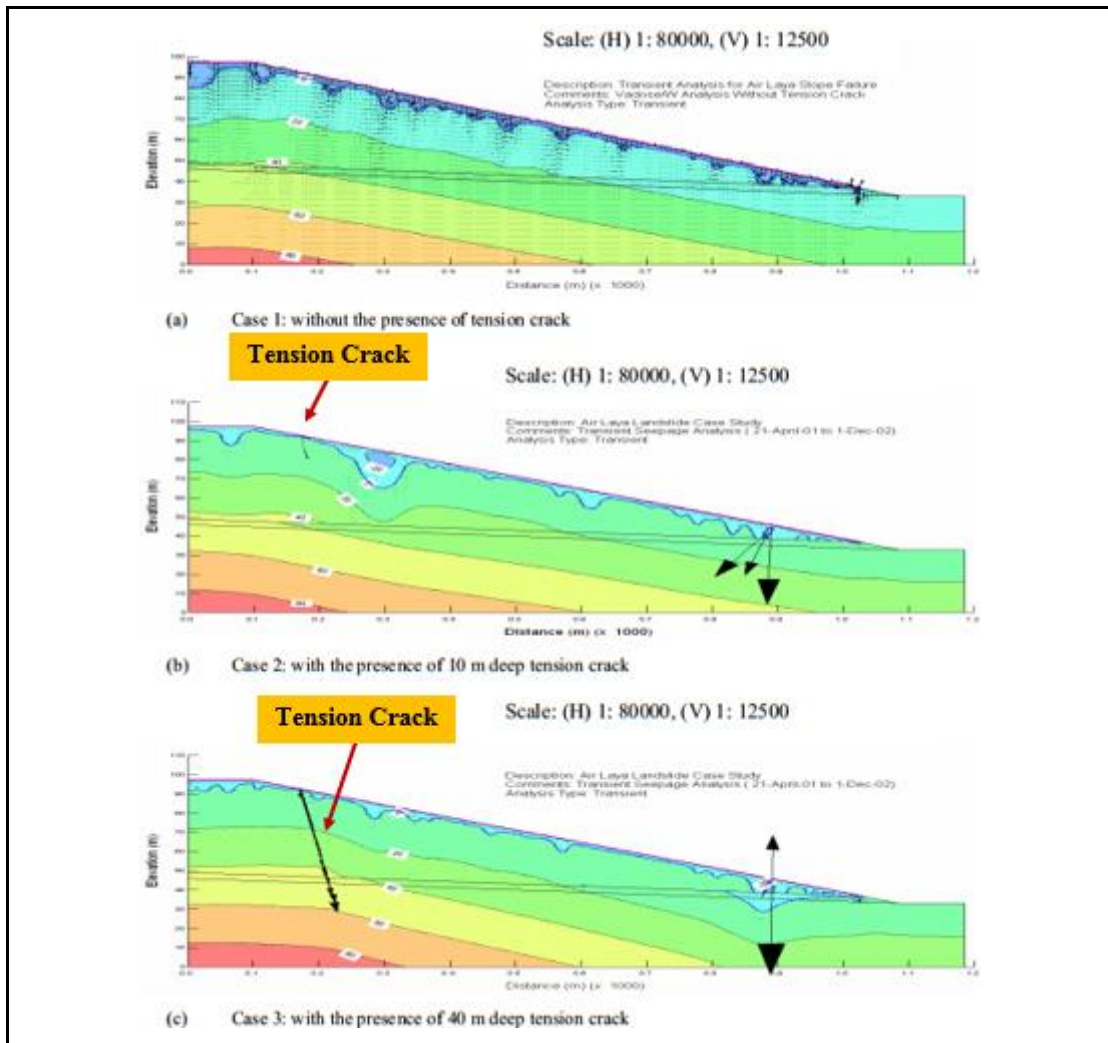
Figure 2.27 Water table and pore water profile at time steps 585 (Gofar *et al.,* 2006)
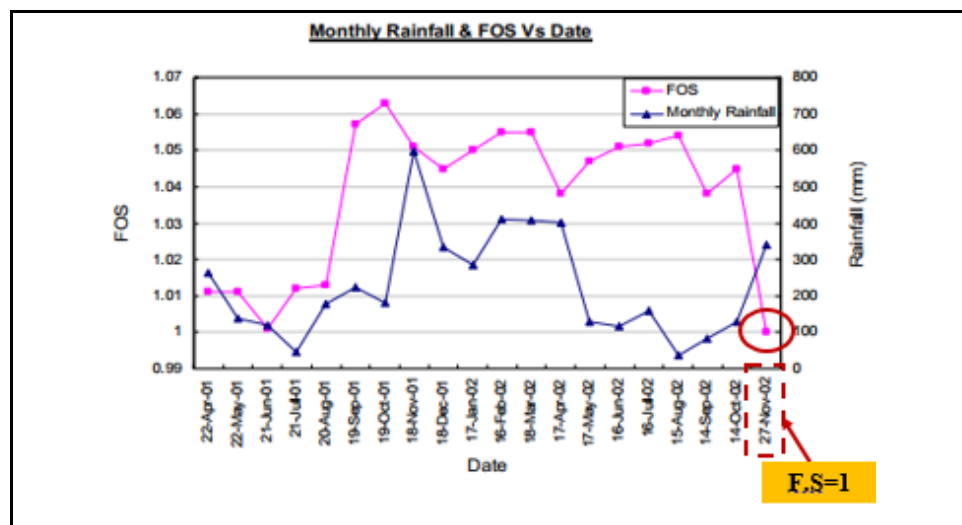
Figure2.28 Monthly rainfall and factor of safety during the period concerned (Gofar *et al.,* 2006)

Some authors are also studied various types of landslide events with the rainfall-induced condition using SEEP/W-SLOPE/W coupled modeling and which are listed in Table 2.8.

Table 2.8 The application of SEEP/W-SLOPE/W coupled modeling in some landslide events

Case Study, Authors, Year	Objective	Methodology	Result
Comparative analysis of contributing parameters for rainfall-triggered landslides in the Lesser Himalaya of Nepal, Dahal *et al.*, 2009	To understand the condition of PWP variations in subsoil layers and to determine the formation of landslide	SEEP/W Transient seepage van Genuchten method SLOPE/W Morgenstern-Price method	Landslide are occurred due to very weak hydro-mechanical and geotechnical soil properties, formation of clay in topsoil, bedrock hydrology, and anthropogenic factors.
Slope stability analysis of transient seepage under extreme climates: case study of typhoon Slope Stability Analysis of Transient Seepage under Extreme Climates : Case Study of Typhoon Nari in 2001, Hsu & Chien, 2016	To improve the previous research method of STABL with SEEP/W and SLOPE/W	SEEP/W Transient seepage Fredlund & Xing method SLOPE/W Ordinary, Bishop, Janbu, and Morgenstern-Price	They have found that the results of SEEP/W and SLOPE/W are more applicable to real-world cases than STABL.

Table 2.8 The application of SEEP/W-SLOPE/W coupled modeling in some landslide events (Continued)

Stability analysis of rainfall-induced typical landslide in Fanjingshan mountain area, Xinwei & Yan, 2016	To provide theoretical base and engineering reference for similar rainfall-induced landslide in the study area.	SEEP/W Transient seepage SLOPE/W	Shihuixi landslide is occurred by rainfalls, and theoretically proved into the failure mechanism of similar landside types in Fanjingshan mountain
Analysis of rainfall-induced landslide on unsaturated soil slopes, Jeong *et al.*, 2017	To determine the root of the activation of landslides in the Umyeonsan region.	SEEP/W Transient seepage van Genuchten method SLOPE/W	The result getting from SEEP/W-SLOPE/W is closely similar to the real condition.

CHA PTER3

METHODOLOGY

The research methodology includes two principal parts. The first part is a 2-D ERI survey, which is employed to identify the geometry of the landslide. The second part is a simulation of SEEP/W-SLOPE/W modeling with rainfall data for estimating PWP variation under the subsoil, F.S., the thickness and the sliding surface of the susceptible slopes. Then, both results from ERI and coupled modeling verified in each other The fieldwork procedure is shown in Figure 3.1.
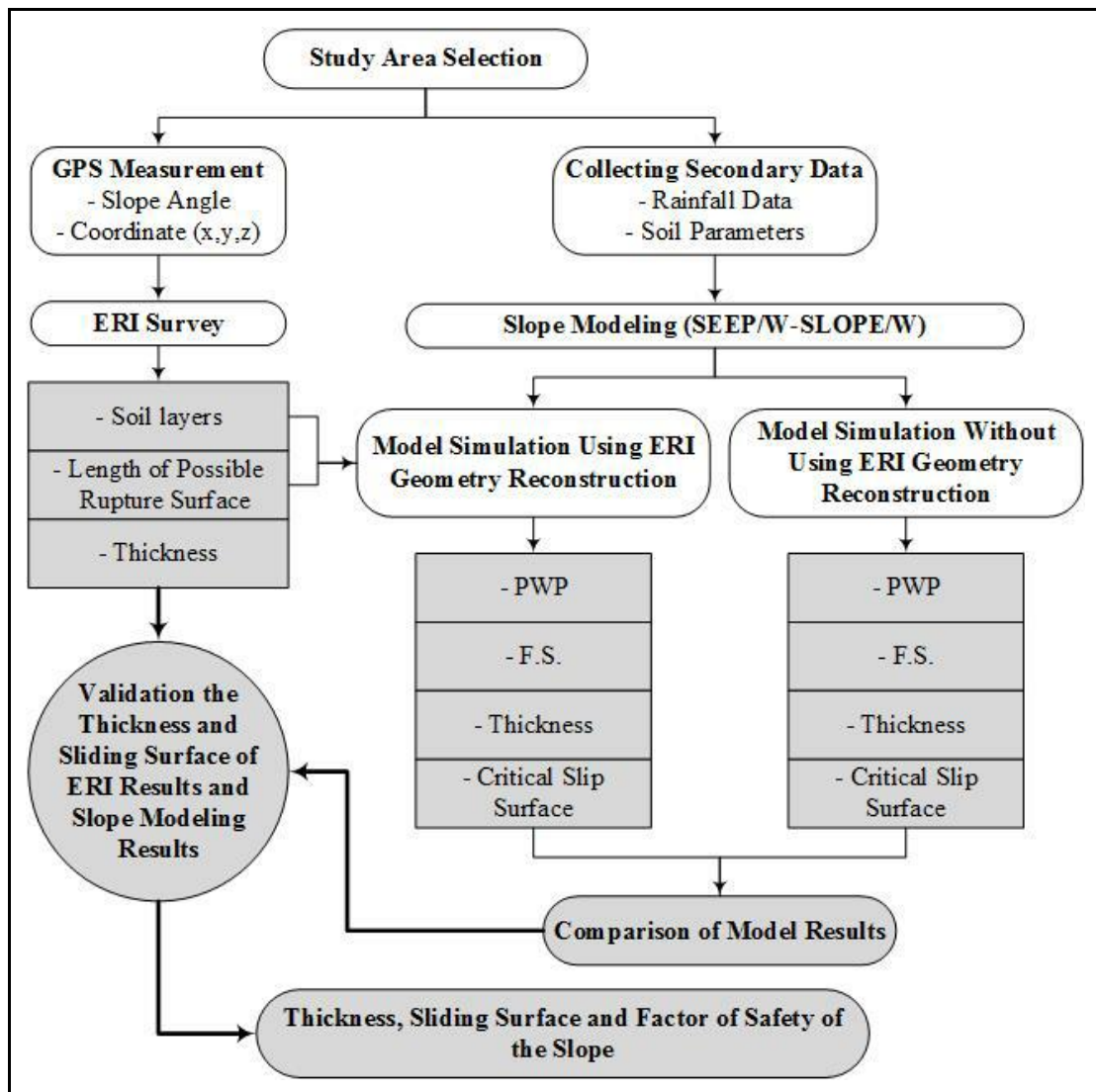

Figure 3.1 Field work procedure

3.1 Study Area Description

In Phuket Island, most of the landslides usually occur in the hillsides area. Therefore, three locations: Location 1 (7° 56' 16.33"N, 98° 17' 25.38"E), Location 2 (7° 51' 47.32"N, 98° 19' 42.39"E) and Location 3 (7° 51' 22.62"N, 98° 19' 16.25" E) are selected in critical areas of Kamala and Chalong districts based on the existed map of the landslide risk area and the past landslide event locations. DEM, geology, and soil properties maps show the formation of soil types (granite soil and weathered sedimentary rock) are the same in the selected areas because they lie along with the same mountain range. Therefore, the 2-D ERI was conducted on the same mountain range.

Location 1 is selected for this study because it was affected landslide in 2005 and very close to the houses, thus it still needs to check whether this location is possible to encounter landslide in the future or not. Location 2 and 3 are selected for observation because they are located not only beside the streams but also near the Chalong dam. The streams are the primary water sources of the dam. If any landslide occurs near the dam site, it might be surely affected by the availability of water quantity and quality. Moreover, this dam was constructed to supply water for 100,000 resident people who live in Chalong, Kata-Karon and Rawai areas (The Phuket News, 2017).

Furthermore, all the selected locations are governed by granitic rock according to the geology and soil properties maps. The previous researchers already recommended that these two types of rocks are very favorable to occur landslide. Figure 3.2 shows the map of the study locations.
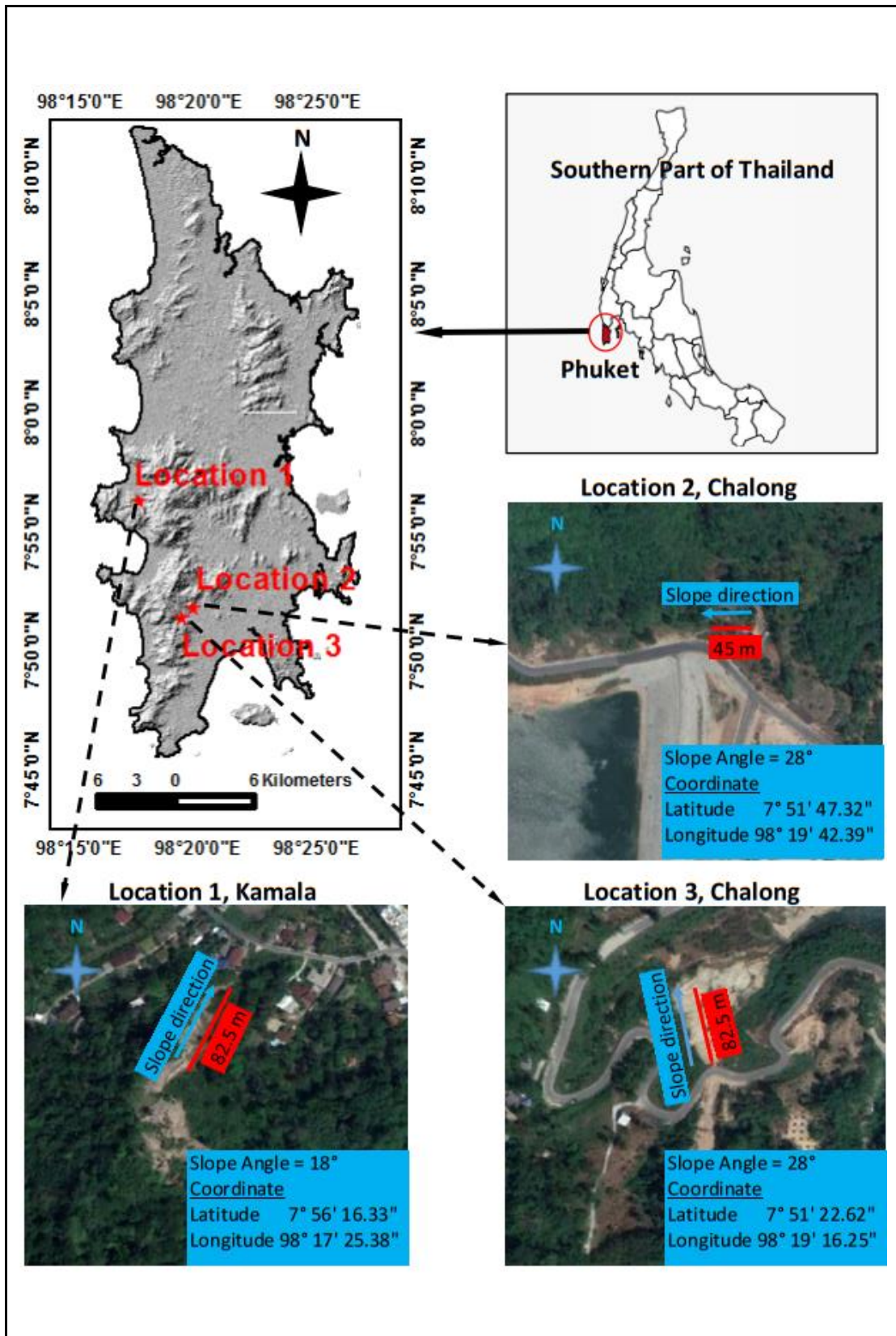
Figure 3.2 Study locations

3.2 Preliminary Studies

In the first stage, the existed data are gathered throughout the Phuket such as geological information, soil properties, and their parameters, and past events of the landslide information (Figure 3.3). Then, the study location was selected based on google earth, and then they were   checked on the field observations. These study locations were adopted based on the hazard map of Soralump, 2007 and flooding and landslide risk locations of DMR, 2017. The geological and topological characteristics of the sliding area were considered by the geological and google maps. The groundwater level data were collected from the well data of DGR, 1998-2012. Also, well data were used to construct the stratigraphy section of soil layers. The locations of groundwater data of Phuket and the interpolated groundwater level map of Phuket are exhibited in Figure 3.4 and 3.5.
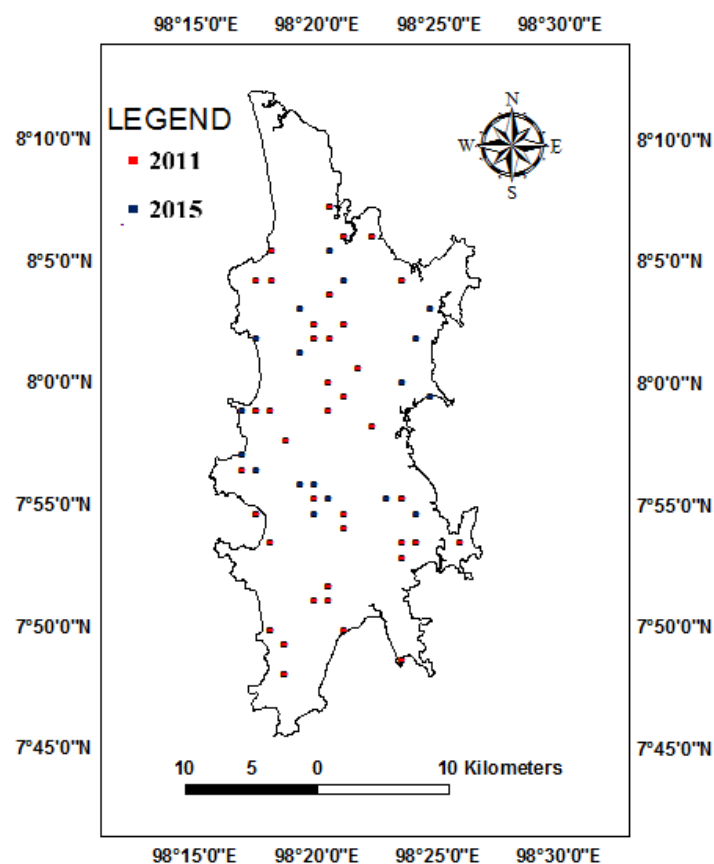
Figure 3.3 Flooding and landslide high risk locations of Phuket for the year 2011 and 2015 (DMR, 2017)
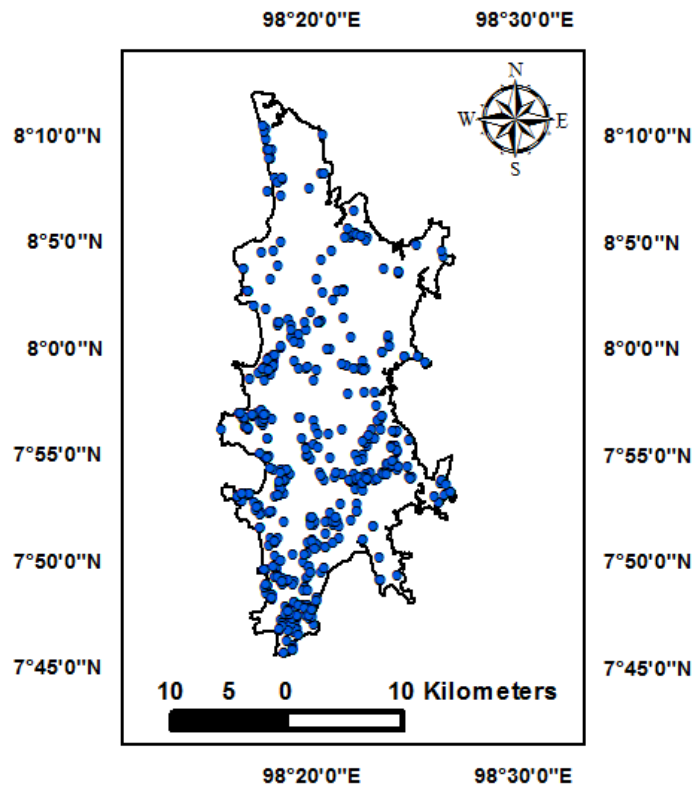
Figure 3.4 Locations of groundwater well in Phuket (DGR, 1998-2012)
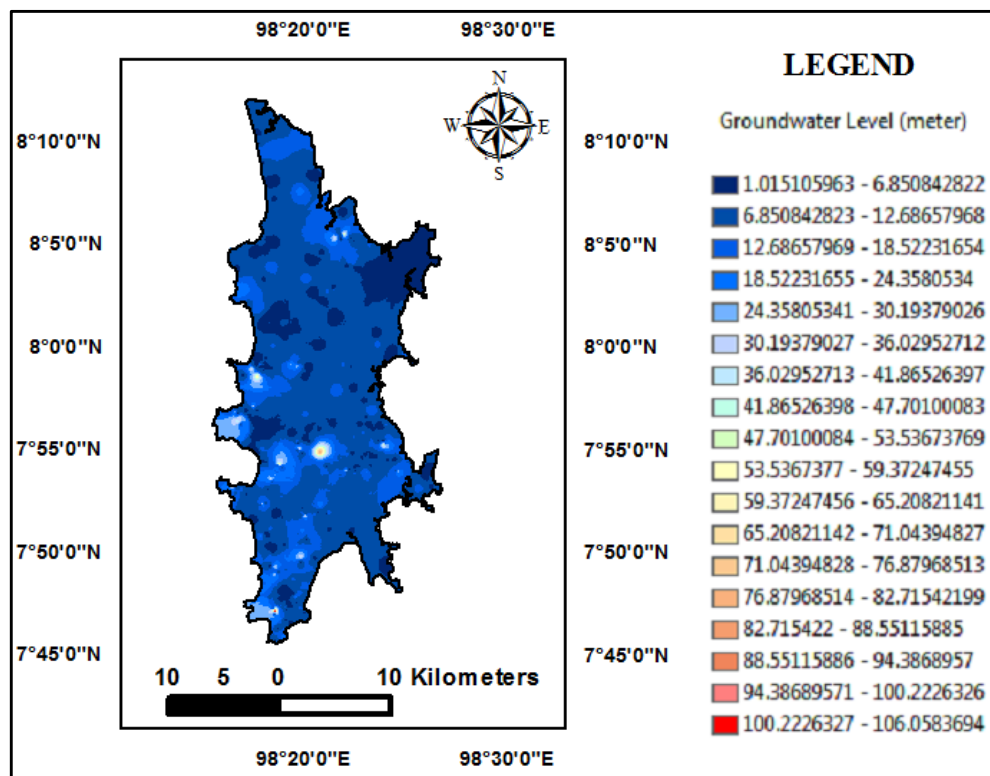
Figure 3.5 Interpolated groundwater level map of Phuket

3.3 Two Dimensional (2-D) Electrical Resistivity Imaging (ERI) Survey

The survey configuration needs to figure out before the field work. Therefore, the required data points are designed using AGI Supersting Administrator software. An example simulation of designed configuration for 2-D ERI survey is demonstrated in Figure 3.6.
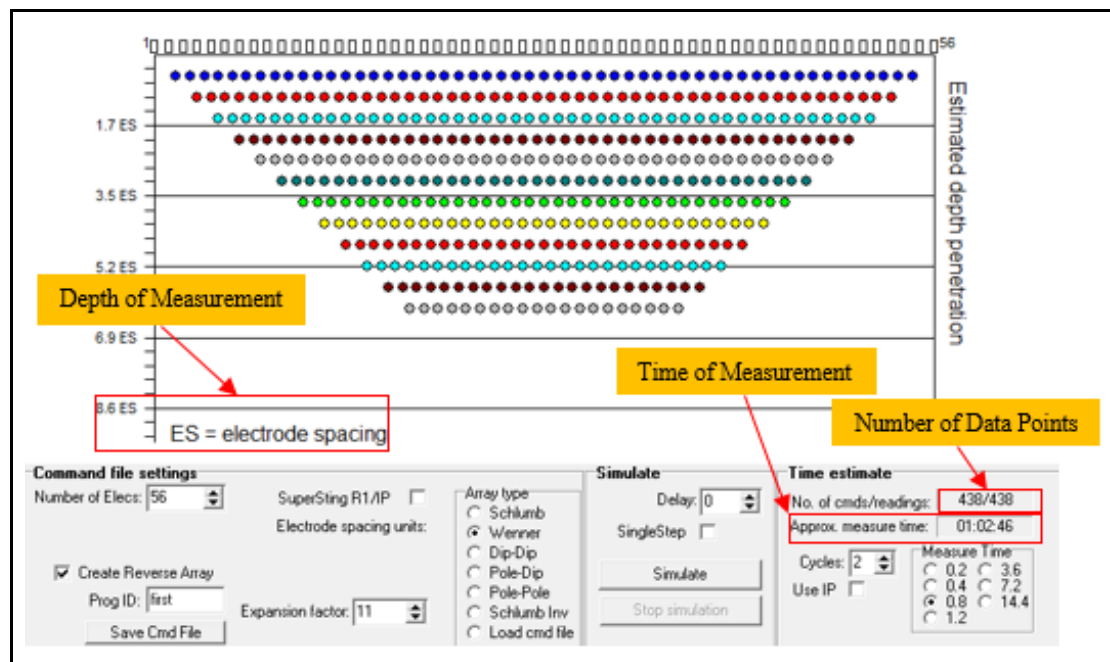
Figure 3.6 Arrangement of electrodes for a 2-D electrical survey line designed by simulation

3.3.1 Two Dimensional (2-D) ERI Data Acquisition

Two dimensional (2-D) ERI data acquisitions were done on the selected locations which are already shown in Figure 3.2. All ERI survey lines orientate parallel to the slope direction. Location 1 has the slope angle of about 18° and Location 2 and 3 have the same slope angle of about 28°. The slope lengths and slope angles are obtained from the GPS measurement. The ERI surveys were done using AGI Supersting R2. The instrument materials used in ERI survey are laid out in Figure 3.7.
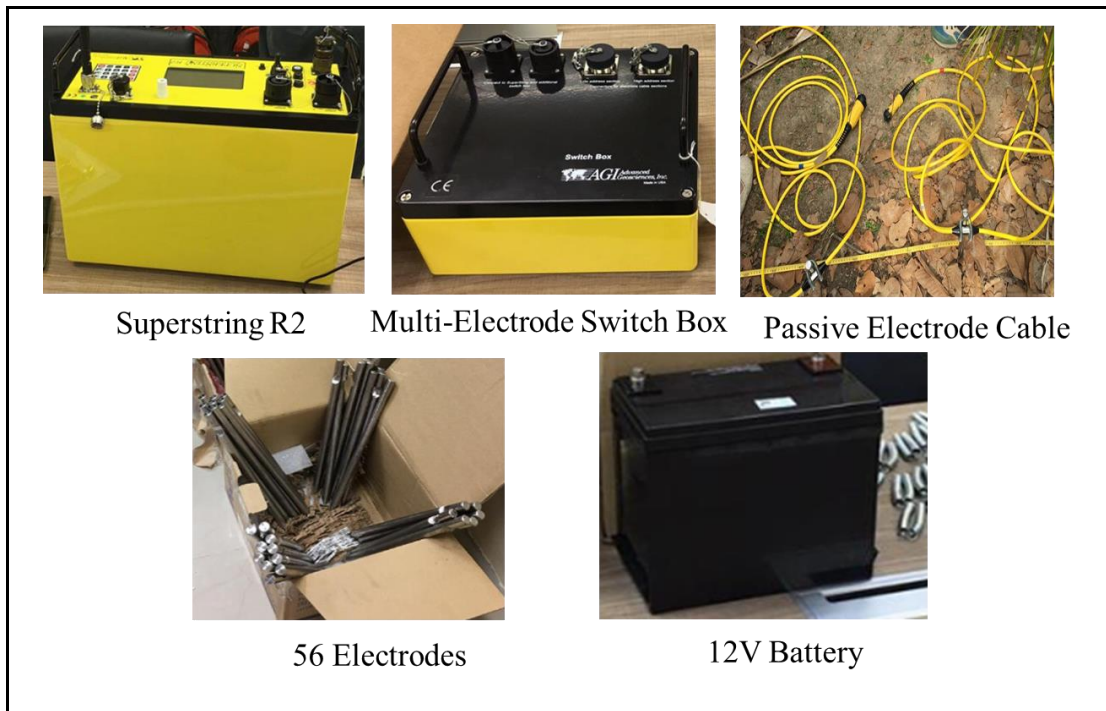
Figure 3.7 Instrument materials for ERI survey

Wenner array with 1.5 m electrode spacing is chosen for all ERI survey lines because this array has a strong signal to noise ratio. Moreover, it is good for resolving vertical changes (Loke, 2004). Nevertheless, Wenner array gives the maximum penetration depth of about 0.2 times of total length survey length (Bernard, 2003). Therefore, the estimated depths of penetration were achieved at 9 m deep of 45 m length and 16.5 m deep of 82.5 m length for Line x and x, respectively. The electrodes spacing and survey lengths are normally considered based on the stratigraphic sections because the existed data show the bedrock is very shallow in the study areas. Moreover, all landslides in Phuket are a shallow type and they usually occur in the weak soil layers. The stratigraphy section for Location 1 shows 10 m thickness of topsoil layer overlays on granite bedrock. While, Locations 2 and 3 show the thickness of the granitic soil layer is about 5 m, and the granite bedrock is occupied at the bottom. Hence, the ERI survey lengths and electrode spacing were confirmed to cover for delineating the thickness and sliding surface of the landslide body. Data acquisitions with parameters for ERI surveys are summarized in Table 3.1.

Table 3.1 Data acquisition parameters for ERI survey

Parameter	Location 1	Location 2	Location 3
Electrode spacing (m)		1.5	
Length of profile (m)	82.5	45	82.5
Apparent investigation depth (m)	~ 16.5	~ 9	~ 16.5
Number of electrodes	56	31	56
Array type		Wenner	
Instruments		AGI Supersting R2, Multi-electrode switching box, Passive electrode cables, 12 V battery, 30 cm electrodes	

Although Hauck *et al.,* 2003 (cited in Ogunsuyi, 2010) mentioned that the perfect resistivity data may be difficult to acquire on the dry surface because of leading to current leakage, this problem was not on the study area because the season was selected in the raining season for the field surveys. In addition, the exact electrode spacing is also set up carefully in ERI survey as the suggested by Oldenborger *et al.,* 2005 (cited in Ogunsuyi, 2010) to avoid misfit errors. Every electrode positions were recorded using etrex 10 GARMIN GPS and its elevation data are used for topographic correction.

3.3.2 Two Dimensional (2-D) ERI Inversion

Measured resistivity data have to be inverted to create a depth section of the subsurface. This can be done by using an iterative procedure called an inversion process. The model is fixed with many rectangular cells. The resistivity of each cell is obtained from the measured apparent resistivity values using an inversion program. The arrangement of model blocks and apparent resistivity datum points called a pseudo-section is shown in Figure 3.8.

The smoothness-constrained least-squares optimization method based on Jacobian matrix equation is commonly used in 2-D and 3-D resistivity inversions. Jacobian matrix equation can be expressed as follows:

$$[J_i'J_i + \lambda_i W'W]\Delta q_i = J_i'g_i - \lambda_i W'W q_{i-1} \qquad (3.1)$$

where J is the Jacobian matrix of partial derivatives or sensitivity, J_i' is the transport Jacobian matrix of partial derivatives or sensitivity, λ is the roughness filter damping factor, W is the matrix of roughness filter, W' is the transport matrix of roughness filter,

Δq_i is the change in model resistivity to be calculated, g is the data misfit (difference between measured and calculated apparent resistivity values), q_{i-1} is the current inversion model.
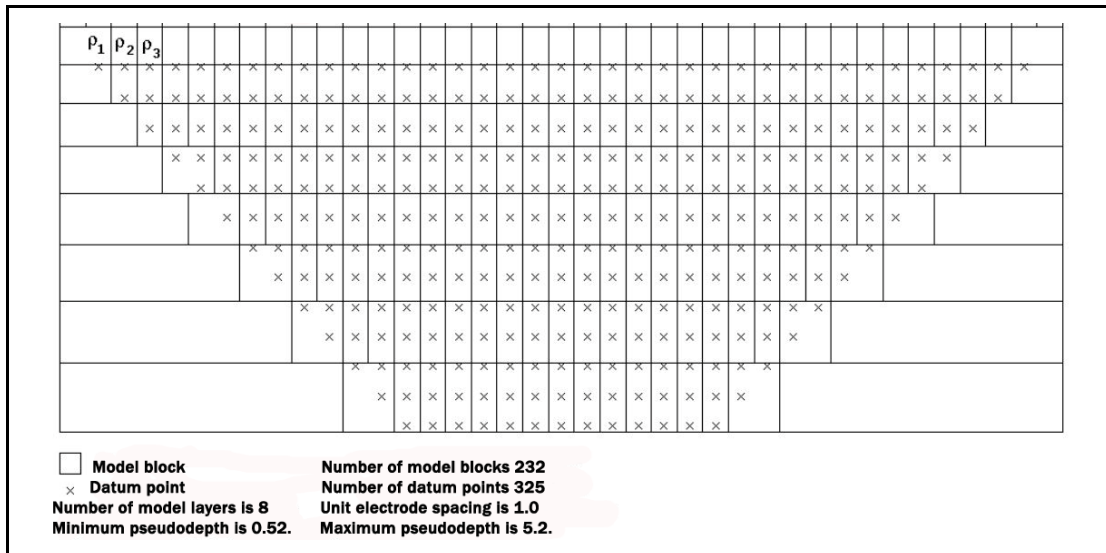
Figure 3.8 Arrangement of model blocks and apparent resistivity datum points (Loke, 2015)

Normally, the model parameter vector, q, contains the logarithm of the model resistivity values. The inversion process is a nonlinear process. Therefore, an initial model is required to solve this problem. Loke, 2004 stated that the functions of the inversion algorithm as follows:

i)   Start by assuming a homogenous model, i.e., all the model cells have the same resistivity.

ii)   Calculate the apparent resistivity values for this model by putting the data misfit, g, in the least-squares equation and calculate Δq.

iii) Calculate the new model $q_i = q_{i-1} + \Delta q$, repeat step (ii) to get the difference between the calculated and measured apparent resistivity values is sufficiently small.

In this study, AGI EarthImager 2-D software is used to convert the raw resistivity data of each survey line to get the lithological interpretation of the subsoil. Terrain files also support to perform the topography correction. All inversions are carried out using smoothness constrained least-squares inversion method because these studies require only the surface resistivity changes in a smooth manner form and then

this method can also attempt to reduce the square of the differences between the observed and calculated apparent resistivity values. The inversion iteration processes are carried out until the difference between the measured data and the model response reach a given threshold. After all iterations processes have finished, the root-mean-square (RMS) error shows a measure of this difference. Figure 3.9 illustrates the sample diagram of 2-D ERI inversion result.
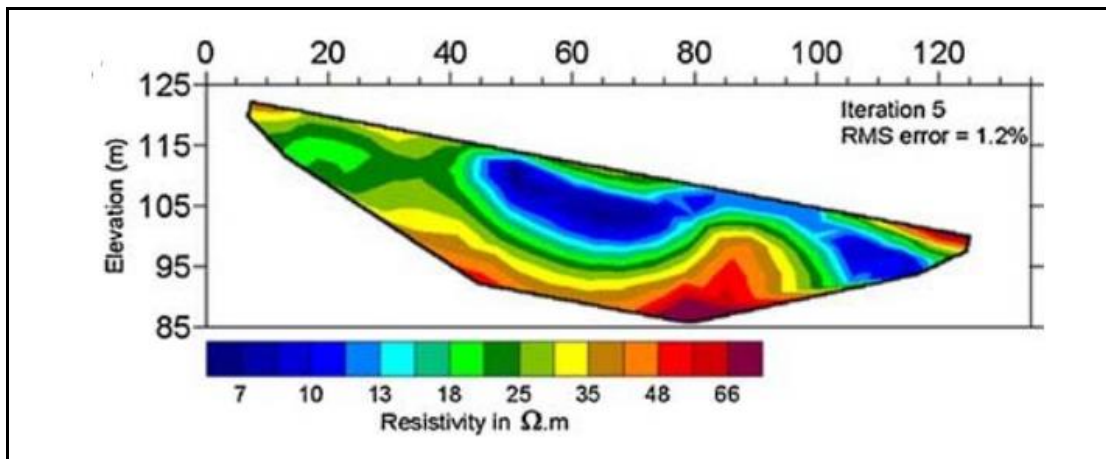
Figure 3.9 Sample diagram of 2-D ERI inversion result

3.4 Seepage Modeling

SEEP/W computer-based program was used to establish the 2-D numerical model. This model is developed by GeoStudio software. Slope geometries were defined from ERI results. Hydro-mechanical parameters for seepage analyses were adopted from DMR, 2011b and which are listed in Table 3.2.

Table 3.2 Hydro-mechanical parameters of clayey gravel and fractured granite

Material	θ_s	θ_r	a	n	m	K_{sat}
clayey gravel	0.46	0.03	0.06	2.53	0.60	2.76×10^{-5}
fractured granite	0.44	0.03	0.04	2.29	0.56	1.68×10^{-5}

θ_s = saturated volumetric water content (m^3/m^3), θ_r = residual volumetric water content (m^3/m^3), a,n,m = curve fitting parameters, K_{sat} = saturated hydraulic conductivity (m/sec)

In the seepage simulation, it works with five steps (GEO-SLOPE International Ltd., 2012a) as follows:

i) The geometry condition (shape of soil layers and groundwater table) is defined, then the model was designed with nodes (1 for triangular mesh and 4 for rectangular mesh) in the profile.

ii) The unsaturated soil permeability parameters (eg. grain size, θ_s, θ_r) is assigned in the program to generates VWC function. The function gives the amount of water contain in the soil depend on the PWP.

iii) Saturated hydraulic conductivity (Ks) is assigned in the program to generates hydraulic conductivity function. The function gives saturated water flow velocity and shape of water content function.

iv) Boundary conditions (null flux boundary is assigned at the bedrock and vertical boundaries; water flux potential seepage face is assigned on the ground surface) are assigned to know the driving force of the water flow.

v) Step (i) to (iii) were done for geometry and material properties of [K] matrix and step (iv) was done for the steady state hydraulic head boundary condition of {H} vector. Then {Q} vector was calculated based on steps (i) to (iv) to determine the flow quantities at the nodes.

Figure 3.10 shows the simulation procedures of SEEP/W model. The sample hydraulic function of SWCC and SPC are mentioned in Figure 3.11 and Figure 3.12.
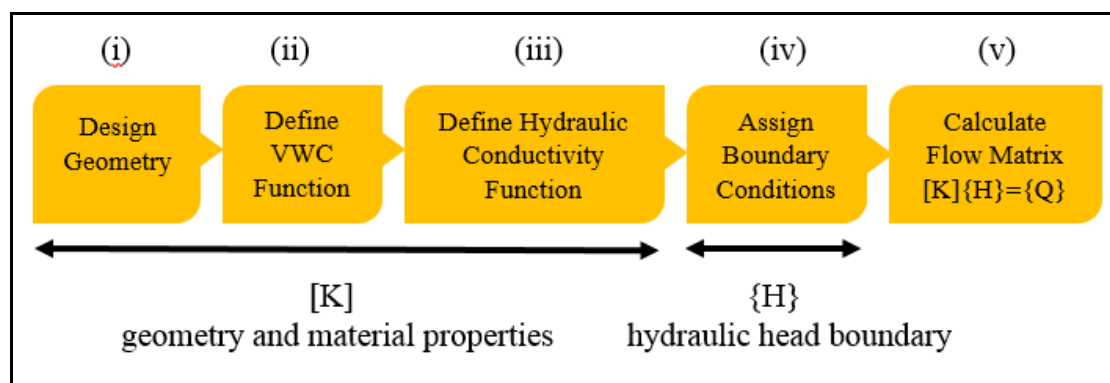
Figure 3.10 SEEP/W simulation procedure for steady seepage condition
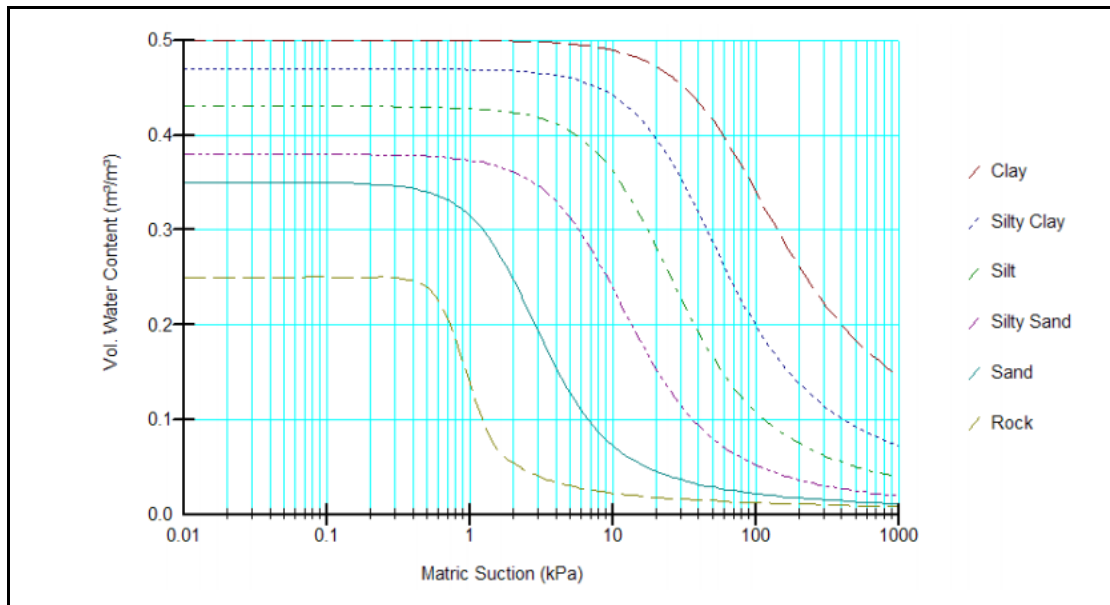
Figure 3.11 A typical soil-water characteristic curve (SWCC)
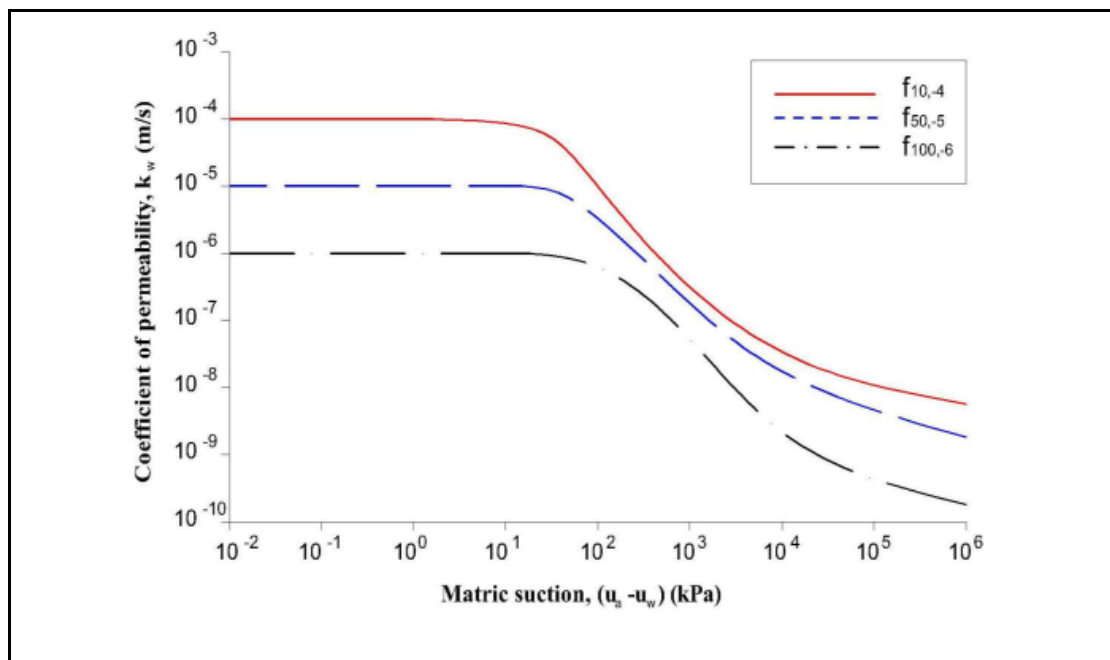
Figure 3.12 A Sample hydraulic conductivity function for unsaturated soil

3.4.1 Procedure to Approach Convergence or Under-relaxation in SEEP/W Modeling

In SEEP/W modeling, the program simulates iterative procedure using Guess iteration method. Equation (2.13) is used to compute repeatedly the amount of change of pressure head of each created nodes until the last two solutions that represent all nodes are very close. The is called the convergence solution and the procedure

reaches in under-relaxation. Trying to reach the convergence or under-relaxation with the help of computer aids is very difficult if the material properties are highly non-linear (Geo-Slope International Ltd ,2012a). To attain the convergence solution, the model simulation was done by the recommendation of Tracy *et al.,* 2016 and the assumptions were as follows:

- Increasing the number of nodes and elements.
- Decreasing the time steps.
- Applying the lower order elements which means do not consider secondary nodes.
- Setting the under-relaxation criteria as much as minimum.

3.5 Slope Modeling

A numerical model, SLOPE/W program, is used to establish a numerical model for the study locations. This model is also developed by GeoStudio software. SLOPE/W program is a mathematical model of the slope simulating package of GeoStudio software, the program can simulate the stability of a slope through complex geometry. The secondary data of the geotechnical parameters for 95% saturated soil layers (Table 3.3) were set up in the model and taken from Mairaing *et al*., 2006. The 95% degree of saturation of soil condition was selected because the slope failure mechanism of Phuket soil types is ranging from 90% to100% (DMR, 2011b). Figure 3.13 (a) shows the correlation between the degree of saturation and effective cohesion and Figure 3.13 (b) shows the correlation between the degree of saturation and friction angle of clayey gravel. Figure 3.14 (a) shows the correlation between the degree of saturation and effective cohesion and Figure 3.14 (b) shows the correlation between the degree of saturation and friction angle of fractured granite. Sample structure of a slope for slope modeling is shown in Figure 3.15.

Table 3.3 The geotechnical parameter of clayey gravel and fractured granite

Material	c' (kPa)	ϕ' (°)	Υ (kN/m^3)
clayey gravel	27.75	38.62	18.66
fractured granite	3.93	37.39	18.02
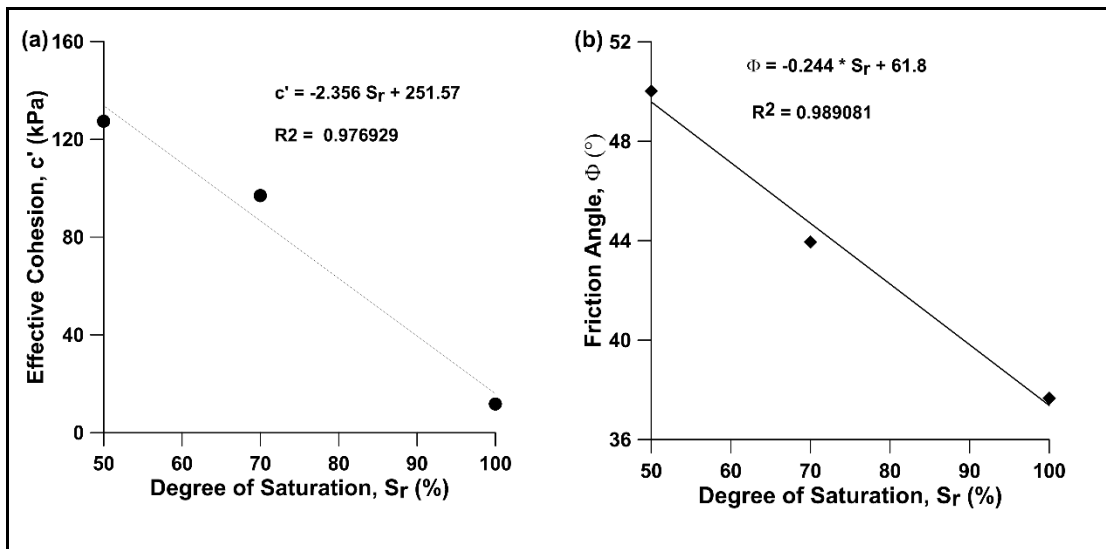
Figure 3.13 Correlation between degree of saturation and (a) effective cohesion (b) friction angle of clayey gravel for Kamala location
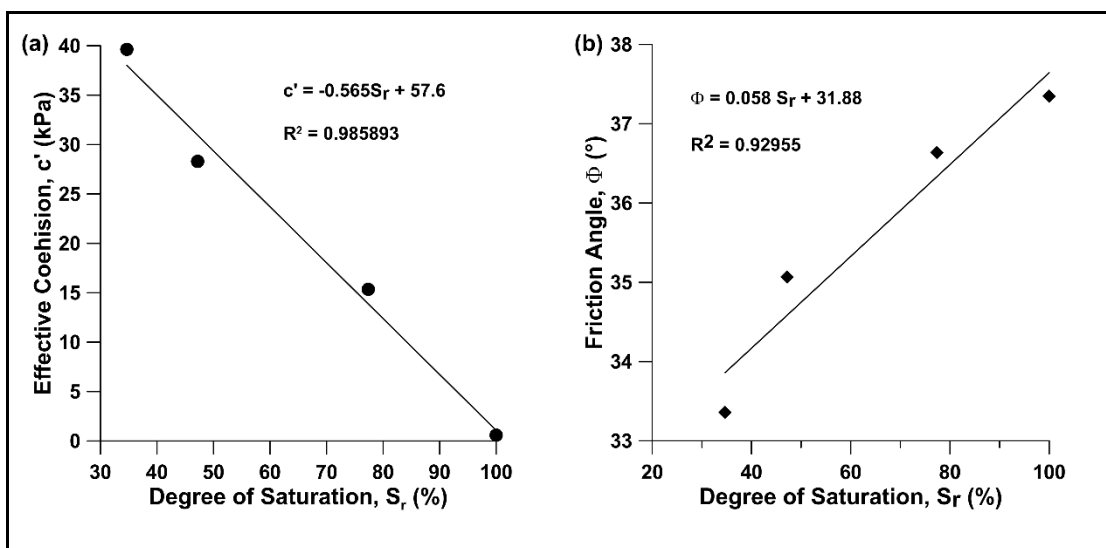
Figure 3.14 Correlation between degree of saturation and (a) effective cohesion (b) friction angle of fractured granite for Chalong location
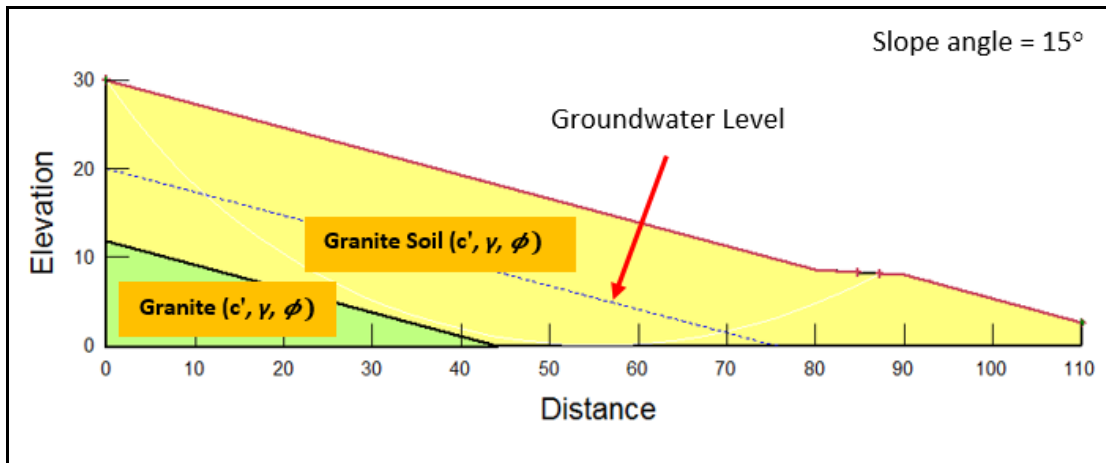
Figure 3.15 Sample structure of a slope for slope modeling

Although SLOPE/W model is based on many methods to simulate the General Limit Equilibrium (GLE), Morgenstern-Price method with circular slip surface was applied in the simulation because this method satisfies not only the moment (F.S$_M$.) but also force (F.S$_F$.) equilibrium of the slope. The GLE of Morgenstern-Price method is described as per equations (2.25-2.30), (2.26) and (2.37).

With respect to the simulation of SLOPE/W modeling, it was conducted in four main steps (GEO-SLOPE International Ltd., 2012b) as follows:

i)   In the first stage of the first iteration, F.S. is calculated by setting normal and shear force to zero in Fellenius's Ordinary Method [(equation 2.15)] to get F.S$_M$.

ii)   In the second stage, F.S. of stage (i) was applied to solve F.S$_M$. and F.S$_F$. equilibrium by assuming the shear force is zero. Four to six times of iterations were done in this stage. The calculated answer F.S$_M$. is relating to Bishop's Simplified method and F.S$_F$. is corresponding to Janbu's Simplified method.

iii)   In the third stage, it considers all interslice forces and applies in stage (ii) F.S. to find GLE F.S. of moment and force. The relation between F.S. through lambda values were plotted as shown in Figure 3.16. The common point of F.S$_M$. and F.S$_F$. were adopted from the plot.
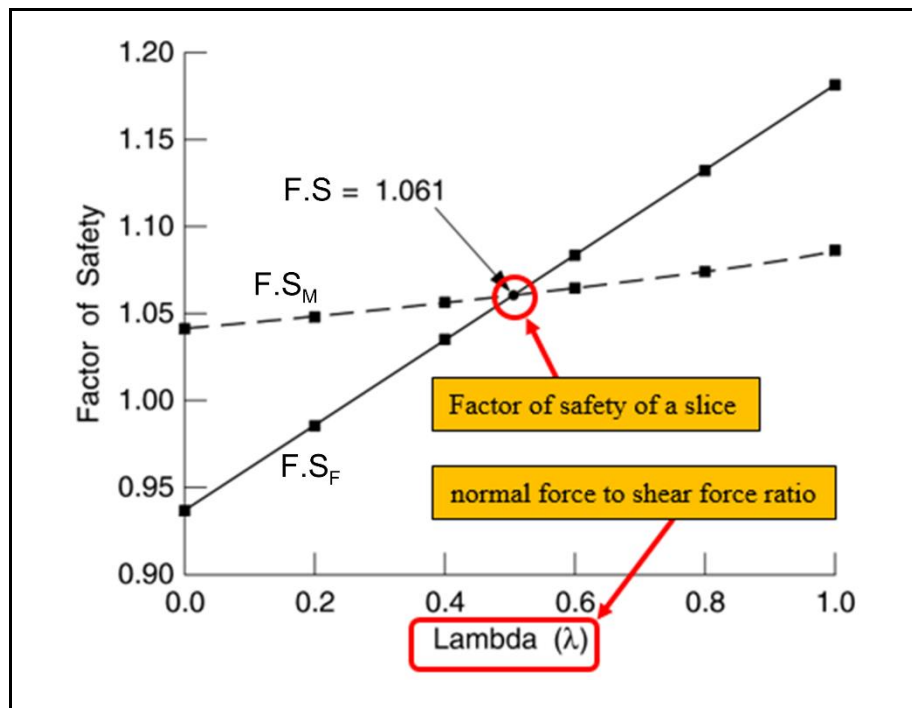
Figure 3.16 Example factor of safety versus lambda plot (GEO-SLOPE International Ltd., 2012b)

iv)   In the final stage, the factor of safety of stage (iii) was used as specific interslice force function to simulate all slope stability methods.

In SLOPE/W modeling, the effective cohesion (c'), the friction angle (ϕ), the unit weight (γ) are important geotechnical parameters. Besides, the slope angle of the study areas and the pore water pressures are also essential parameters because they are affected to the safety factor and the sliding thickness.

3.6 SEEP/W-SLOPE/W Coupled Modeling

SLOPE/W modeling was coupled with SEEP/W modeling. In this condition, SEEP/W is called a parent analysis and SLOPE/W is called a child analysis. The SWCC and SPC are two main functions of SEEP/W analysis and these were transferred to the SLOPE/W modeling to analyze the stability of the slope. As a result, the PWP distribution, the hydraulic pressure head and flow direction under subsoil during a transient time were obtained from SEEP/W analysis and F.S. relating to rainfall duration is an outcome result of SLOPE/W modeling. The procedure for combined modeling is illustrated in Figure 3.17.
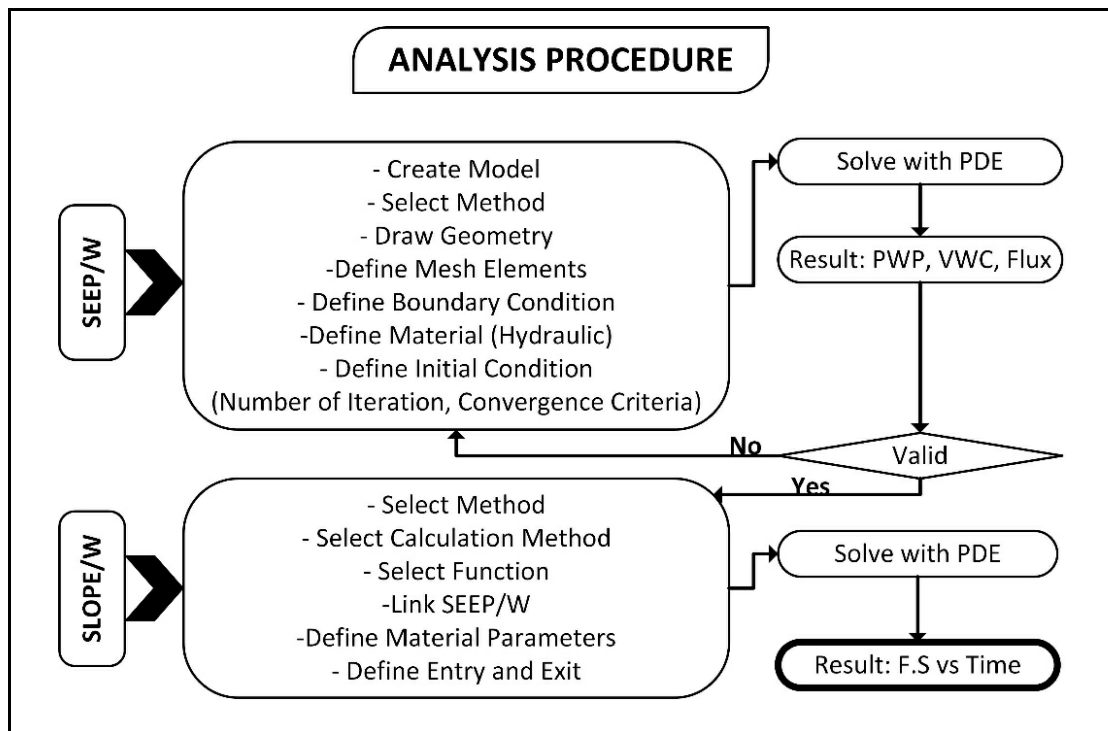
Figure 3.17 The schematic procedure of combined SEEP/W-SLOPE/W

A coupled simulation of SEEP/W-SLOPE/W was done on two study areas: Location 1 (Kamala) and Location 2 (Chalong). While Location 3 (Chalong) was not considered for doing simulation because the area is on a dam construction site as a man-made (artificial) slope. In addition, the ERI result of the Location 3 shows that the subsurface of the slope is governed by granite bedrock only. Slope geometries of the model were constructed based on (i) DGR well data (ID- 671) near study area for Location 1 and (ii) outcrop cutting bank near study area for Location 2 which are illustrated in Figure 3.18 (a) and (b). Both Location 1 and Location 2 profiles were constructed into quadrilateral and triangle mesh elements. For Location 1, the side length of a mesh was made by 0.8 m, while Location 2 was 0.5 m. For Guess iteration, 4-integration order for quadrilateral elements and 1-integration order for triangle elements is applied during model simulation. Table 3.4 shows the acceptable integration orders for mesh elements recommended by GEOSLOPE International Ltd., 2012a.
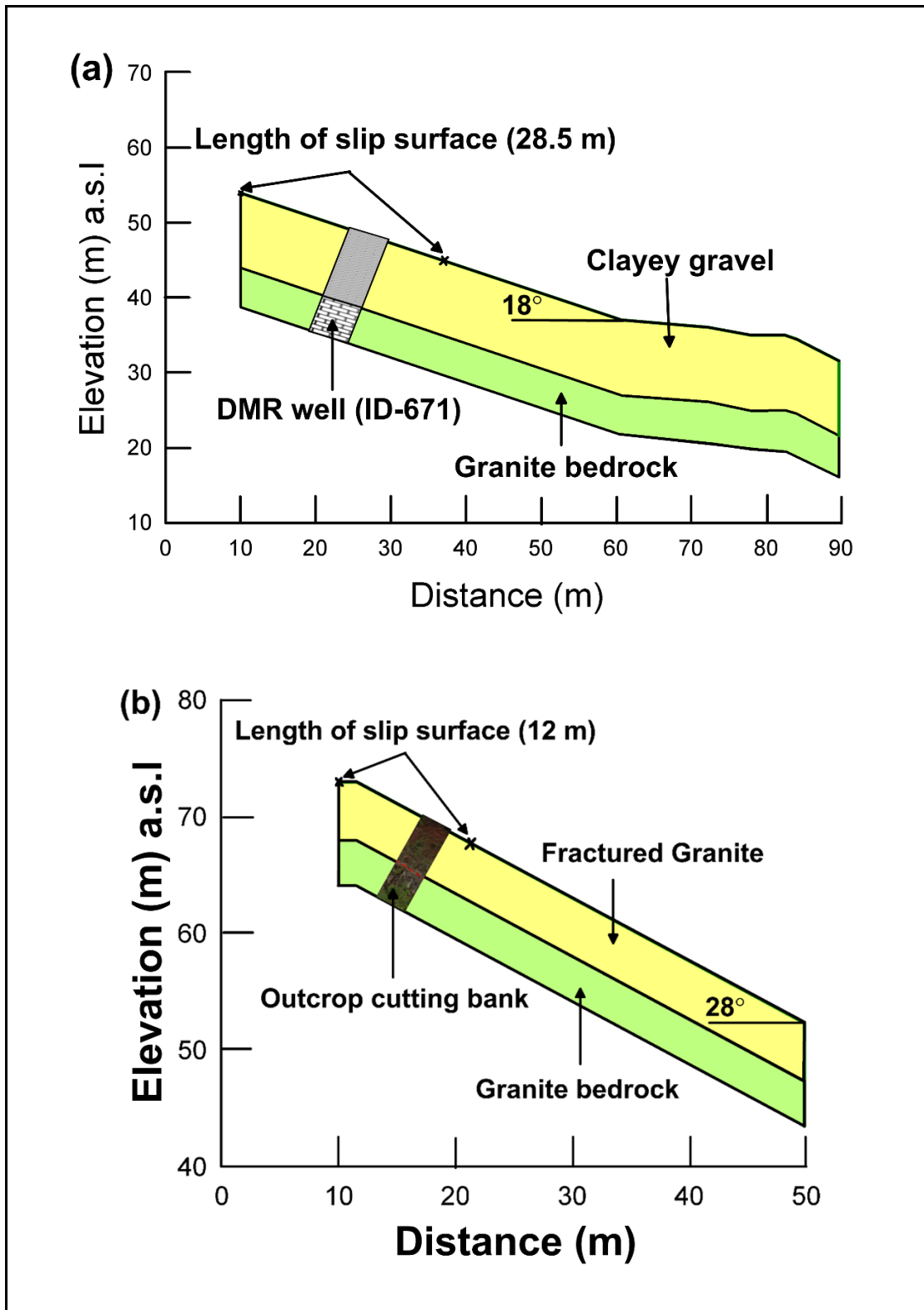
Figure 3.18 The slope geometries of (a) Location 1 and (b) Location 2 for without using ERI geometry reconstruction

Table 3.4 Acceptable element integration orders

Mesh Element	Internodes	Integration Order
Quadrilateral	No	4
Quadrilateral	Yes	9
Triangle	No	1
Triangle	Yes	3

* Triangle element with no internodes is not recommended to use as primary mesh element.

Mesh elements of Location 1 were 1262elements with 1383 nodes, while Location 2 was 815 elements and 917 nodes. Side lengths 0.5 m and 0.8 m are used in this study because mesh element sizes are influenced in seepage modeling (GEOSLOPE International Ltd., 2012a; Tracy *et al*., 2016).

The initial water table is essential in the coupled modeling of SEEP/W-SLOPE/W because the main function of this combined modeling is to consider the variation of PWP, then the stability was calculated f a slope depending on PWP. Therefore, the initial water table is assigned along the 90% granite bedrock for both locations with maximum negative pressure head of 5 m. The assumed value of initial PWP -5 kPa was imposed in each simulation to avoid unrealistic negative PWP in each simulation. The grain sizes of the top layer in each location were assumed as the same size and homogeneous, thus the hydraulic conductivity is equal between the horizontal and the vertical directions. van Genuthen (1980) criterion [equation (2.9-2.18)] is used to estimate SWCC and SPC.

The initial hydro-mechanical parameters which are already shown in Table 3.2 were input in the models. To implement the transient seepage analyses, Location 1 is used rainfall data during 14-days (06/06/2018-29/06/2018), while Location 2 used 20-days (10/05/2018-29/05/2018) rainfall data. These rainfall data are taken from ESSAND Geo-monitoring stations during 2018 as listed in Table 3.5 and Table 3.6. Instead of using the hourly time step, the daily time step was considered because the rainfall data are not successive. If the time span is not successive, it may affect the analysis (GEOSLOPE International Ltd., 2012a). Therefore, 14-time steps and 20-time steps were set as water flux for Location 1 and 2, respectively. Due to a limitation, the maximum infiltration rate was considered as the same as the permeability

for the soil layers. Figures 3.23 and 3.24 show the input SWCC and SPC functions in unsaturated soils for Location 1 and 2.

Table 3.5 24-hr precipitation data of PSU Rain Station to apply in transient seepage analysis for Location 1 (Kamala)

Date (d/m/y)	Rainfall Intensity (mm/hr)	Rainfall Intensity (m/sec)
16/06/2018	20.60	5.72E-6
17/06/2018	45.40	1.26E-5
18/06/2018	78.40	2.18 E-5
19/06/2018	5.60	1.56E-6
20/06/2018	35.80	9.94E-6
21/06/2018	1.40	3.89E-7
22/06/2018	0	0
23/06/2018	0.40	1.11E-7
24/06/2018	10.60	2.94E-6
25/06/2018	12.40	3.44E-6
26/06/2018	59.60	1.66E-5
27/06/2018	0	0
28/06/2018	0	0
29/06/2018	6.80	1.89E-6

Table 3.6 24-hr precipitation data of PMBC Rain Station to apply in transient seepage analysis for Location 2 (Chalong)

Date (d/m/y)	Rainfall Intensity (mm/hr)	Rainfall Intensity (m/sec)
10/05/2018	38.80	1.08E-5
11/05/2018	3.60	1.00E-6
12/05/2018	14.60	4.06E-6
13/05/2018	2.80	7.78E-7
14/05/2018	0.60	1.67E-7
15/05/2018	0	0
16/05/2018	9.00	2.05E-6
17/05/2018	27.00	7.50E-6

Table 3.6 24-hr precipitation data of PMBC Rain Station to apply in transient seepage
analysis for Location 2 (Chalong) (Continued)

18/05/2018	12.20	3.39E-6
19/05/2018	1.00	2.78E-7
20/05/2018	0	0
21/05/2018	0	0
22/05/2018	0	0
23/05/2018	0	0
24/05/2018	78.60	2.18E-5
25/05/2018	0	0
26/05/2018	9.40	2.61E-6
27/05/2018	0.40	1.11E-7
28/05/2018	8.60	2.39E-6
29/05/2018	17.00	4.72E-6
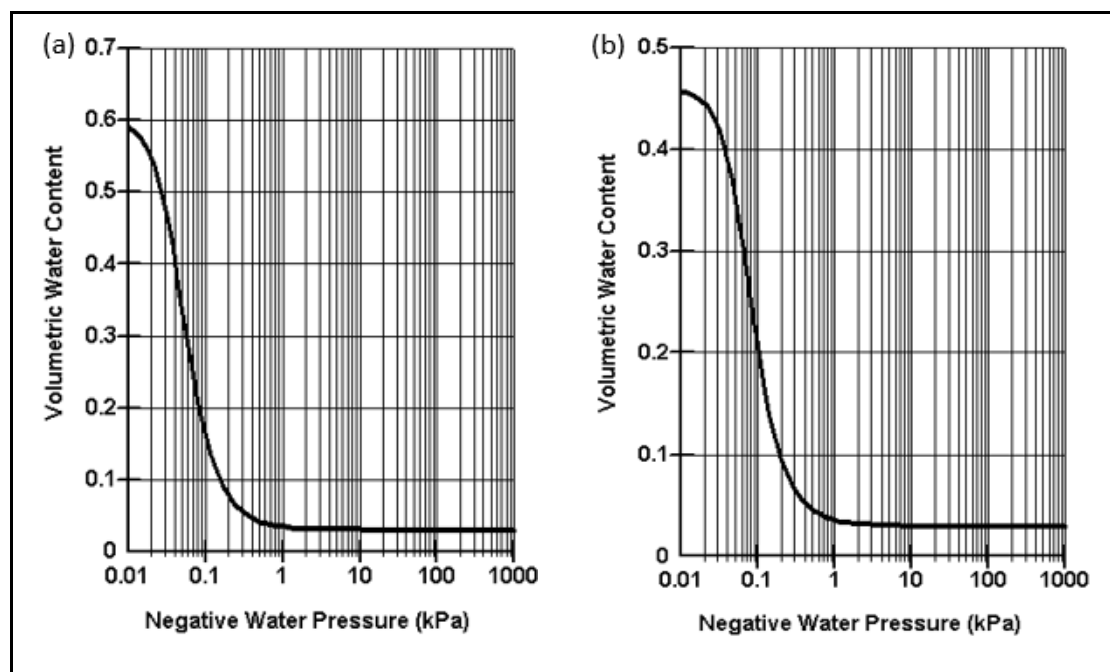
Figure 3.19 The SWCC function used in seepage model simulation for (a) Location 1
and (b) Location 2
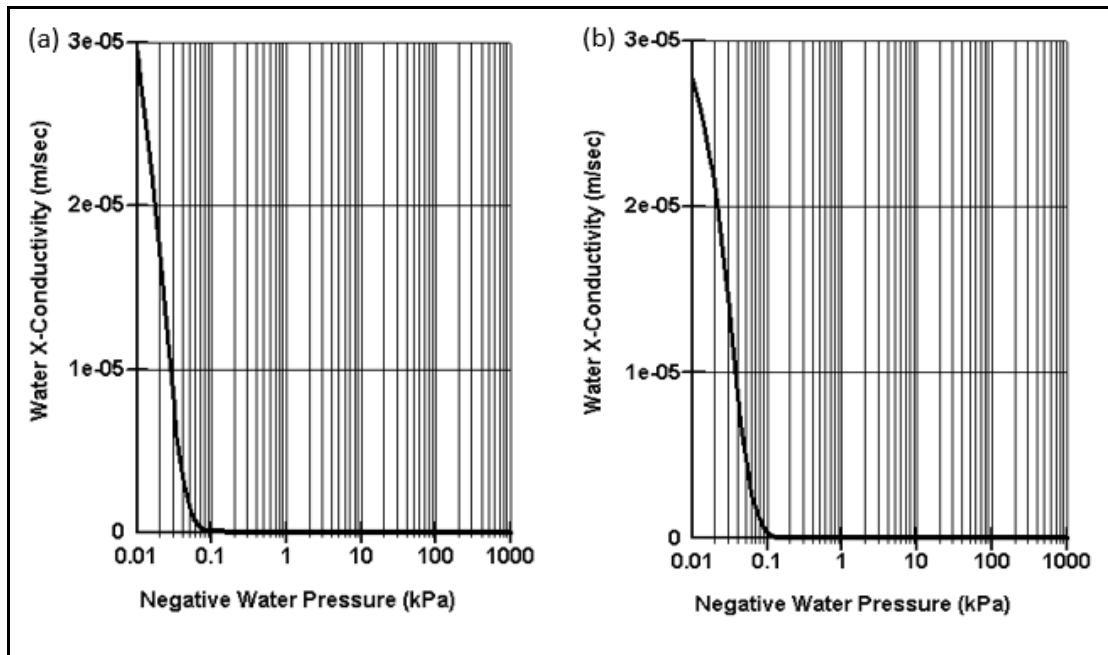
Figure 3.20 The SPC function used in seepage model simulation for (a) Location 1 and
        (b) Location 2

Seepage analysis has used to consider the underground water movement, the boundary condition is very important for studying steady state seepage or transient seepage (GEO-SLO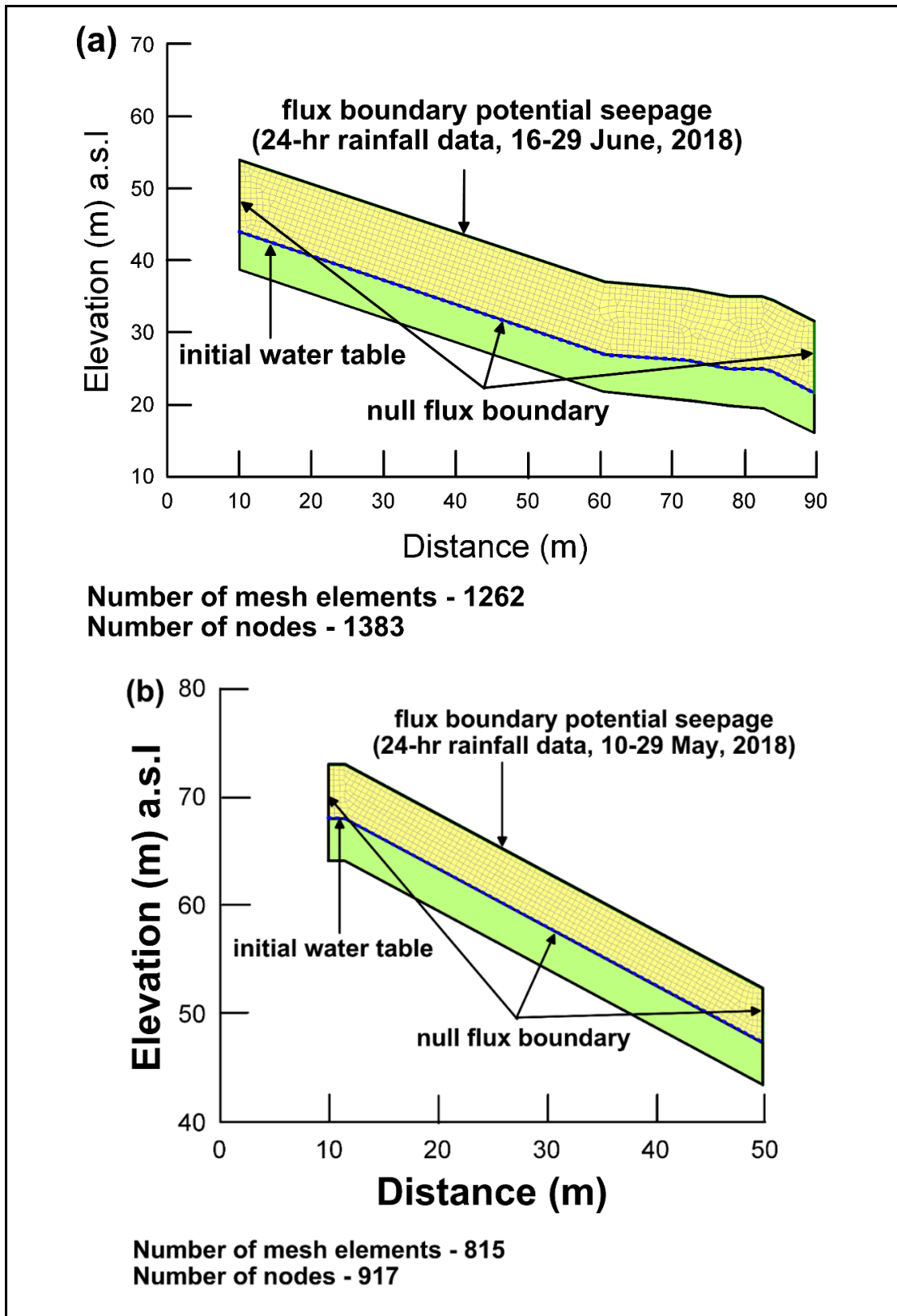PE International Ltd., 2012a). In this study, the hydraulic condition of the bedrock was neglect (Dahal *et al*., 2009; Crosta and Negro, 2003; Dapporto *et al*., 2002) because the 24-hr rainfall data is very short period for bedrock infiltration (Dahal *et al*., no 2009). Therefore, the 90% fresh granite layer was considered as impervious bedrock. Along the impervious granite bedrock for both locations was considered as a null flux boundary. The daily 24-hr rainfall data were assigned as transient flux potential seepage along the slope surface. The vertical upslope vertical and downslope boundaries were set as an unnatural impermeable border and assigned the null flux boundaries for avoiding the side effects. Evapotranspiration process was not considered in this study due to data limitation. The boundary condition of the model for both Location 1 and Location 2 are presented in Figure 3.25.

(a)

flux boundary potential seepage
(24-hr rainfall data, 16-29 June, 2018)

initial water table

null flux boundary

Elevation (m) a.s.l

Distance (m)

Number of mesh elements - 1262
Number of nodes - 1383

(b)

flux boundary potential seepage
(24-hr rainfall data, 10-29 May, 2018)

initial water table

null flux boundary

Elevation (m) a.s.l

Distance (m)

**Number of mesh elements - 815**
Number of nodes - 917

Figure 3.21 Finite element description model of (a) Location 1 and (b) Location 2 for
without using ERI geometry reconstruction

3.7 Validation of Sliding Surface and Thickness of Landslide Mass

The interpretation of 2-D ERI results were done using Giao *et al.*, 2008's concept of granite rock resistivity range in Phuket (Table 3.7). The possible sliding surface of ERI inversion was situated at the low resistivity layer (ranging from 5-150 Ωm, which refers high water content or moisture content or clay) (Lapenna *et al.*, 2003; Drahor *et al.*, 2006; Pánek *et al.,* 2008; Jomard *et al.*, 2010; Chambers *et al.*, 2011; Grandjean *et al.*, 2011; Yilmaz, 2011; Perrone *et al.,* 2014). In addition, very weathered granite layer (100-1000 Ωm) also was seen as the sliding surface (Nordiana *et al.,* 2017). Low resistivity zone is the possible landslide zone because the increment of soil water content can generate the movement of the land mass in this zone, thus the thickness of this zone can be estimated as the thickness of landslide mass. But the low resistivity zone range is varied from one location to another depending on geology structure. Furthermore, in the slope stability modeling results, the sliding surface is dependent on the slope parameters, i.e., geological parameters (c', ϕ and γ), groundwater table, and slope angle. Both 2-D ERI and coupled slope modeling results were validated with each other to confirm the thickness and the sliding surface of the landslide. Figure 3.26 illustrates the validating sample of the thickness and sliding surface of (a) 2-D ERI result and (b) slope modeling result.

Table 3.7 Geo-electrical range of granite in Phuket (Giao *et al*., 2008)

Material	Resistivity Range (Ωm)
Granite residual soil (no corestones)	<300
Completely weathered granite soil (<50% corestones)	300-600
Granite soil (50-90% block of rock)	600-1000
Granite bedrock (90% fresh granite)	1000-1800
Fresh granite	>1800
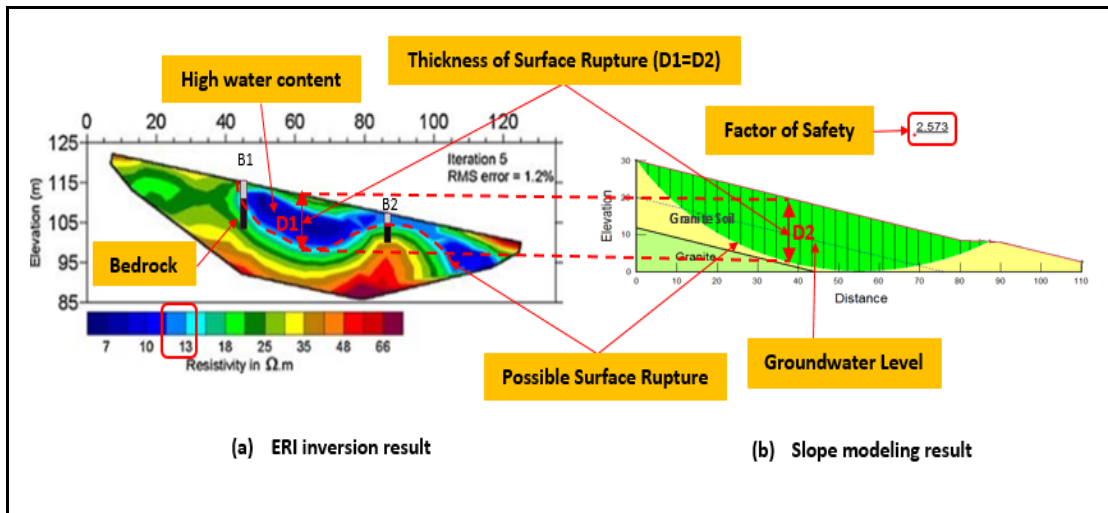
Figure 3.22 The validation of the thickness and surface rupture of (a) ERI result and (b) Slope modeling result

CHAPTER 4
RESULT AND DISCUSSION

4.1 Result and Interpretation for Electrical Resistivity Survey

A topographic correction was applied for all survey lines. After the inversion of the ERI datasets, the vertical axes in the inverted resistivity section refers above sea level (a.s.l) elevations in meter and the horizontal axis shows the slope distance in the meter. The logarithmic value of the apparent resistivity in ohm meter unit as shown in the vertical color scale bar is at the right side of the profile. The results of the ERI inversion data are mentioned below follows:
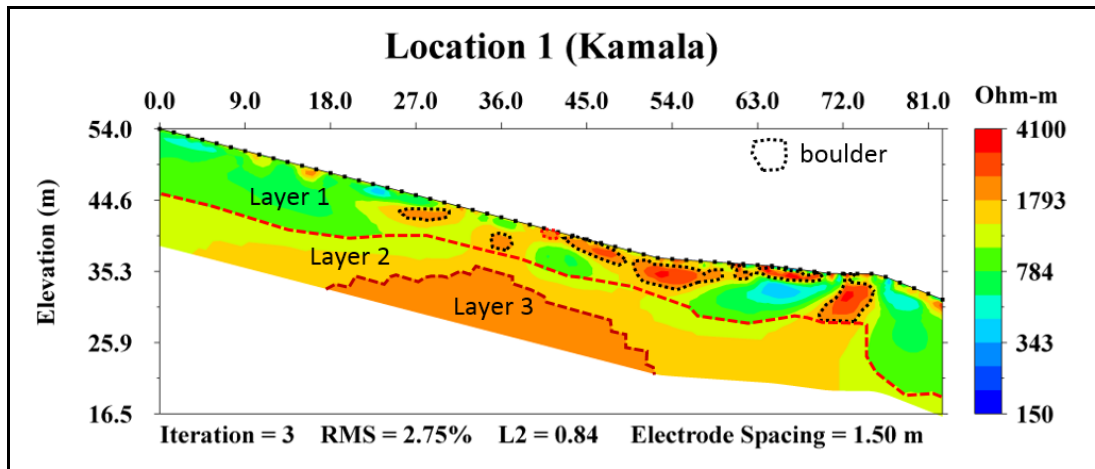
(i) Location 1 (Kamala)

For this location, the stratigraphic section (Figure 4.1) was created based on DGR well data which is located near the study area (about 260 m). Stratigraphy section shows topsoil (clayey gravel) is laid down over granite bedrock. It confirms the eroded path (Figure 4.2) in the study area. The interpretation was carried out depending on the stratigraphic section and Table 3.4. In this resistivity section, the ERI inversion dataset (Figure 4.3) was obtained RMS error of 2.52% with three iterations by removing 3.2% of measured resistivity data. Figures 4.4 shows data misfit cross-plot of the resistivity section. The resistivity profile was divided into three layers. Layer 1 with resistivity of <1000 Ωm was interpreted as clayey gravel and some boulders are distributed in this layer. Then the Layer 2 with resistivity ranges of 1000 Ωm-1800 Ωm was interpreted as 90% fresh granite bedrock and Layer 3 with resistivity of >1800 Ωm was interpreted as fresh granite bedrock.
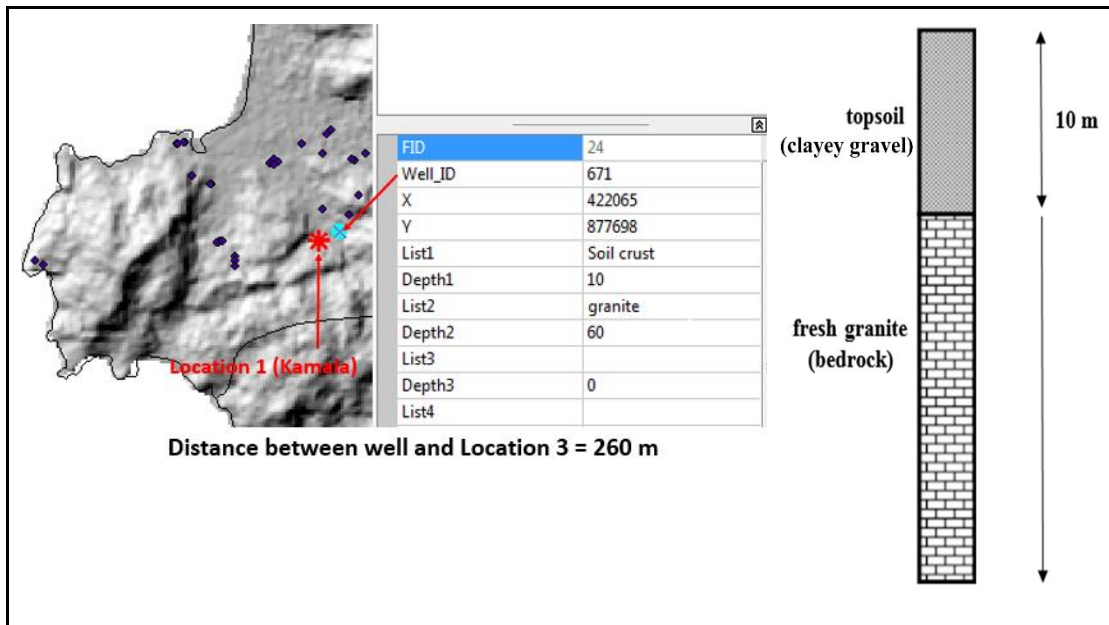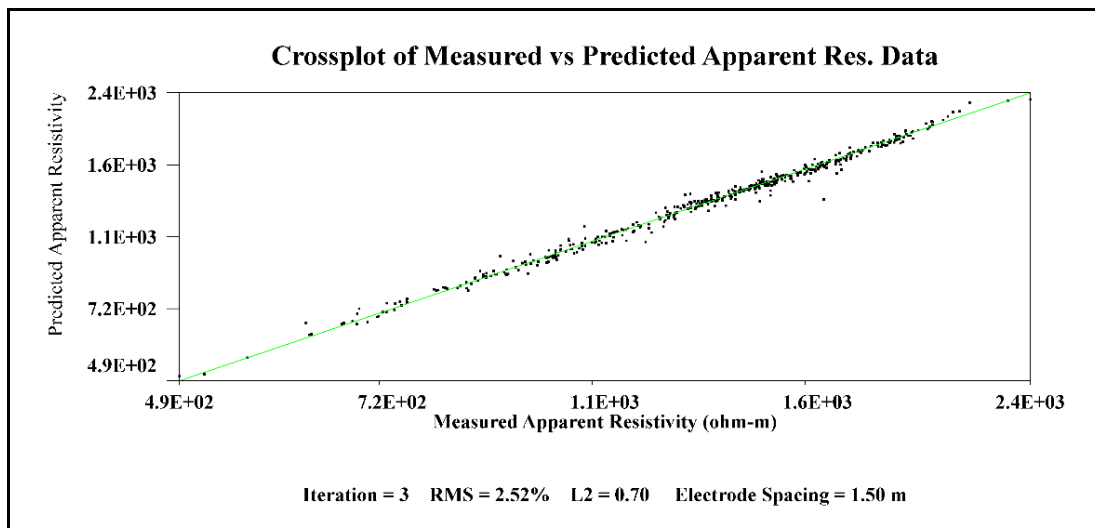
Figure 4.1 The location of DGR well near Location 1 and its stratigraphic section

Figure 4.2 Location 1 shows clayey gravel exposed on the ground surface
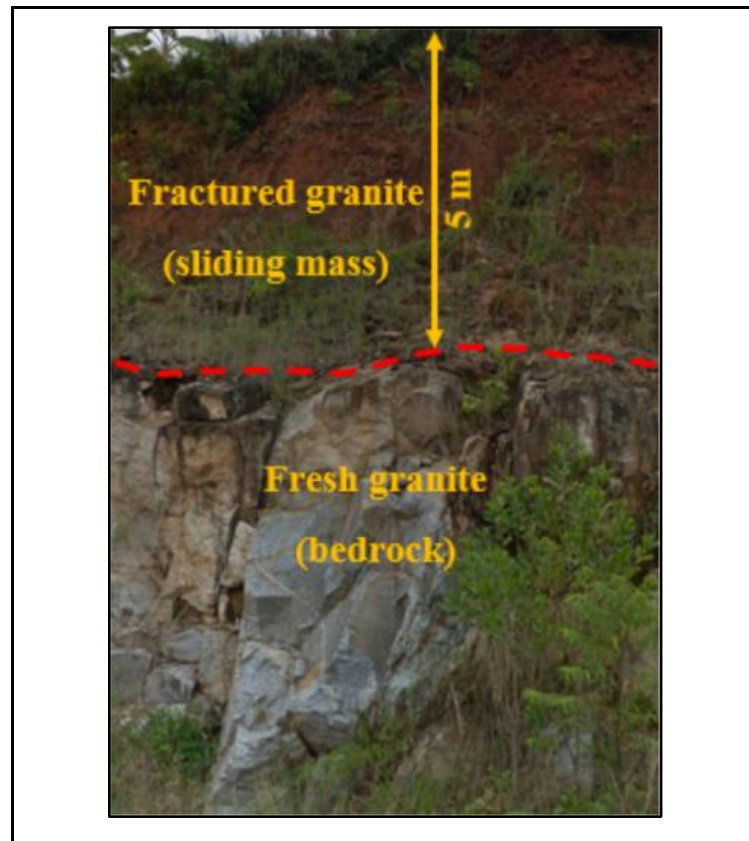
Figure 4.3 Resistivity profile of Location 1 (Kamala)

Figure 4.4 ERI data misfit cross-plot diagram of Location 1

(ii) Location 2 (Chalong)

   The interpretation was done based on the outcrop cutting bank (Figure 4.5) and Table 3.4. According to the field result, the resistivity data was inverted with RMS error of 2.23% and two iterations. Any resistivity data point was not necessary to remove data misfits for inversion processes. The ERI inversion result of Location 2 (Chalong) is displayed in Figure 4.6, while Figures 4.7 shows data misfit cross-plot of the resistivity section. The resistivity profile shows two layers, i.e., Layer 1 with resistivity of < 1000 Ωm was interpreted as fractured granite mixed with debris materials, stone, and sand. The resistivity range of 1000 - 1800 Ωm in Layer 2 was interpreted as 90% fresh granite bedrock.

Figure 4.5 The outcrop cutting bank near Location 2 and 3
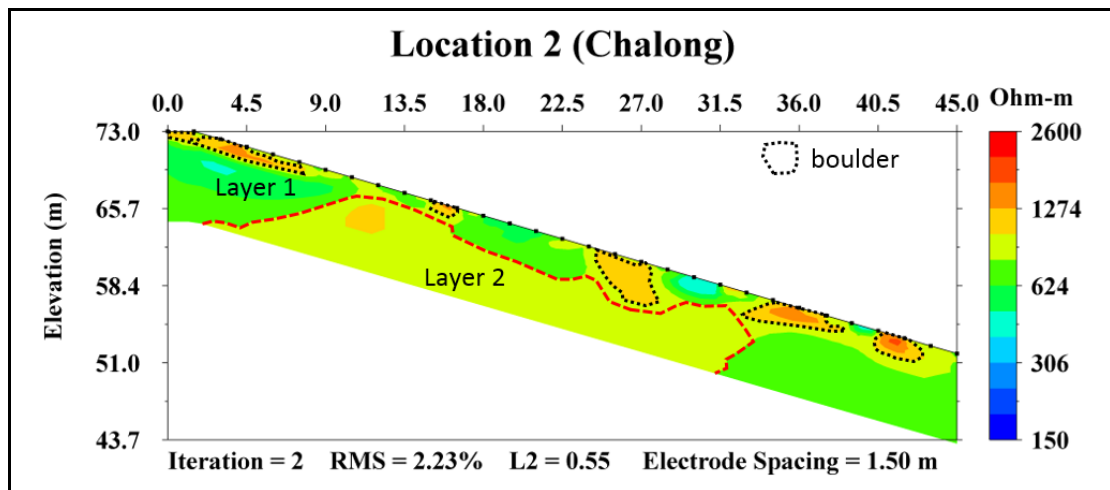
Figure 4.6 Resistivity profile of Location 2 (Chalong)

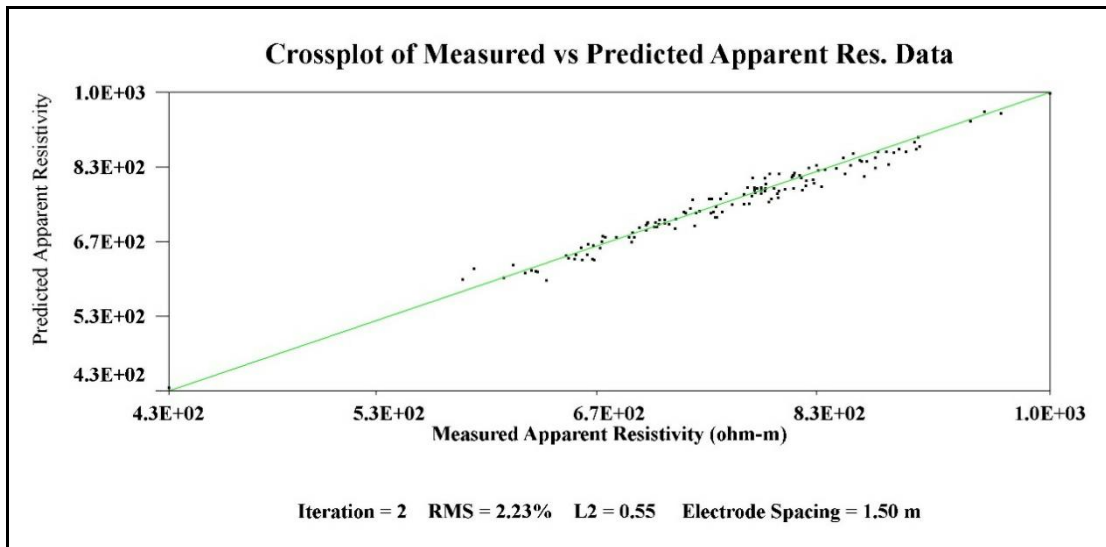**Figure 4.7** ERI data misfit cross-plot diagram of Location 2

(iii) ERI Line 3, Location 3 (Chalong)

The interpretation of this inverted resistivity section was done as the same as Location 2. In this resistivity section, five iterations were done without deleting any error of the resistivity data with RMS error of 2.62%. The inversion result of ERI Line 3 was displayed in Figure 4.8 and 4.9. According to the inversion result, only one layer was found in this study area which has a resistivity range of >1800 Ωm. The ERI result was interpreted as fresh granite bedrock because the location was destructed for the dam construction site (Figure 4.10). However, some locations shown the resistivity profile accompanying low resistivity values of water accumulation in fractures. These fractures were not from a nature and they were abnormally formed due to excavation or vibration. The debris materials, granitic soil, and water occupied in these fractures.
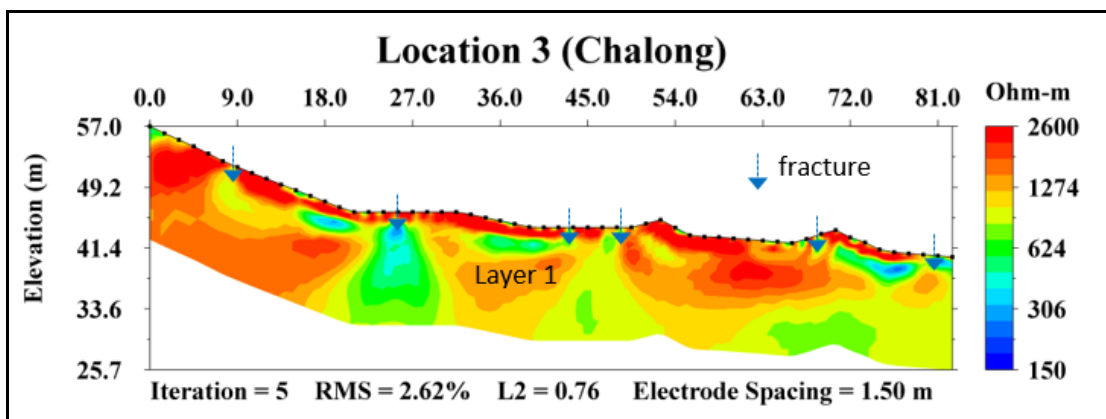

Figure 4.8 Resistivity profile of Location 3 (Chalong)
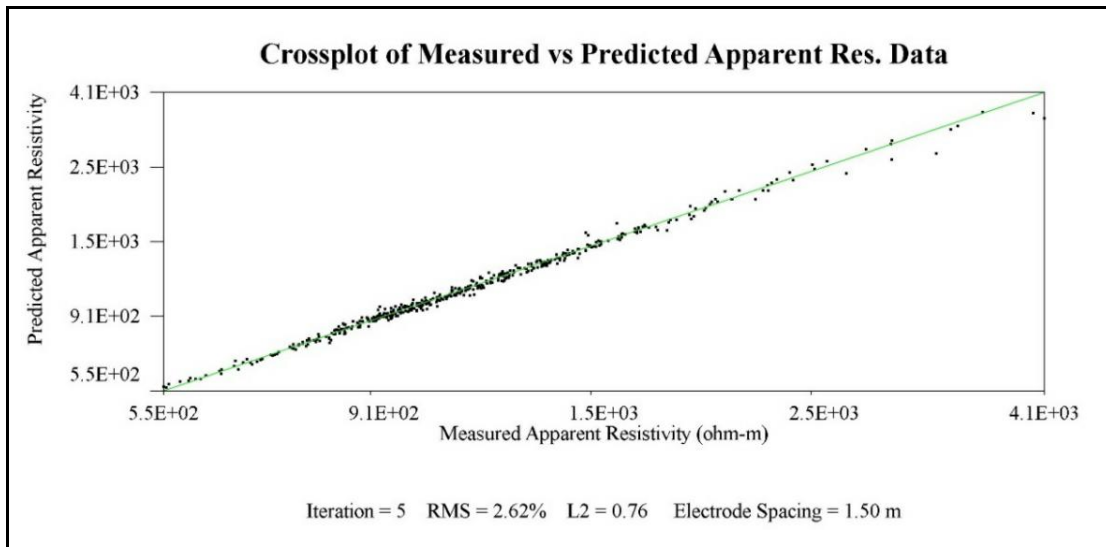
Figure 4.9 ERI data misfit cross-plot diagram of Location 3

Figure 4.10 The excavated area of Location 3 shows the ground surface is exposed with granite bedrock

4.2 Seepage Simulation Results

Transient seepage simulation was done for both locations. Figure 4.11 presents the water conductivity over matric suction. Location 1 reached the convergence state (input and computed conductivity functions are matched and coincided) at the iteration time of 57 times, while Location 2 was 472 times. Figure

4.12 indicates the number of non-converged nodes over the number of iterations. Moreover, each seepage simulation reached the under-relaxation condition (towards zero). The results of convergence and under-relaxation criteria indicate the model simulations are fully solved without errors.
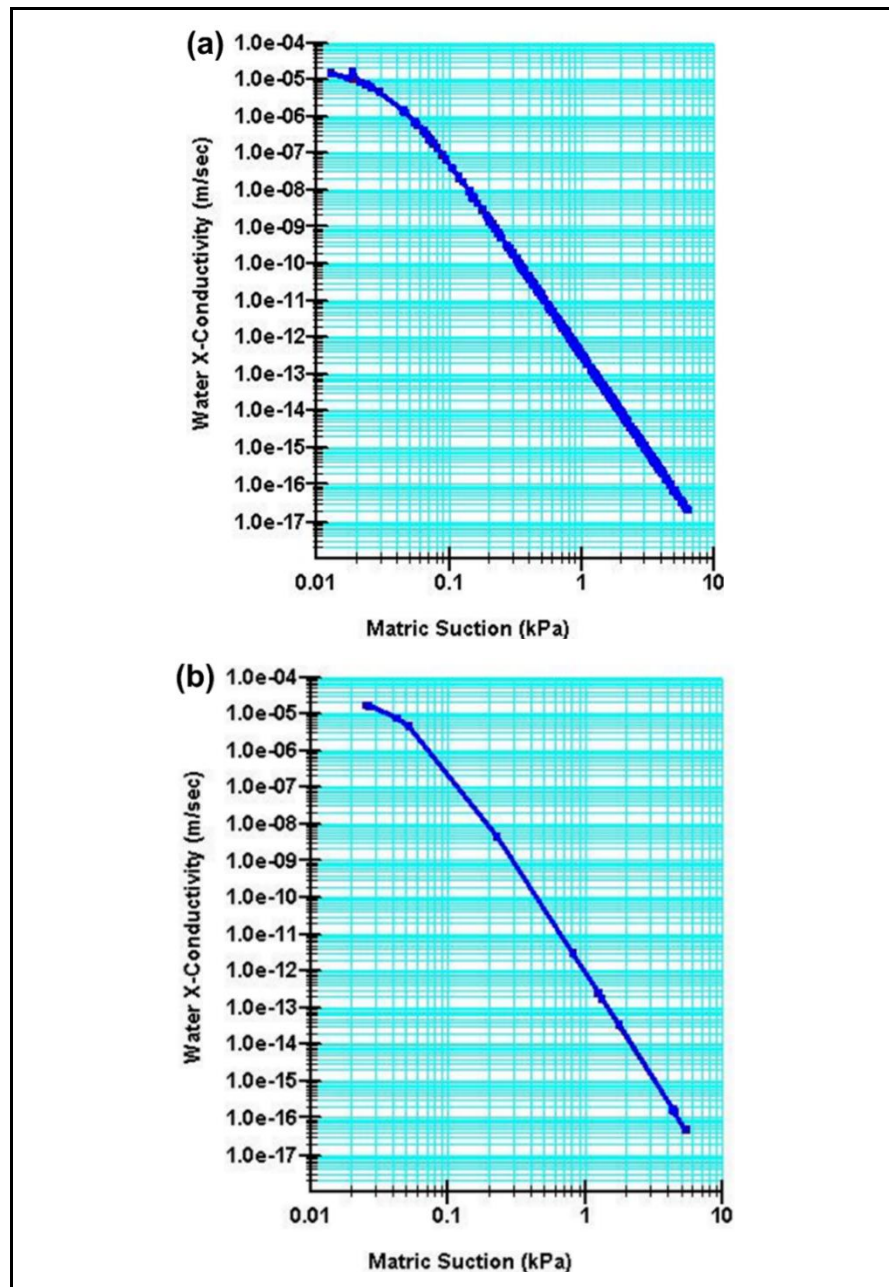
Figure 4.11 The output result of conductivity versus matric suction graph for without using ERI geometry reconstruction, which represents a converged solution for (a) Location 1 and (b) Location 2
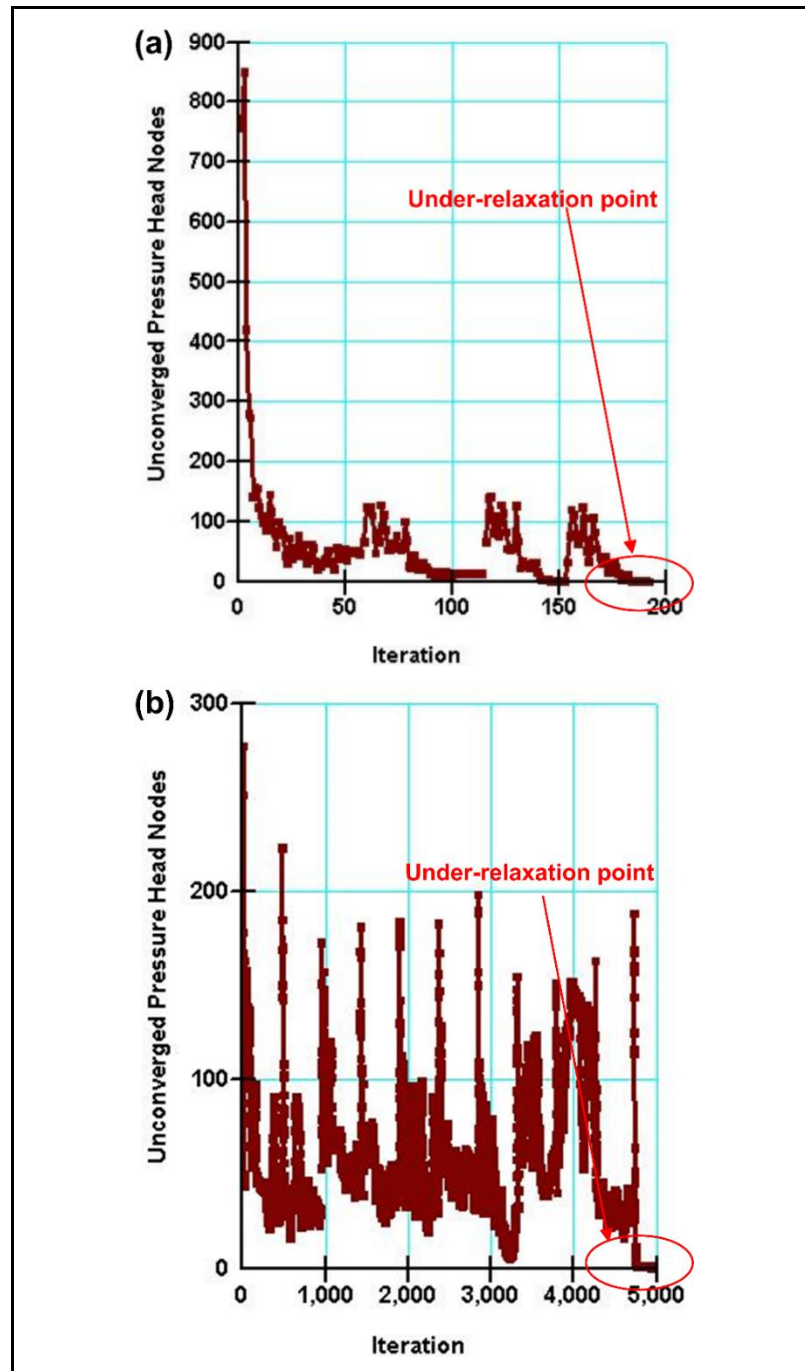
Figure 4.12 The output result of non-converged nodes versus number of iterations graph for without using ERI geometry reconstruction, which represents an under-relaxation state for (a) Location 1 and (b) Location 2

Figure 4.13 (a) shows PWP distribution over time for Location 1. In this simulation, the first 6-time steps (June16-21) seem that the clayey gravel layer starts to absorb water showing in the PWP changes from negative to positive. Anyway, at the

time steps-7 and 8 (June 22-23), no rainfall and a few rainfall made for decreasing the PWP. Then, the PWP was rising up immediately after the time step 8 (23 June) and maximum PWP appears at the time step-11. This is because the soil gained the water amount enough from the accumulated rainfalls. After that the PWP went down accompanied with two days successive unrainy days.

For Location 2 (Figure 4.13(b)), the medium amount of rainfall intensity at the first 8 time steps (10-17 May) changed the subsoil condition into the partially unsaturated condition which showed the trend of PWP from negative to positive. Then the PWP was increased suddenly at the time step-9, even the low amount of rainfall. After the time step-9, the PWP was sharply decreased to the time step 14 (23 May) due to less amount of rainfall. Then, the PWP re-increased at the time step 15 (24 May) due to the maximum rainfall. However, the peak PWP did not appear at the time step-15, but the small amount of rainfalls supports the PWP getting the peak at the last time step-20 (May 29).
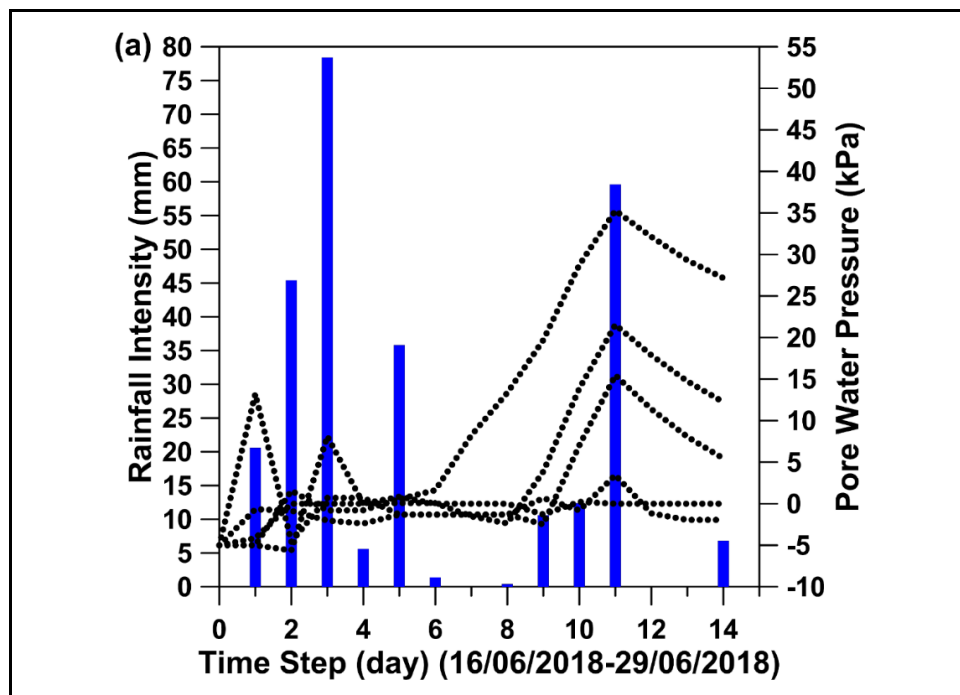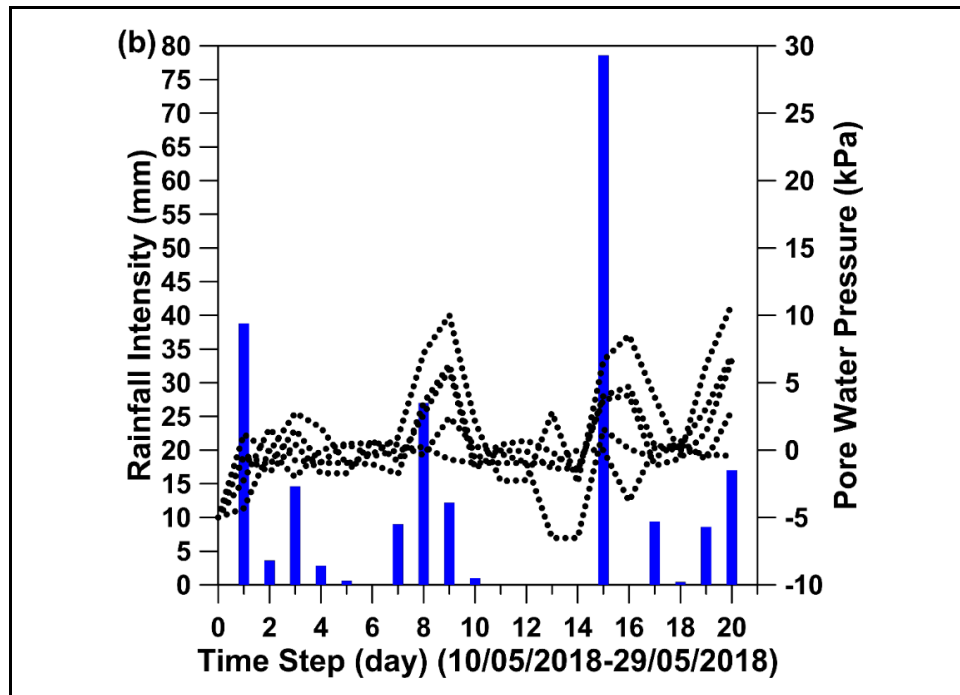
Figure 4.13 Transient seepage pore water pressure distribution over time with rainfall
optimize in critical slip surface at (a) Location 1 and (b) Location 2 for
without using ERI geometry reconstruction

Figure 14 (a) and (b) illustrate the PWP condition after 14-days rainfall
20-days rainfall for Location 1 and 2, respectively. Location 1 indicates the changes of
PWP in the subsoil were highly developed and the maximum PWP of 120 kPa was seen
at the base of the slope. Similarly, the Location 2 also showed the development of PWP
under the subsoil. The maximum PWP of 50 kPa was found at the base of the slope.
The PWP along the wetting front in each location reached a positive number meaning
the subsoil was totally saturated due to infiltration.
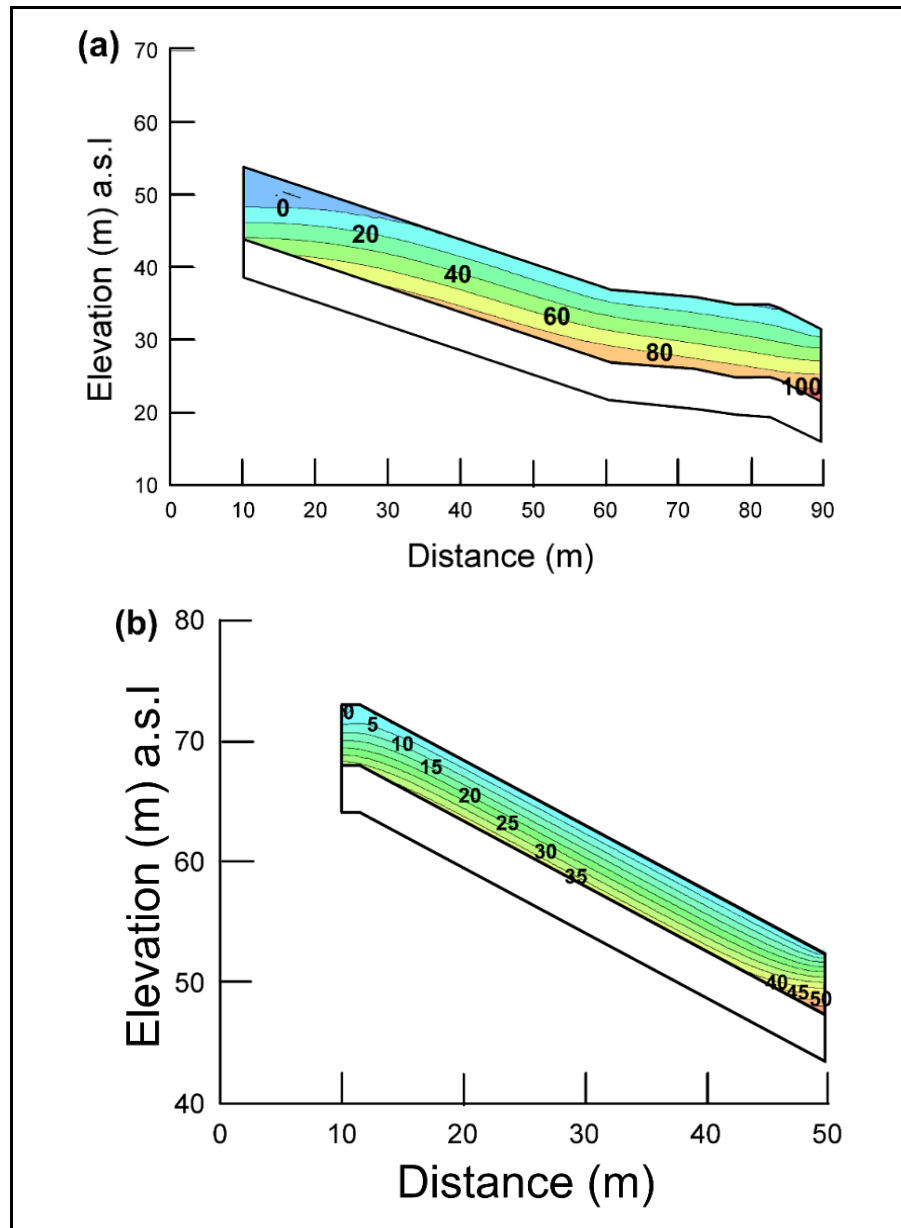
Figure 4.14 PWP (kPa) distribution of (a) Location 1 under 14-days rainfall and (b) Location 2 under 20-days rainfall for without using ERI geometry reconstruction

Figure 4.15 (a) and (b) indicate the hydraulic head of Location 1 and Location 2. Both locations show the infiltration is in the form of vertical direction which means water moved under the subsoil in the horizontal direction from the top of the slope to the bottom of the slope and seepage flow processes took place in each location.
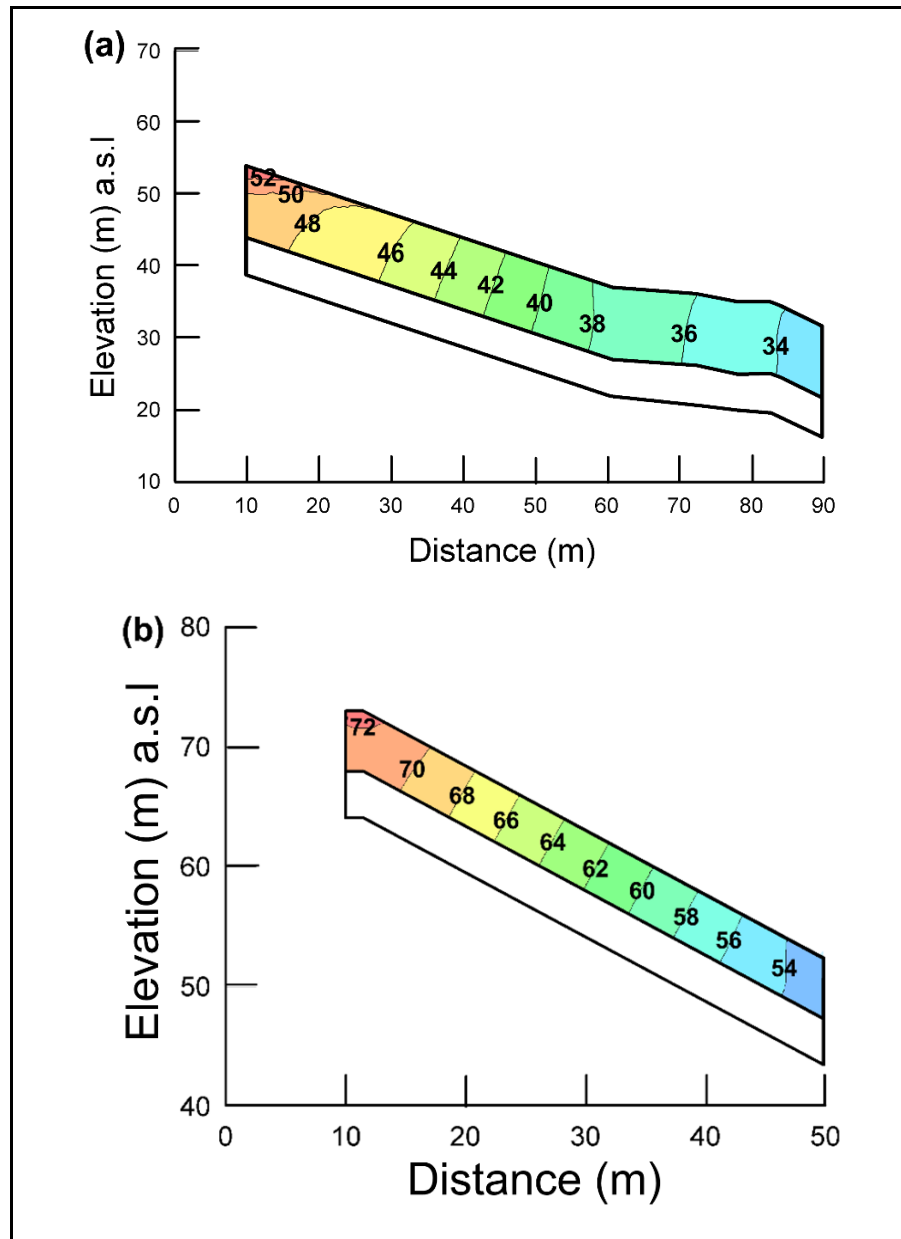
Figure 4.15 Hydraulic head (m) distribution of (a) Location 1 under 14-days rainfall
and (b) Location 2 under 20-days rainfall

4.3 Slope Modeling of Without Using ERI Geometry Reconstruction Results

The parent analysis (SEEP/W simulation) directly linked to the analysis of SLOPE/W for conducting the slope stability analysis. Morgenstern-Price's method depicted in equation (2.35) and (2.36) with a half-sine function used in each simulation for determining the F.S. The user specified half-sine function was not considered because the study objective is to estimate the thickness of the slip surface. For all the

geotechnical parameters, 95% saturation was applied in this study because Phuket's granitic soils are usually failure when they reached 90-100% degree of saturation (DMR, 2011b). The minimum value of friction angle due to suction (ϕ_b) was adopted from Mairaing, 2006. Where the angle between matric suction and shear strength for Location 2 was nearly uniformed, but Location 1 was quite variations. Theoretically, the maximum value of ϕ_b should not exceed the original friction angle. Therefore, ϕ_b value for Location 1 and 2 were 38.62 ° and 27.12°, respectively. Figure 4.16 (a) and (b) show the friction angle due to matric suction for Location 1 and 2 from DMR, 2011b. The parameters used in slope modeling were listed in Table 3.5. Trial and error method was used to estimate the entry and exist type within the mentioned length of sliding surface, then models were done with a convergence iteration setting of 100 times. Figure 4.17 (a) and (b) illustrate F.S. distribution over time with rainfall at Location 1 and 2. For Location 1, the minimum F.S. of 3.884 was found at the time step 11 (26 June). It was very high under induced-rainfall on that date. This is because of very low suction takes place to the soil layer which was already discussed in seepage analysis. For Location 2, F.S. was totally dependent on the rainfall intensity, the first 8-days accumulated rainfall (10-17 May) abruptly changed F.S. After time step 15 (maximum rainfall intensity), the changes of F.S. depended on the amount of rainfall intensity; thus the lowest F.S. of 1.554 was found at the final time step 20 (29 May). The critical sliding surfaces for each location with the lowest F.S. after slope stability simulation are exhibited in Figure 4.18 (a) and (b). Figure 4.19 (a) and (b) show the F.S. vs. Lambda graph, the graphs show the moment limit equilibrium did not affect the F.S. and only force equilibrium influenced in Location 1. Whereas, in Location 2, both moment and force influenced in the equilibrium state. These graphs are useful to identify the types of the landslide. Generally, an active moment limit equilibrium represents rotational landslide, while an active force equilibrium represents translational landslide. Figure 4.20 (a) and (b) illustrate the information of the computed sliding surface occurred in slice-17 of each location. The closed force polygons referred the Morgen-Price method was fully satisfied both moment and force equilibriums.
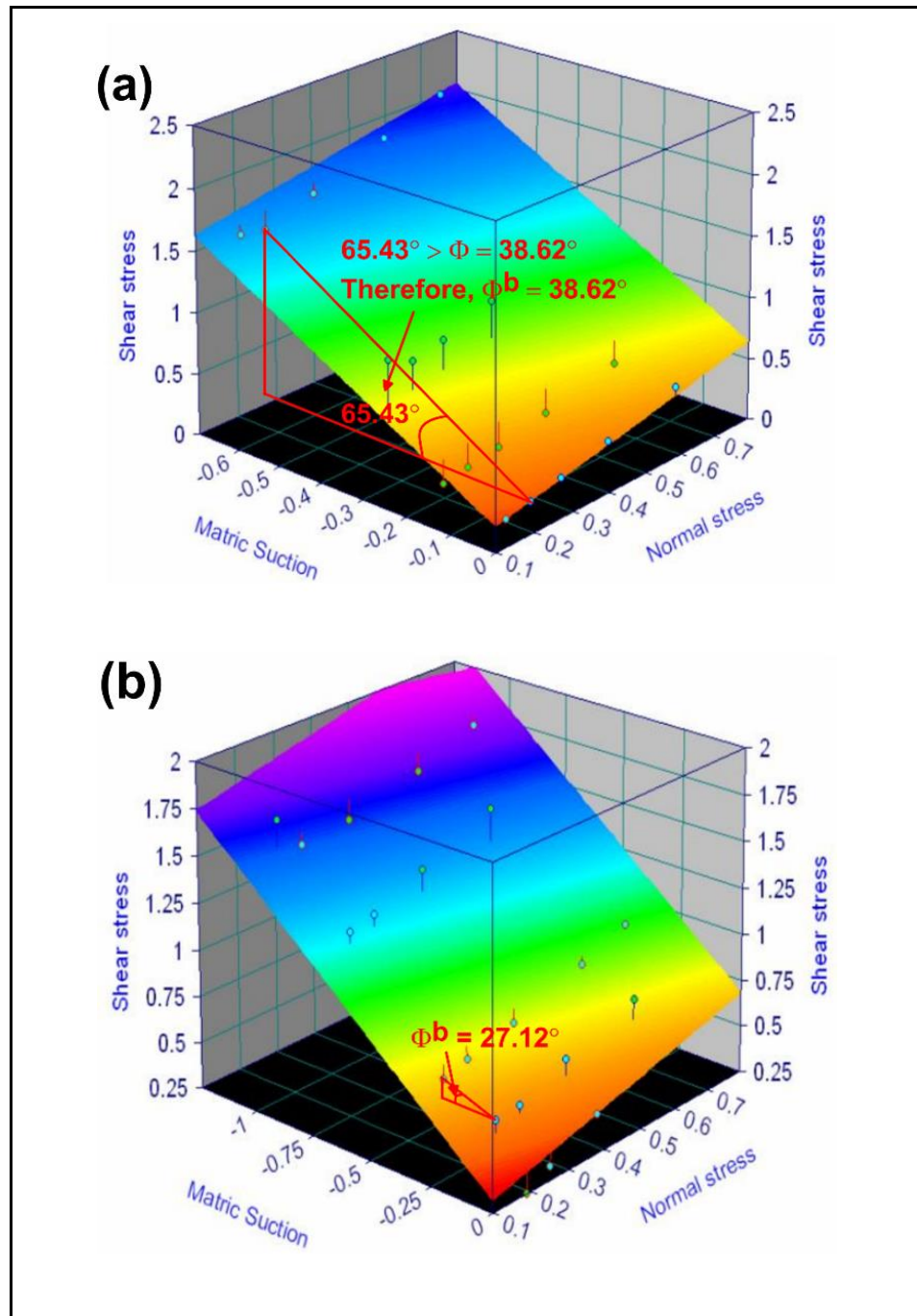
Figure 4.16 Friction angle due to matric suction for (a) Location 1 and (b) Location 2
(DMR, 2011b)
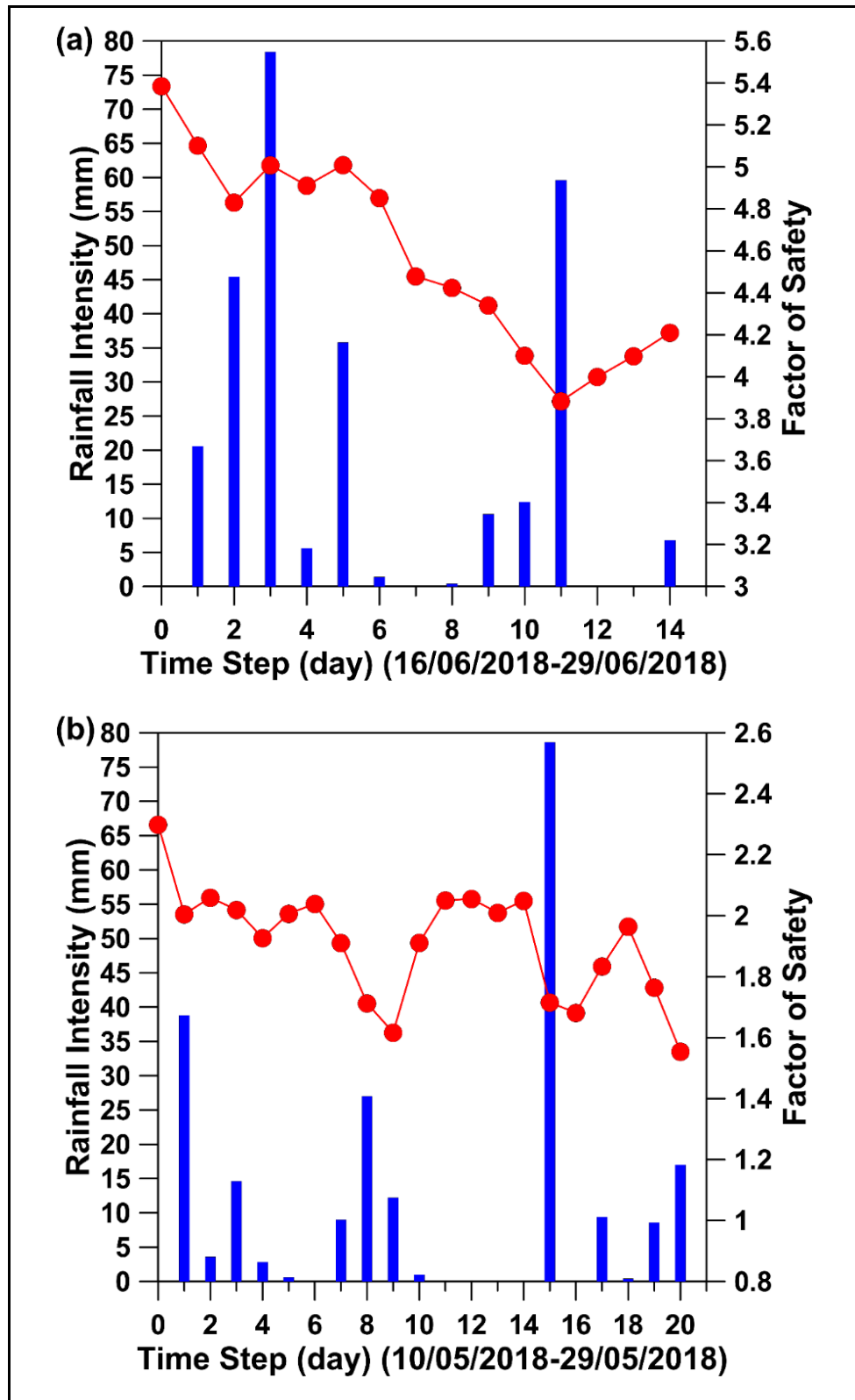
Figure 4.17 The lowest state factor of safety distribution over time with rainfall of (a) Location 1 and (b) Location 2 for without using ERI geometry reconstruction
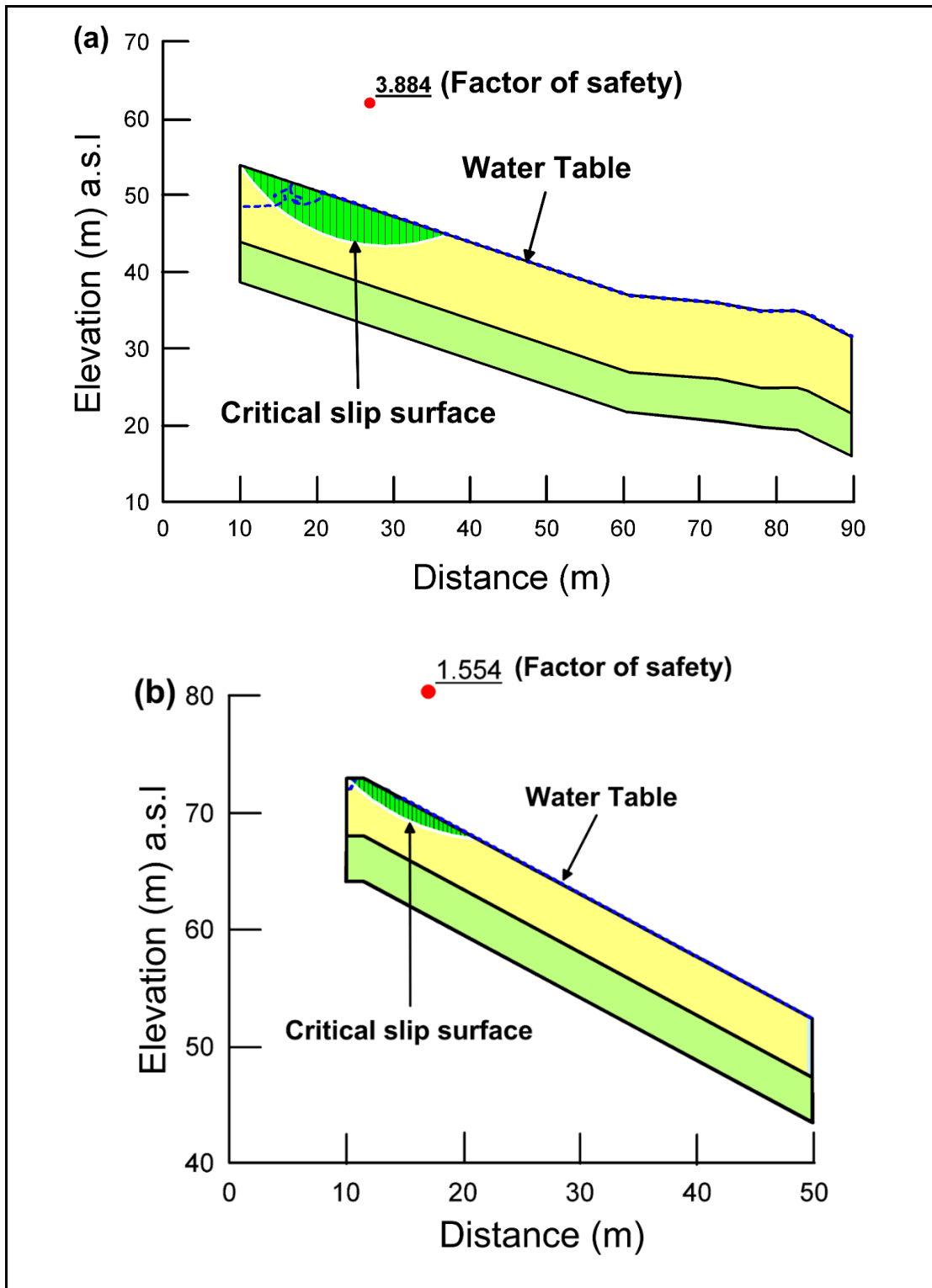
Figure 4.18 The critical slip surfaces after slope stability modeling with water table at (a) Location 1 and (b) Location 2 for without using ERI geometry reconstruction
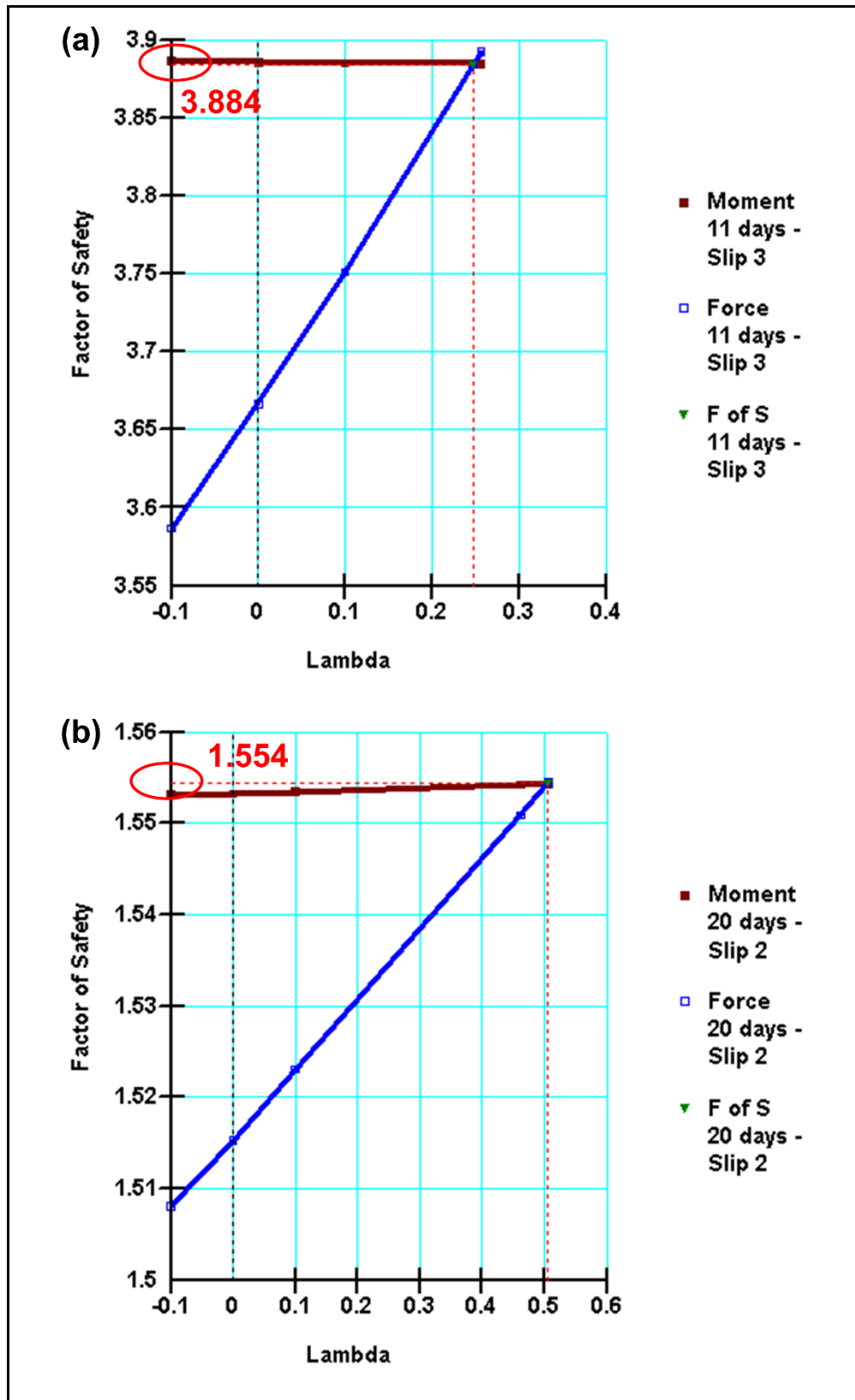
Figure 4.19 Factor of Safety verses Lambda graph for (a) Location 1 and (b) Location 2 for without using ERI geometry reconstruction
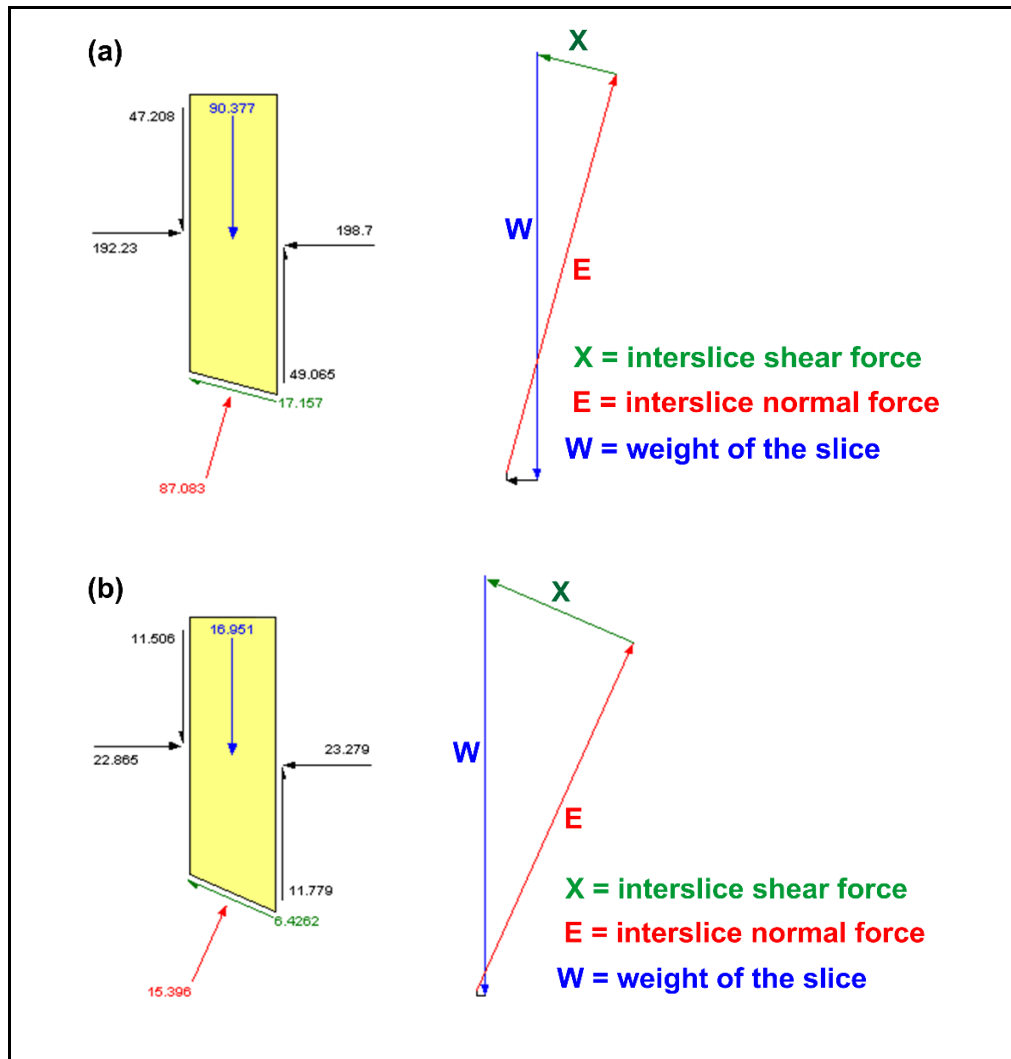
Figure 4.20 The critical state slice information at slice 17 for (a) Location 1 and (2) Location 2 for without using ERI geometry reconstruction

4.4 Reconstruction of Landslide Model Geometry using ERI

The reconstructed geometry of both slope models were illustrated in Figure 4.21 (a) and (b). The same mesh element size of the original models was used for both locations.

The boundary definition for Location 1 was the same as the previous model, but it was a little different from the previous model of Location 2. The base boundary is necessary to define as null flux boundary by assuming totally bedrock. It is possible to define because the outcrop cutting bank near this location shows the bedrock is too shallow. Therefore, the base boundary of the reconstructed model is very

close to the bedrock. The other boundary definitions for Location 2 were the same as the previous model. The redefined boundary conditions of reconstructed models are shown in Figure 4.22 (a) and (b).
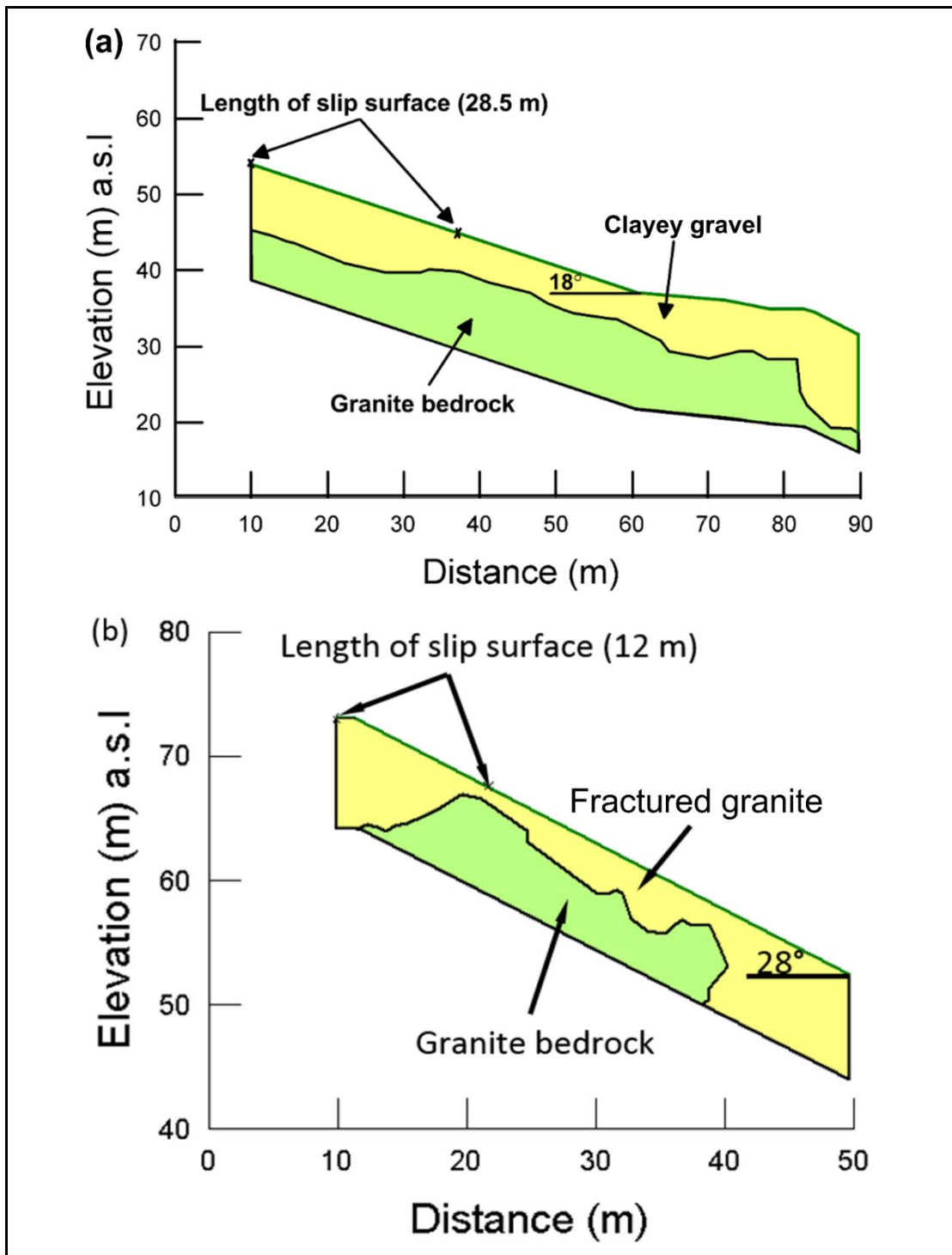
Figure 4.21 The slope geometries of (a) Location 1 and (b) Location 2 for using ERI geometry reconstruction

(a)

Number of mesh elements - 902
Number of nodes - 1133

(b)

Number of mesh elements - 851
Number of nodes - 965
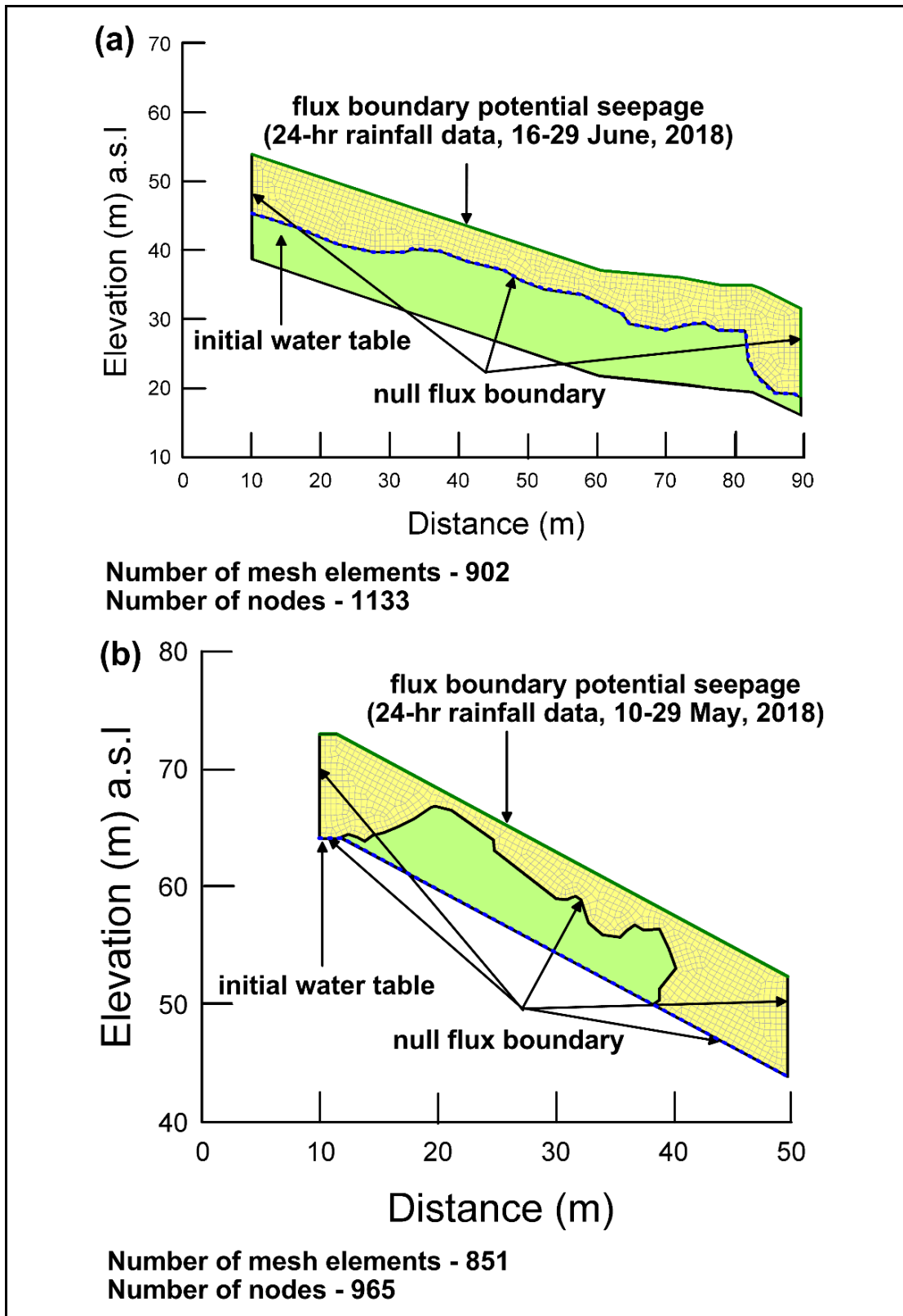
Figure 4.22 Finite element description model of (a) Location 1 and (b) Location 2 for using ERI geometry reconstruction

4.5 Reconstruction of Landslide Model Geometry Using ERI Results

Figure 4.23 (a) and (b) present the water conductivity over matric suction for Location 1 and 2. Figure 4.24 (a) and (b) indicate the number of non-converged nodes over the number of iterations for Location 1 and 2.
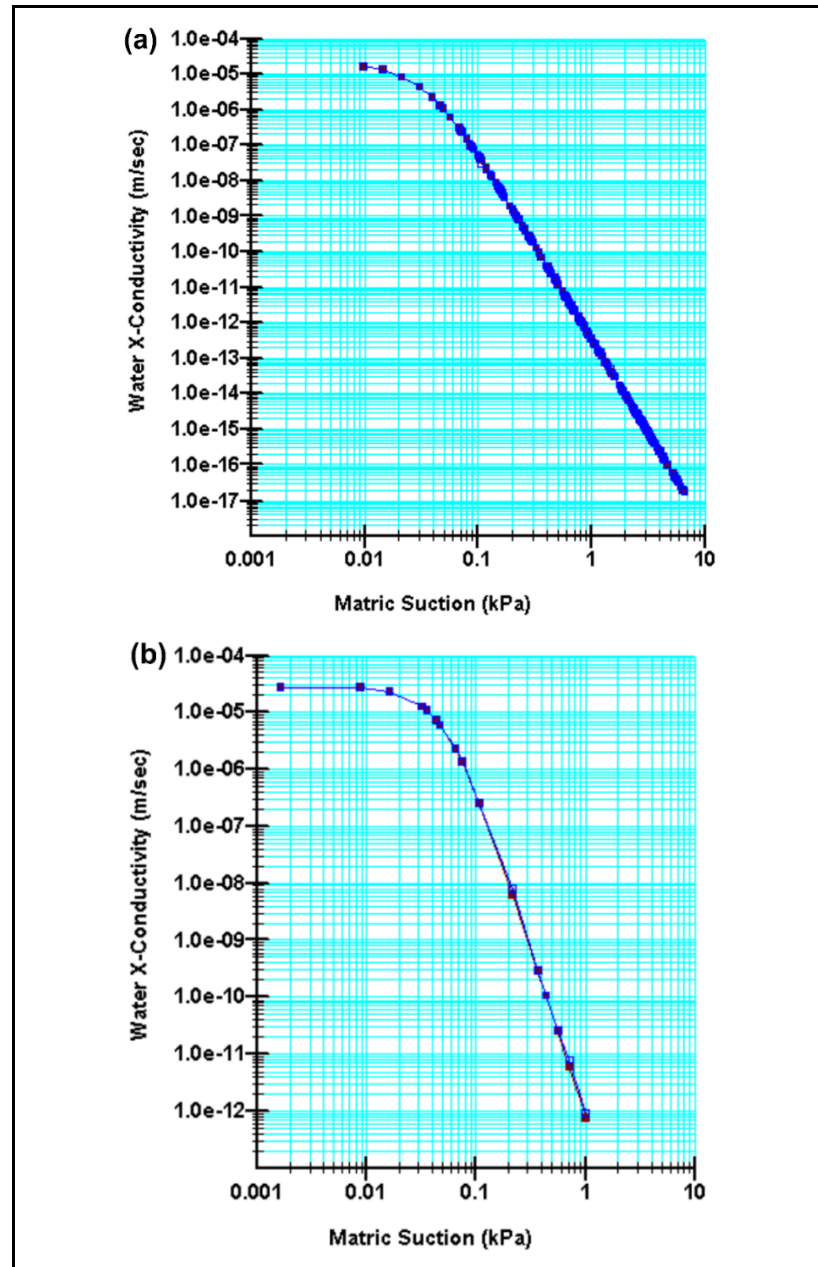
Figure 4.23 The output result of conductivity versus matric suction graph for using ERI geometry reconstruction, which represents a converged solution for (a) Location 1 and (b) Location 2
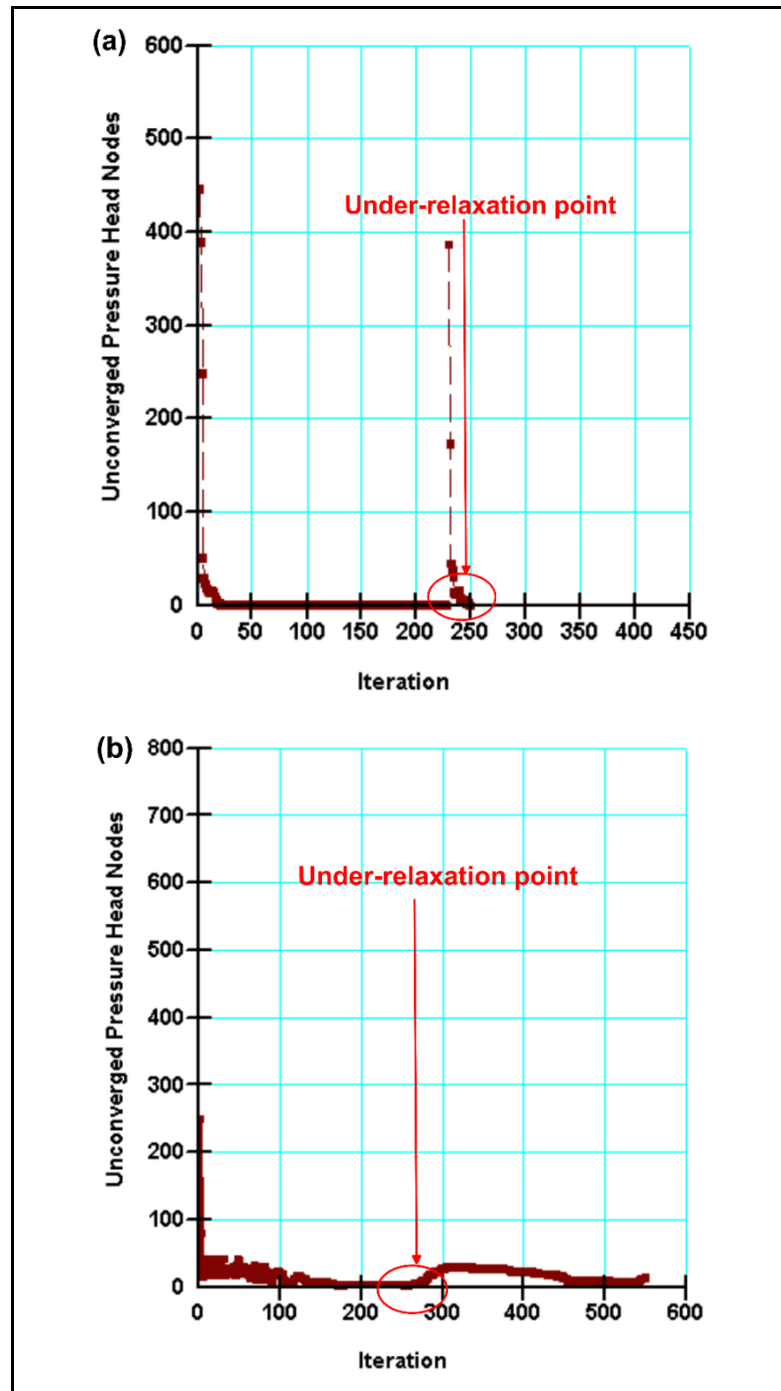
Figure 4.24 The output result of non-converged nodes versus number of iterations graph for using ERI geometry reconstruction, which represents an under-relaxation state for (a) Location 1 and (b) Location 2

Transient seepage simulation was done again for both locations. Figure 25 (a) shows PWP distribution over time for Location 1. In this simulation, much amount of PWP did not see at the first 3 time steps (16-18 June), then the PWP was

rising up immediately after the time step 3 (18 June). It seems the soil stored water amount enough for saturation due to the first 3-day rainfall. Starting from time step 6 (21 June), the variation of PWP went nearly constantly to last day (29 June). The peak condition of PWP occurred at the time step 11 (26 June).

For Location 2 (Figure 25 (b)), the medium amount of rainfall intensity at the first 7 time steps (10-16 May) changed the subsoil into the partially unsaturated condition influencing the trend of PWP from negative to positive. Then the PWP was increased suddenly at the time step 8-9, the PWP was sharply decreased to the time step 14 (23 May) due to less and no rainfall. Anyway, the peak rainfall at the time step 15 produced the PWP re-increasing at the last time step (29 May).
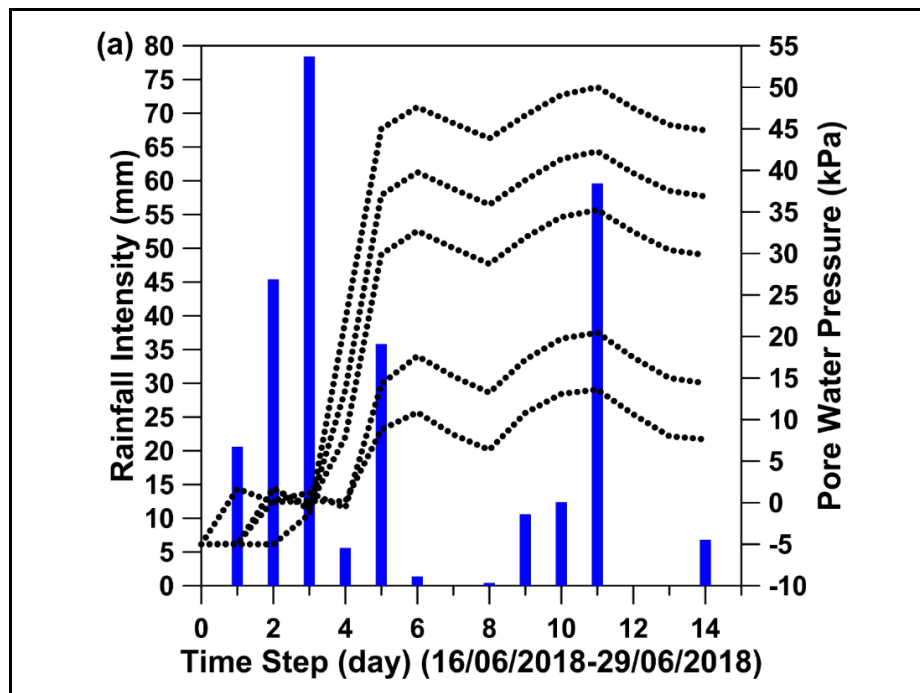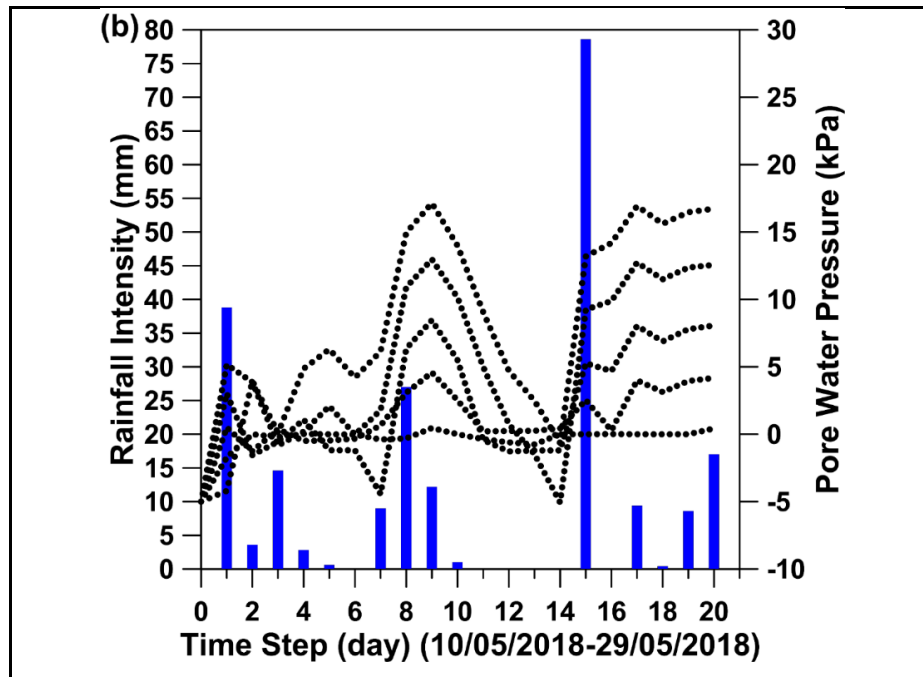
Figure 4.25 Transient seepage pore water pressure distribution over time with rainfall optimize in critical slip surface at (a) Location 1 and (b) Location 2 for using ERI geometry reconstruction

Figure 26 (a) and (b) illustrate the PWP condition after 14-days rainfall Location 1 and 20-days rainfall for Location 1 and 2, respectively. In this reconstructed models, Location 1 indicated the changes of PWP in the subsoil were highly developed and the maximum PWP of 140 kPa was seen at the base of the slope. The amount of PWP was higher than the previous models. The same condition in the Location 2 was also found at the base of the slope with PWP of 80 kPa. Hydraulic head changes due to seepage flows were the same as the previous models as shown in Figure 4.27 (a) and (b).
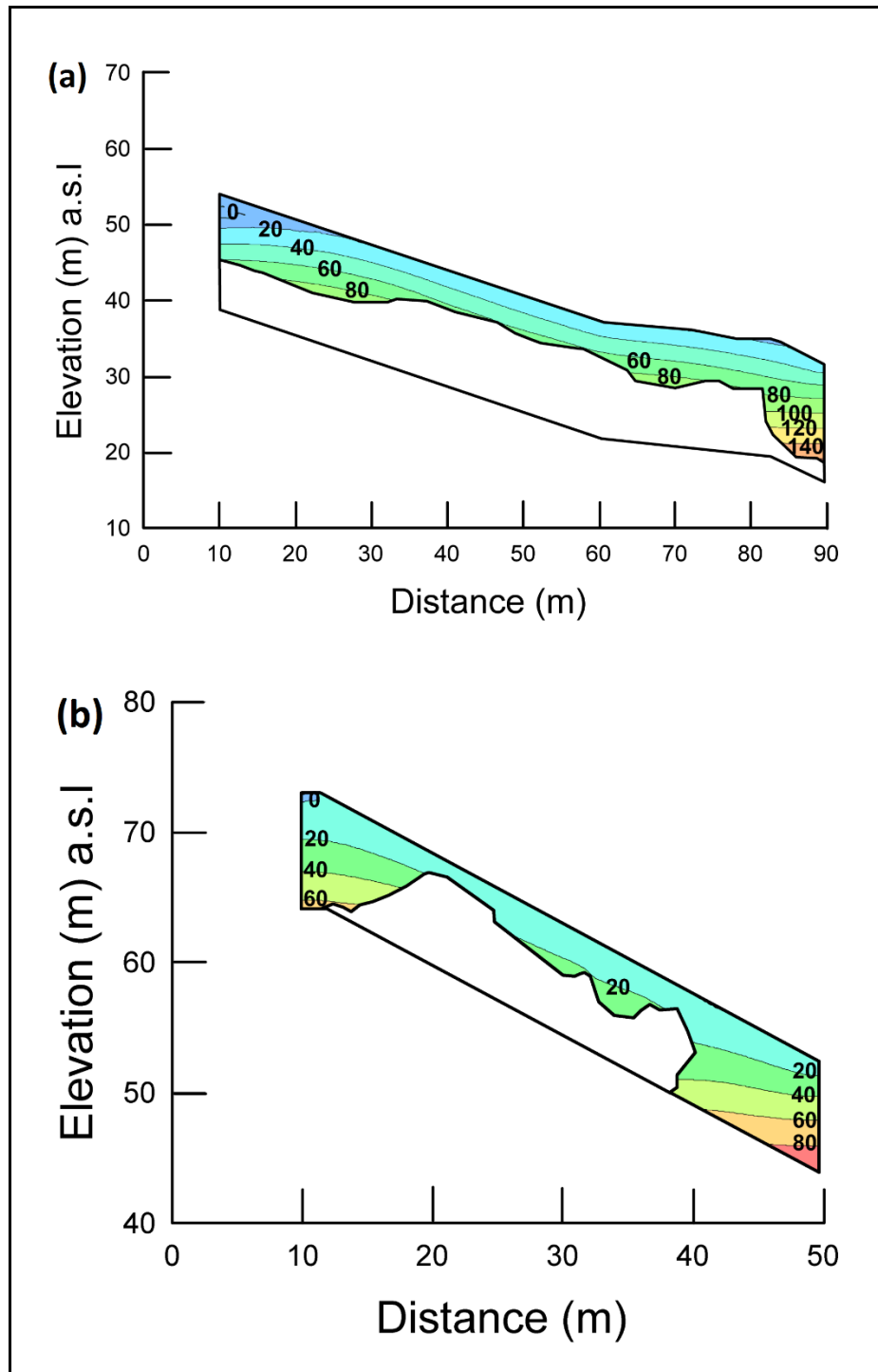
Figure 4.26 PWP (kPa) distribution of (a) Location 1 under 14-days rainfall and (b) Location 2 under 20-days rainfall for using ERI geometry reconstruction
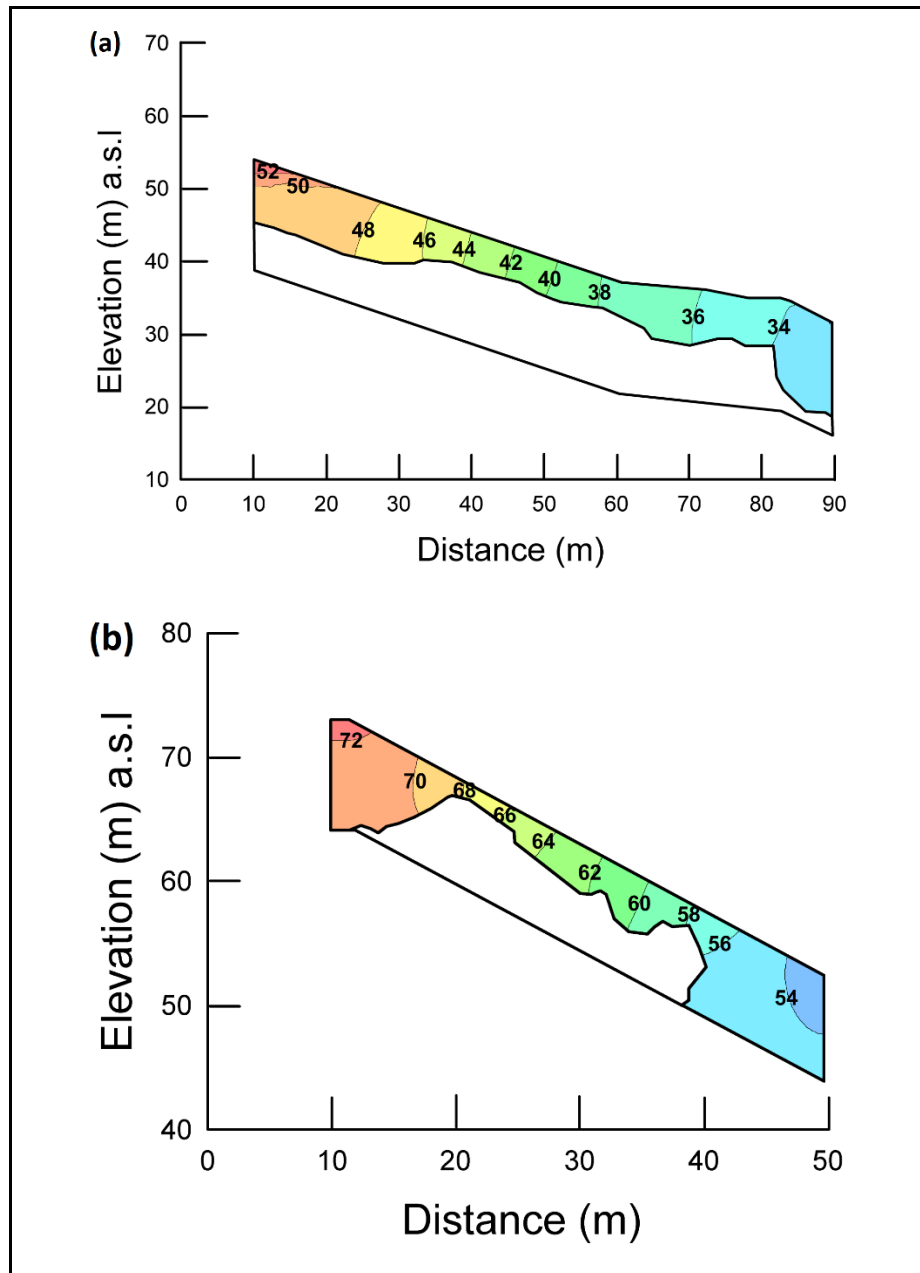
Figure 4.27 Hydraulic head (m) distribution of (a) Location 1 under 14-days rainfall and (b) Location 2 under 20-days rainfall for using ERI geometry reconstruction

Furthermore, Figure 4.28 (a) and (b) illustrate the F.S. distribution over time with rainfall in Location 1 and 2. For Location 1, the variation of F.S. was almost the same as the previous simulation. The lowest F.S. value (3.484) was at the time step 11. On the other hands, the F.S. was totally different from the previous simulation at the time step 17-18 (26-27 May) for Location 2. The critical sliding surface of each

location with F.S. after slope stability simulation was exhibited in Figure 4.29 (a) and (b).
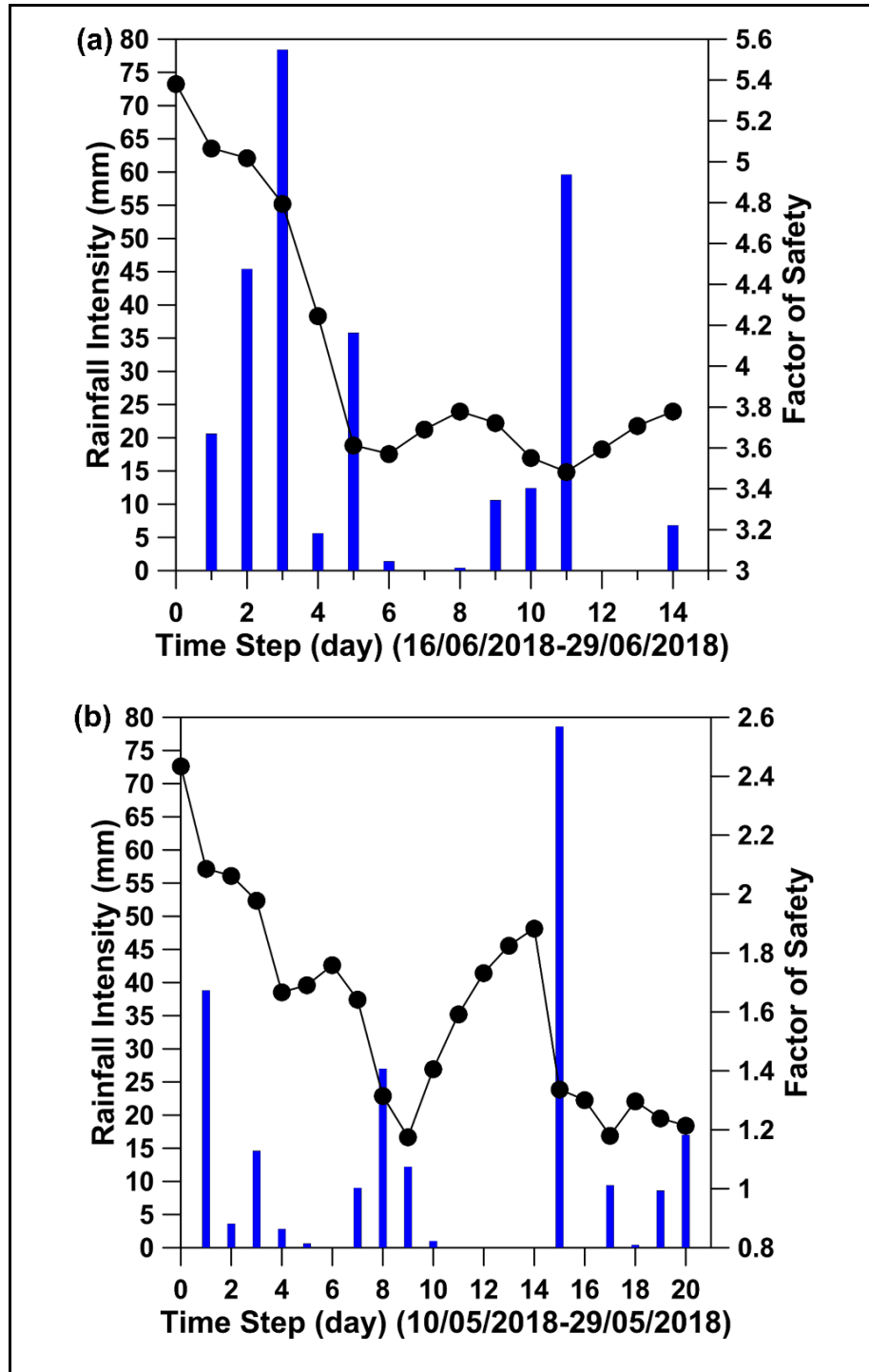
Figure 4.28 The lowest state factor of safety distribution over time with rainfall of (a) Location 1 and (b) Location 2 for using ERI geometry reconstruction
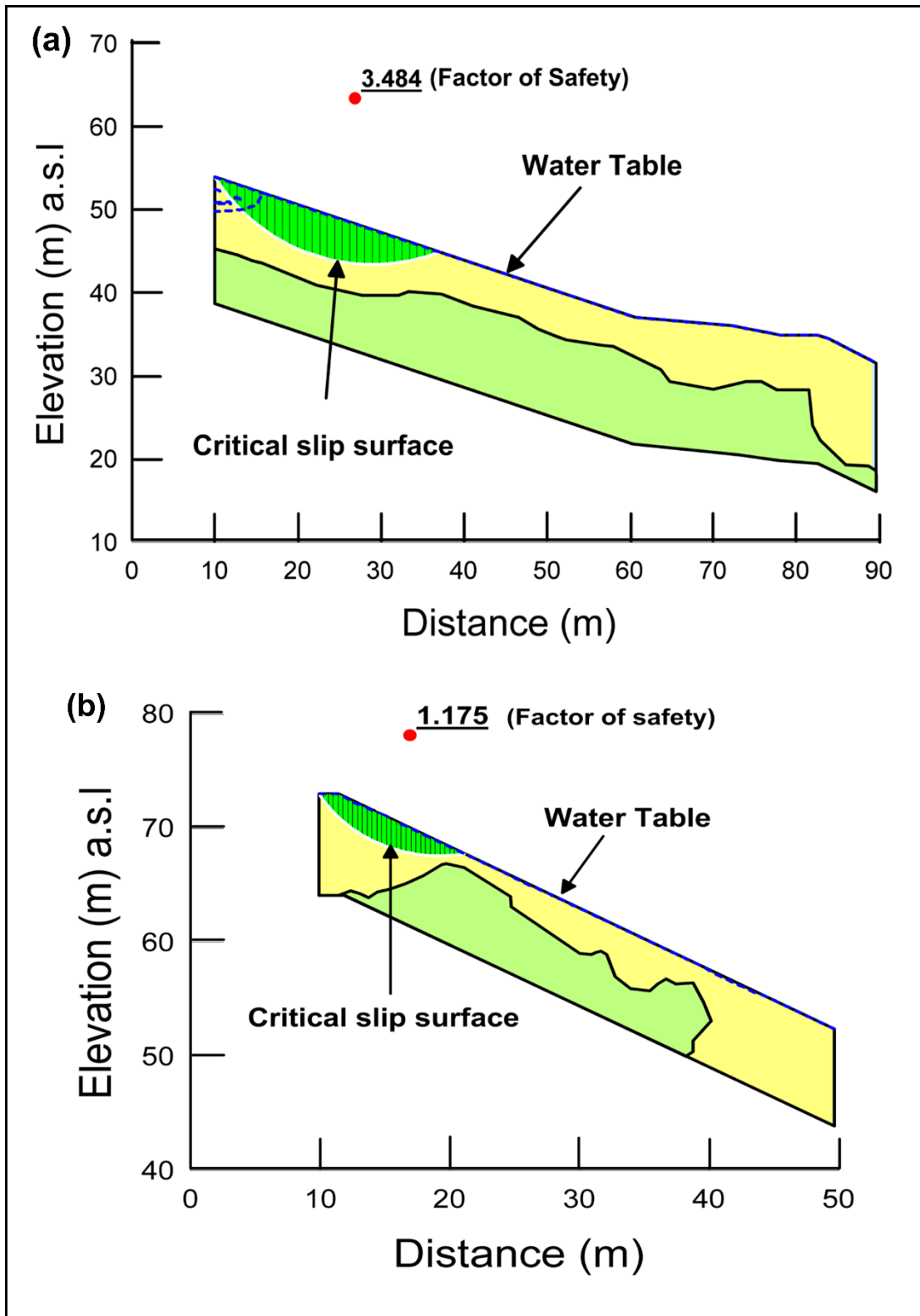
Figure 4.29 The critical slip surfaces after slope stability modeling with water table at (a) Location 1 and (b) Location 2 for using ERI geometry reconstruction

4.6 Safety Factor Comparison between Conventional Model Geometry and Reconstructed Model Geometry

For Location 1, the F.S. in the simulation of the conventional model was changed after time step 5 (20 June), whereas the F.S. of the reconstructed model changed directly starting from the first time step. After time step 5, the trends of the F.S. changed over time were quite the same for both models. Both model results show the lowest F.S. at the time step 11 (26 June). In addition, the trend of F.S. over time for Location 2 was almost the same before the time step 16 (14 May). However, at the time step 16-17, it was found that the F.S. trends contradicted between conventional model and reconstructed model. The last 3-time steps show the same trends of decreasing F.S. The lowest F.S. indicated that the reconstructed model was at the time step 20, the conventional model was at the time step 9. The comparison of the F.S. between the reconstructed and conventional models is shown in Figure 4.30 (a) and (b).
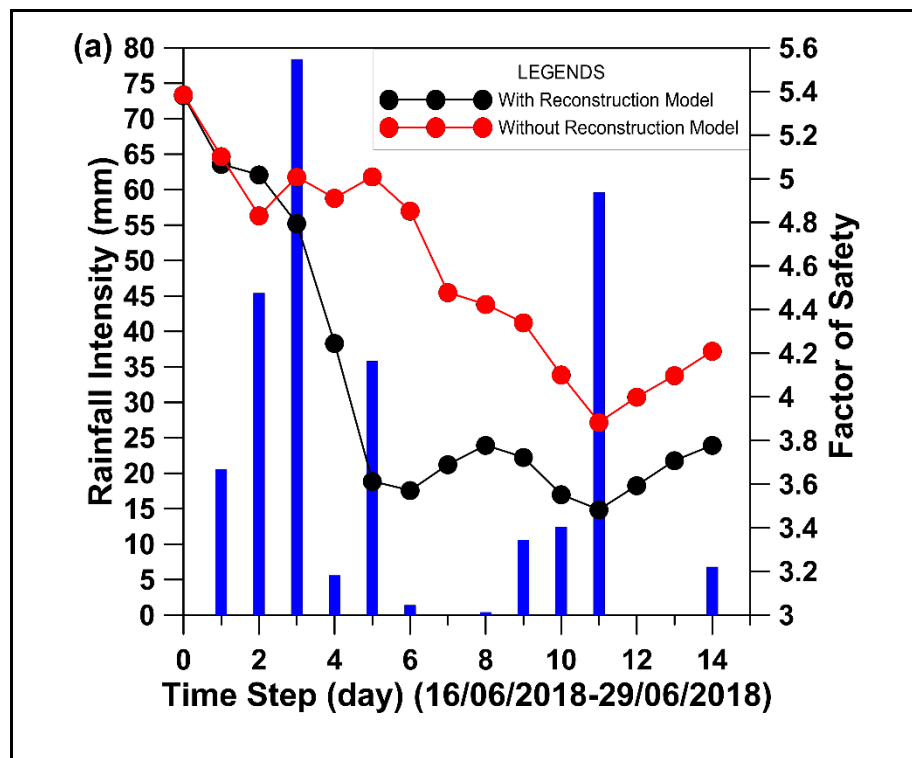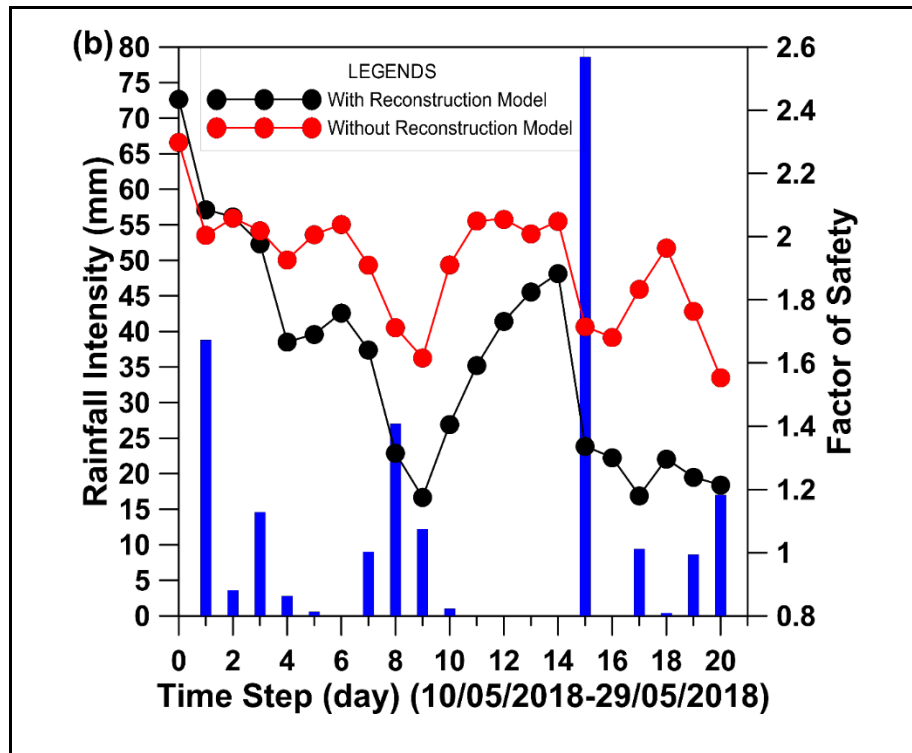
Figure 4.30 The comparison of factor of safety between using ERI geometry reconstruction and without using ERI geometry reconstruction

Surveying the subsurface geometry along the steep slopes of the fractured granite mountains in Phuket is difficult using conventional techniques, i.e., the drilling and borehole methods. Therefore, ERI is supported to detach the subsurface geometry. Moreover, ERI can successfully identify the presence of moisture content under the subsoil. This helps to define the susceptible sliding surface between the active and in-active zones. Generally, the interface between the active and non-active zones of the resistivity profile is usually defined as the susceptible sliding surface for studying the landslide with ERI. This interrelation hypothesis has been deemed to identify the sliding surface.

Based on the above concept, the susceptible sliding surface of Location 1 was defined at a slope distance of 13.5 m with the depth of ~4.7 m where were accumulated with a low resistivity zone of about 624 Ωm (clayey gravel). In the simulation results, even the transient seepage was considered as a flux boundary, the F.S. was still high in both simulations (conventional and reconstructed models). This is because slope angle and soil properties were dominant on the slope. Moreover, the

sliding surface from simulation results of both reconstructed and conventional models was located at the depth of about 5.4 m and 5.5 m corresponding with the factor of safeties of 3.884 and 3.484 in Location 1, respectively. These F.S. values were acceptable in comparing with the ADPC, 2008 report. ADPC observed the landslide cases in Phuket and they have found that the slope angle 18° has the F.S. greater than 1.8 as a low potential landslide. Heavy and prolonged rainfall also cannot change the stability of the slope to reach the failure state because it is an in-active landslide.

In the same ways, the possible sliding surface was defined for Location 2 at a slope distance 5.5 m with the depth of about 2.5 m showing in the ERI result of resistivity value of about 465 Ωm (granitic soil). This resistivity range was accumulated with moisture content and these layers are possible to store water when heavy and prolonged rainfall. In this location, boulders at the top of the resistivity profile was considerable to occur sliding when the contact area at the base of the rock and fractured soil entraps enough amount of water. The top layer of the fractured granite was totally weathered and swell which means the soil can absorb water easily. Slope modeling results show the thickness of critical sliding surface in this location was 1.6 m and 2.5 m with the factor of safeties of 1.554 and 1.175 for conventional and reconstructed models, respectively. The reconstructed model was acceptable comparing with the ADPC, 2008 report. ADPC observed that the slope angle greater than 26° has the F.S. ≤ 1.3. This F.S. is quite low compare than Location 1 because the slope angle is high (28°) and its soil type is weak. Therefore, ADPC recommended that such a slope angle is a high potential landslide. Heavy and prolonged rainfalls like a disaster rainfall can make the F.S. of the slope under 1. The comparison of slidng surface and thickness between ERI result and slope modeling result of both Location 1 and 2 are displayed in Figure 4.31 and 4.32.

The conventional model is a general simulation to check the PWP and F.S. because it does not simulate on the actual soil layer and it considers only the estimated planar of soil layer depths. On the other hands, the reconstructed model is totally considered on the real shape of the subsoil layer. The comparison of different model results is already presented in section 4.7. The over-estimated F.S. was 0.441 at the time step-11 and 0.4 at the time step-9 for Location 1 and 2, respectively. Based on these results, it can be easily noticed the effective ways to solve the mislead assessment

of the susceptible landslide area, the integrated method of ERI and coupled slope modeling is suggested to conduct for studying the landslide research.
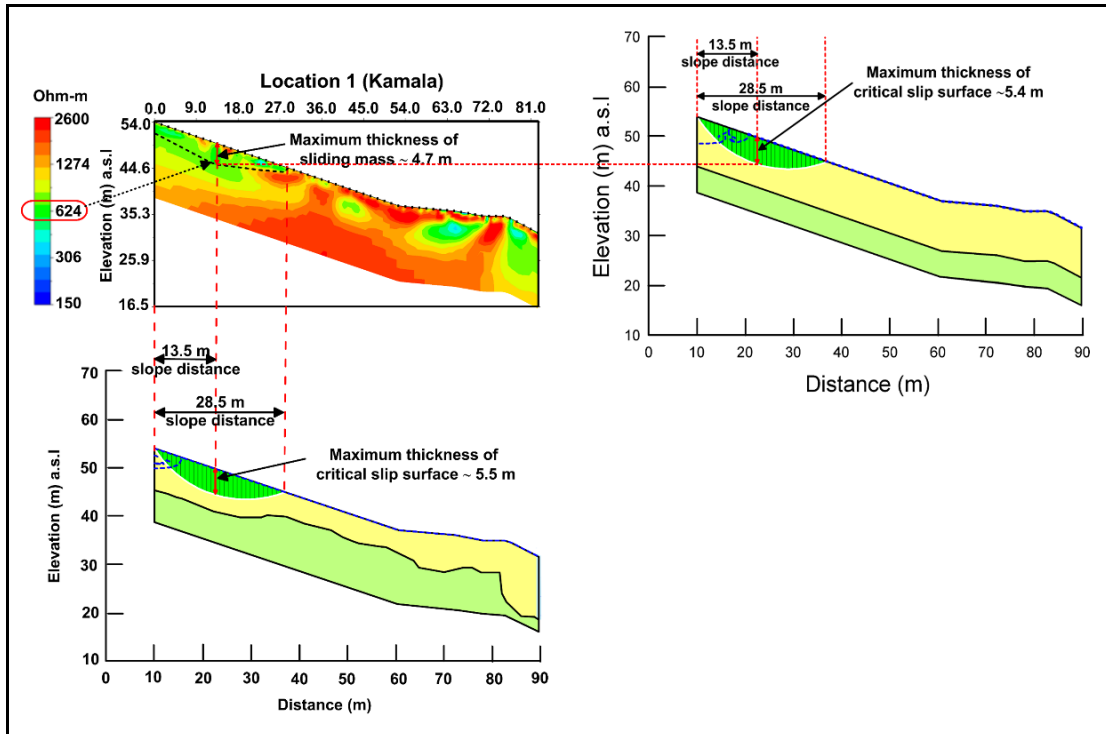
Figure 4.31 The comparison of sliding surface and thickness between ERI result and slope modeling result of Location 1
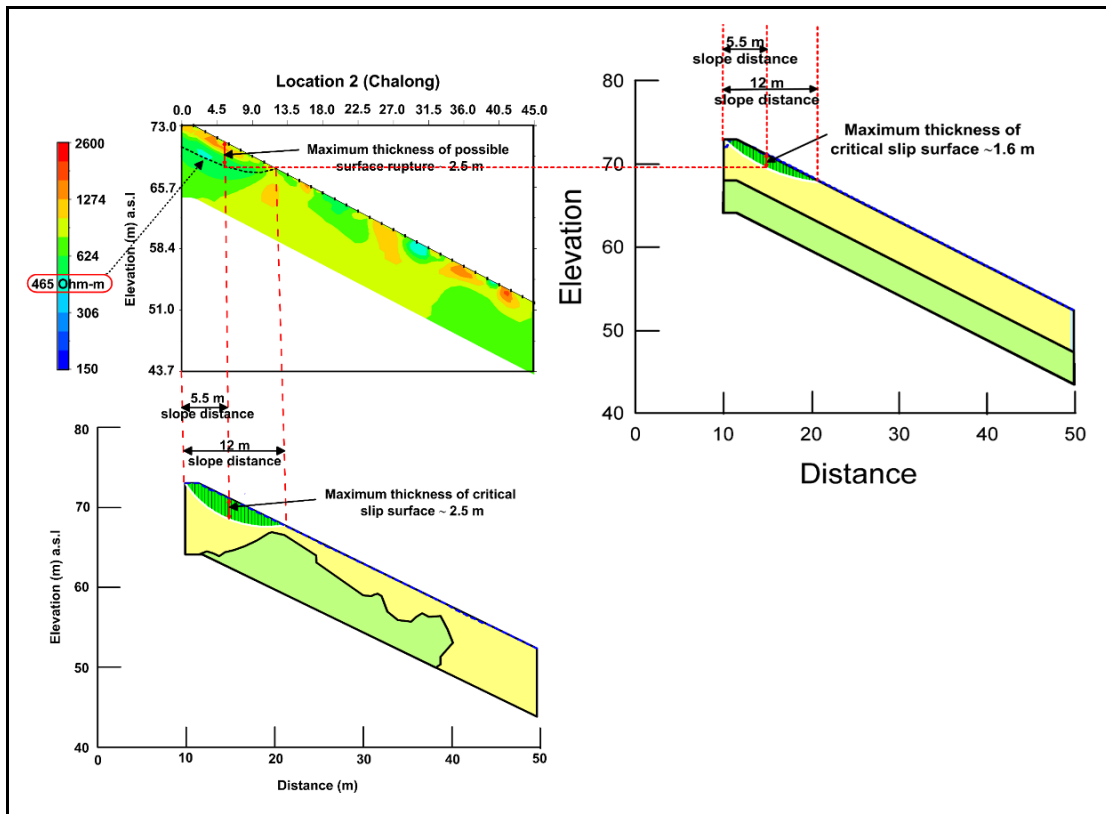
Figure 4.32 The comparison of sliding surface and thickness between ERI result and slope modeling result of Location 2

CHAPTER 5
CONCLUSION

5.1 Determination of Sliding Surface and Thickness of Landslide

Studies are done on the past landslide area, natural slope and manmade undercut. The past landslide area, Location 1 has the clayey gravel. The permeability of such soil type is very low. Even though the ERI result shows this soil layer has a moisture content, the stability is very high (F.S. = 3.884 for without using ERI geometry reconstruction and F.S. = 3.484 for using ERI geometry reconstruction) and very less tendency to occur landslide because the slope angle, soil permeability and infiltration rate are possible to allow surface runoff while raining and the rate of saturation also might be very low. Location 1, therefore, can be inferred that it is an inactive landslide area. The permeability of fractured granite at Location 2 is higher than Location 1 and the slope angle has also medium range. In this location, the successive and high amount of rainfall conditions can be seen as very tendency to increase the PWP. But, the PWP results show there is no negative PWP near the front water table. This means the imposed rainfall data suffices to saturate the soil. But, the stability analysis result (F.S. = 1.554 for without using ERI geometry reconstruction and F.S. = 1.175 for using ERI geometry reconstruction) is still higher. The inputted heavy and prolonged rainfall cannot change the stability of the slope under 1. But the slope stability condition might influence the unexpected future climate changes. Therefore, it can be concluded that Location 2 is an active area under heavy and prolonged rainfall. The manmade undercut, Location 3 already reached to the granite bedrock due to the excavation which can be clearly seen in ERI result and on-ground condition. Therefore, coupled slope modeling of SEEP/W-SLOPE/W is not considered such an artificial slope because this study already neglected the bedrock hydrology. Thence, Location 3 cannot be seen any sliding mass on the slope. But its ERI result can confirm the granite bedrock resistivity range (>1800 Ωm) and this resistivity range helps to assign the other locations bedrock layer.

In this study, only the location 2 is notable the rainfall-induced condition makes reducing the strength of the slope. This means the heavy and prolonged rainfall influences the stability of the slope. But the slope geometry, the hydro-mechanical and geological properties of the soil layers are also concerned as other triggering parameters to occur landslide. Location 1 and 2 ERI results show the surface ruptures and thicknesses likewise SLOPE/W results show the maximum thicknesses of surface ruptures and the factor of safety. These two different results obliviously can be seen the maximum thickness of Location 1 is about 5m at a slope distance 13.5 m and Location 2 is about 2.5 m at a slope distance 5.5 m.

Generally, investigation of the landslides using ERI can show the interface of the high conductive zone and low conductive zone. By surveying parallel to the slope and perpendicular to the slope, the sliding plain area of the slope can be defined. From this assumption, the area and thickness of the slope, the volume of the sliding mass can be easily estimated. Therefore, it can be concluded that ERI provides an easy method on the slope for investigating the susceptible landslide based on the determination of the sliding surface and the geometry of the landslide. The slope modeling likewise supports the critical slip surface of a slope and its stability under rainfall-induced condition.

Finally, it can be suggested that the integration of geophysical method (ERI) and geotechnical method (slope modeling) is a very useful technique for mitigation processes such as cutting and filling processes, construction of embankments, retaining walls and canals. Then, this integrated method can apply to establish the landslide risk assessment of Phuket.

There are many landslides around Phuket. Some landslide locations may be still active, and some areas are in the hazard. Researching the hazard locations near the critical areas using integrated ERI technique and coupled slope modeling of SEEP/W-SLOPE/W should be done for preventing the landslide in the future.

5.2 Reconstruction of Landslide Model Geometry Using ERI

In practical, the soil layers are not planar shapes. The concave shape of the bedrock can entrap more water compare than planar shape and convex shape. The

presence of water or moisture content is favorable to occur landslide. Moreover, ERI provides the presence of water or moisture content locations as well as the real soil layers to define the sliding length and to construct the model geometry in slope modeling. Using the reconstructed model geometries enhanced the slope modeling simulation results. Therefore, the thickness of the sliding surface of the reconstruction of landslide model geometry using ERI were very close to the ERI results. Moreover, the results helped to avoid the over-estimation of the stability of the slope.

5.3 Research Gaps and Further Study

This research is done with a lot of limitations such as i) interpretation of ERI results were confirmed with a single lithology ii) secondary parameters of hydro-mechanical and geotechnical properties of soils were used for slope modeling and iii) only the 2018 maximum and successive precipitation data were used for transient seepage simulations. Therefore, for future studies, more lithological information from the well data should be used to verify the ERI. Then by providing i) the in-situ hydro-mechanical and geological updated data ii) the rainfall data especially the data of during monsoon and storm in the integrated methods, it is hoped that the simulation results will be enhanced. Finally, using the proposed integrated methods for slope model simulation with updated data is expected that it can degrade the impact of landslides in the future.

REFERENCES

Acharya, K. P., Bhandary, N. P., Dahal, R. K., and Yatabe, R. (2016). "Seepage and Slope Stability Modeling of Rainfall-Induced Slope Failures in Topographic Hollows". *Geomatics, Nat. Hazards Risk,* 7(2), 721–746.

Asian Disaster Preparedness Center (ADPC), Department of Mineral Resources (DMR) and Geotechnical Engineering Research and Development Center (GERD). (2008). "Landslide Mitigation Demonstration Project for Patong City: Capacity Enhancement for Landslide Impact Mitigation (RECLAIM II)*, Bangkok, Thailand*". Carried Act as a Part of the Asian Program for Regional.

Bernard, J. (2003). "Short Note on the Depth of Investigation of Electrical Methods". *Source: Google Search*, (July). Retrieved from http://www.iris-instruments.com/Pdf_file/Resistivity_Imaging/methods_depth_investigation.pdf

Bichler, A., Bobrowsky, P., Best, M., Douma, M., Hunter, J., Calvert, T., and Burns, R. (2004). "Three-Dimensional Mapping of a Landslide Using a Multi-Geophysical Approach: The Quesnel Forks Landslide". *Landslides*, 1(1), 29–40.

Bishop A.W. (1955). "The Use of the Slip Circle for the Stability Analysis of Slopes". Géotechnique, 5(1), 7–17.

Brand, E. W. (1981). "Some Thoughts on Rain-Induced Slope Failures". *Proc., Soil Mechanics and Foundation Engineering*, 3, 373–376.

Brooks, S.M. and Richards, K.S. (1994). "The Significance of Rainstorm Variations to Shallow Translational Hillslope Failure". *Earth Surf. Process. Landforms*, 19(1), 85–94.

Brown, G., Buravas, S., Charaljavanaphet, Jalichandra, N., Johnston, W., Sresthaputra, V., and Taylao, G. (1951). "Geologic Reconnaissance of the Mineral Deposits of Thailand". *US Geological Survey, Bulletin*, 984, 1–183.

Chambers, J. E., Wilkinson, P. B., Kuras, O., Ford, J. R., Gunn, D. A., Meldrum, P. I., and Ogilvy, R. D. (2011). "Three-Dimensional Geophysical Anatomy of an Active Landslide in Lias Group Mudrocks, Cleveland Basin, UK". *Geomorphology*, 125(4), 472–484.

Charoenpong, S., Suwanprasit, C., and Thongchumnum, P. (2012). "Impacts of Interpolation Techniques on Groundwater Potential Modeling Using GIS in Phuket Province, Thailand". *33rd Asian Conference on Remote Sensing 2012, ACRS 2012*, 1, 732–738.

Chotikasathien, W. and Soralump, S. (2007). "Landslide Investigation and Hazard Mapping in Phuket Province". *GEOTHAI'07 Conf., Geology of Thailand: Towards Sustainable Development and Sufficiency Economy*. Retrieved from http://library.dmr.go.th/Document/Proceedings-Yearbooks/M_1/2007/ 12716.pdf.

Crosta, G. B., and Negro, P. D. (2003). "Observations and Modeling of Soil Slip-Debris Flow Initiation Processes in Pyroclastic Deposits : the Sarno 1998 Event". *Nat. Hazards Earth Syst. Sci.,* 3, 53–69.

Dahal, R. K., Hasegawa, S., Yamanaka, M., Dhakal, S., and Prakash, N. (2009). "Comparative Analysis of Contributing Parameters for Rainfall-Triggered Landslides in the Lesser Himalaya of Nepal". *Environ. Geol.*, 58(3), 567-586.

Dapporto, S., Aleotti, P., Casagli, N., Polloni, G., Dapporto, S., and Aleotti, P. (2002). "Analysis of Shallow Failures Triggered by the 14-16 November 2002 Event in the Albaredo Valley , Valtellina (Northern Italy)". *HAL Id : hal-00296905*.

Department of Groundwater Resource (DGR). (2010). "*Completed Report: Groundwater Well Observation, Study of Specific Network Groundwater Well, and Groundwater Consumption Evaluation for Groundwater Management*". D.M. Printing Co., LTD, Bangkok, Thailand.

Department of Groundwater Resource (DGR). (2012). "*Final Report: Groundwater Conservation and Recovery from Summer Flooding in Southern Thailand*". Groundwater Conservation and Recovery Institution, Bangkok.

Department of Mineral Resource (DMR). (2011a). "Geology of Thailand". Retrieved from https://doi.org/10.1144/GOTH.

Department of Mineral Resource (DMR). (2011b). "Study of Landslide-Flood Behavior in the Selected Area for Developing of Warning Method and Criteria, Thailand". *Research Fund (TRF)*.

Drahor, M. G., Göktürkler, G., Berge, M. A., and Kurtulmuş, T. Ö. (2006). "Application of Electrical Resistivity Tomography Technique for Investigation of Landslides: A Case from Turkey". *Environ. Geol.*, 50(2), 147–155.

Ekanayake, J.C., and Phillips, C.J. (1999). "A Model for Determining Thresholds for Initiation of Shallow Landslides under Near-Saturated Conditions in the East Coast Region". *NZ. J. Hydrol.*, 38–128.

Fellenius, W. (1936). "Calculation of the Stability of Earth Dams". *Proc., Second Congress of Large Dams*, 4, 445-463.

Frattini, P., Crosta, G., and Sosio, R. (2009). "Approaches for Defining Thresholds and Return Periods for Rainfall-Triggered Shallow Landslides". *Hydrol. Process.*, 23, 1444–1460.

Fredlund, D.G., and Krahn, J. (1977). "Comparison of Slope Stability Methods of Analysis". *Can. Geotech. J.*, 14, 3, 429–439.

Fredlund, D.G., Krahn, J., and Pufahl, D. (1981). "The Relationship Between Limit Equilibrium Slope Stability Methods". *Proc., 10th International Conference. Soil Mechanics and Foundation Engineering*, (Stockholm, Sweden), 3, 409-416.

Fredlund, D.G. and Xing, A. (1994). "Equations for the Soil-Water Characteristics Curve". *Can. Geotech. J.,* 31, 533–546.

GEO-SLOPE International Ltd. (2012a). **"*Seep Modeling with SEEP/W"*.** Calgary, Alberta., Canada T2P 2Y5. Novemver 2012 Edition.

GEO-SLOPE International Ltd. (2012b). "Stability Modeling with SLOPE/W". Calgary, Alberta, Canada T2P 2Y5.

GEO-SLOPE International Ltd. (2012c). **"**Factors Controlling Rainfall-Induced Instability". Retrieved from http://downloads.geo-slope.com/ geostudioresources/examples/9/0/SlopeW/Factors%20Controlling%20Rainfall -Induced%20Instability.pdf.

Giao, P. H., Weller, A., Hien, D. H., and Adisornsupawat, K. (2008). "An Approach to Construct the Weathering Profile in a Hilly Granitic Terrain Based on Electrical Imaging". *J. Appl. Geophys.*, 65, 30–38.

Gofar, N., Lee, L.M., and Asof, M. (2006). "Transient Seepage and Slope Stability Analysis for Rainfall-induced Landslide: A Case Study". *Malaysian Journal of Civil Engineering*, 18(1), 1–13

Grandjean, G., Gourry, J. C., Sanchez, O., Bitri, A., and Garambois, S. (2011). "Structural Study of the Ballandaz Landslide (French Alps) Using Geophysical Imagery". *J. Appl. Geophys.*, *75*(3), 531–542.

Institute for Social and Environmental Transition-International (ISET), Thailand Environment Institute (TEI), and Vietnam National Institute for Science and Technology Policy and Strategy Studies (NISTPASS) (2013). "Mekong-Building Climate Resilient Asian Cities: M-BRACE". Institute of Social and Environment Transition-International Bangkok, Thailand, p98.

Highland, L. M., and Bobrowsky, P. (2008). "The Landslide Handbook _ A Guide to Understanding Landslides". *Landslides*, 129. https://doi.org/Circular 1325

Hsu, C., and Chien, L. (2016). "Slope Stability Analysis of Transient Seepage under Extreme Climates : Case Study of Typhoon Nari in 2001". *J. Mar. Sci. Tech.,* 24, 3, 399–412.

Iverson, R. M. (2000). "Landslide Triggering by Rain Infiltration". *Water Resour. Res.*, 36(7), 1897–1910.

Janbu, N. (1954). "Applications of Composite Slip Surfaces for Stability Analysis". *In Proc., European Conference on the Stability of Earth Slopes, Stockholm*, 3, 39–43.

Jeong, S., Lee, K., Kim, J., and Kim, Y. (2017). "Analysis of Rainfall-Induced Landslide on Unsaturated Soil Slopes". *Sustainability (Switzerland)*, 9(7), 1–20.

Jomard, H., Lebourg, T., Guglielmi, Y., and Tric, E. (2010). "Electrical Imaging of Sliding Geometry and Fluids Associated with a Deep-Seated Landslide (La Clapière, France)". *Earth Surf. Process. Landforms*, 35(5), 588–599.

Jomard, H., Lebourg, T., and Tric, E. (2007). "Identification of the Gravitational Boundary in Weathered Gneiss by Geophysical Survey: La Clapière Landslide (France)". *J. Appl. Geophys.*, 62(1), 47–57.

Kong S. O. (2016). "Hydrogeological Characterization and Groundwater Analysis with Reference to (Urban, Tourists, and Economic) Development of Phuket Areas, Thailand". (*Master's Thesis, Prince of Songkla University, Phuket, Thailand*).

Lapenna, V., Lorenzo, P., Perrone, A., Piscitelli, S., Sdao, F., and Rizzo, E. (2003). "High-Resolution Geolectrical Tomographies in the Study of Giarrossa Landslide (Southern Italy)". *Bull. Eng. Geol. Environ.*, 62(3), 259–268.

Lee, L. M., Gofar, N., and Rahardjo, H. (2009). "A Simple Model for Preliminary Evaluation of Rainfall-Induced Slope Instability". *Eng. Geol.*, 108(3–4), 272–285.

Loke, M. H. (2004). "Tutorial: 2-D and 3-D Electrical Imaging Surveys", 2004 Revised Edition, 136.

Loke, M. H., (2015). "2-D and 3-D ERT Surveys and Data Interpretation", Turin, Italy, 10th September, 2015. Piedmont Regional Order of Geologists Pasi Geophysics. 1–246.

Mairaing, W., Chantawarangul, K., Kongsomboon, T., and Soralump, S .(2006). "A Study of Landslide Behavior in Phuket Province" .*Thailand Research Fund (TFR).*

Mitchell, A.H.G., Yung, B., and Jautaranipa, W. (1970). "The Phuket Group, Peninsular Thailand: a Paleozoic Geosynchinal Deposit". *Geol. Mag.*, 107, 411–428.

Morgenstern, N.R., and Price, V.E. (1965). "The Analysis of the Stability of General Slip Surfaces". *Geotechnique*, 15, 79–93.

Mualem, Y. (1976). "A New Model for Predicting the Hydraulic Conductivity of Unsaturated Porous Media". *Water Resour. Res.*, 12(3), 513–522.

Mukhlisin, M., Idris, I., Wan-Yaacob, W. Z., Elshafie, A., and Taha, M. R. (2011). "Soil Slope Deformation Behavior in Relation to Soil Water Interaction Based on Centrifuge Physical Modeling". *Int. J. Phys. Sci.*, 6(13), 3126–3133.

Muntohar, A. S., Ikhsan, J., and Soebowo, E. (2013). "Mechanism of Rainfall Triggering Landslides in Kulonprogo, Indonesia". *Geo-Congress 2013*, (December 2014), 452–461.

Naderi, M. A. (2013). "Determination of the Critical Slip Surface in Slope Stability Analysis". (*Master's Thesis, Eastern Mediterranean University, Gazimağusa, North Cyprus*).

Natural Resources. (2017). "What Are Landslides and How Do They Occur?" *Washington Geological Survey*. Retrieved from https://www.dnr.wa.gov/geology

Oluwafemi (Femi) Ogunsuyi, (2010). "Geophysical Characterization of Peace River Landslide". (*Master's Thesis, University of Alberta, Edmonton, Alberta, Canada*).

Pánek, T., Hradecký, J., and Šilhán, K. (2008). "Application of Electrical Resistivity Tomography (ERT) in the Study of Various Types of Slope Deformations in Anisotropic Bedrock: Case Studies from the Flysch Carpathians". *Stud. Geomorphol. Carpatho-Balcanica*, XLII, 57–73.

Pantanahiran, W. (2005). "Using GIS and Remote Sensing for the Delineation of Risk Disaster Areas in Phuket, Thailand". *Asian Association on Remote Sensing - 26th Asian Conference on Remote Sensing and 2nd Asian Space Conference, ACRS 2005*, *1*(June), 261–270.

Papagianakis, A. T., and Fredlund, D. G. (1984). "A Steady State Model for Flow in Saturated–Unsaturated Soils". *Can. Geotech. J.*, 21(3), 419–430.

Perrone, A., Lapenna, V., and Piscitelli, S. (2014). "Electrical Resistivity Tomography Technique for Landslide Investigation: A review". *Earth-Science Rev.*, 135, 65–82.

Petley, D. N., Mantovani, F., Bulmer, M. H., and Zannoni, A. (2005). "The Use of Surface Monitoring Data for the Interpretation of Landslide Movement Patterns". *Geomorphology*, 66(1–4 SPEC. ISS.), 133–147.

Phuket Gazette. https://thethaiger.com/news/landslide (2007-2017).

Rahimi, A., Rahardjo, H., and Leong, E. C. (2010). "Effect of Hydraulic Properties of Soil on Rainfall-Induced Slope Failure". *Eng. Geol.*, 114(3–4), 135–143.

Richards, L.A. (1931). "Capillary Conduction of Liquids Through Porous Mediums". *J. Appl. Phys.,* 1, 318–333.

Samouëlian, A., Cousin, I., Tabbagh, A., Bruand, A., and Richard, G. (2005). "Electrical Resistivity Survey in Soil Science: A Review". *Soil Tillage Res.*, 83(2), 173–193.

Singhroy, V. (2009). "Satellite Remote Sensing Applications for Landslide Detection and Monitoring". *Landslides--Disaster Risk Reduct.*, 143–158.

Soralump, S. (2010a). "Corporative of Geotechnical Approach for Landslide Susceptibility Mapping in Thailand". *Conf., Geotechnique and Geosynthetics for Slopes, 27-30 July, 2010 Chiangmai, Thailand*.

Soralump, S. (2010b). "Rainfall-Triggered Landslide: From Research to Mitigation Practice in Thailand". *Geotech. Eng.*, 41(1).

Soralump, S. (2007). "Corporation of Geotechnical Engineering Data for Landslide Hazard Map in Thailand", EIT-JSCE Joint Seminar on Rock Engineering 2007: Corporation of geotechnical engineering data for landslide hazard map in Thailand, (March).

Soralump, S., and Kulsuwan, B. (2004). "Landslide Risk Prioritization of Tsunami Affected Area in Thailand", (August 2006). International Symposium on Environmental Engineering and 5th Regional Symposium on Infrastructure Development in Civil Engineering., Philippines.

Telford, W. M., Geldart, L. P., and Sheriff, R. E. (1990). "Applied Geophysics". Second Edition. *Published by the press Syndicate of the University of Cambridge*. https://doi.org/10.1180/minmag.1982.046.341.32

The Phuket News. http://www.thephuketnews.com, Sunday 23 April, 2017.

Tracy, F. T., Brandon, T. L., and Corcoran, M. K. (2016). "Transient Seepage Analyses in Levee Engineering Practice". A Final Report. *ERDC TR-16-8*.

USGS. (2004). "Landslide Types and Processes". *Highway Research Board Special Report*, (July), 1–4. https://doi.org/Fact Sheet 2004-3072

Van Genuchten, M.T. (1980). "A Closed-Form Equation for Predicting the Hydraulic Conductivity of Unsaturated Soils". *Soil Sci. Soc. Am. J.*, 48, 703–708

World Weather and Climate Information, Retrieved from https://weather-and-climate.com/average-monthly-precipitation-Rainfall,Phuket, Thailand.

Xinwei, L., and Yan, E. (2016). "Stability Analysis of Rainfall-Induced Typical Landslide in Fanjingshan Mountain Area". *EJGE*, 4985–4996.

Yilmaz, S. (2011). "A Case Study of the Application of Electrical Resistivity Imaging for Investigation of a Landslide along Highway". *Int. J. Phys. Sci.*, 6(24), 5843–5849.

VITAE

Name NAUNG NAUNG HTWE

Student ID 6030420009

Educational Attainment

Degree	Name of Institution	Year of Graduation
Master of Science (Earth System Science)	Prince of Songkla University Phuket Campus	2019

List of Publications

1. Puttiwongrak A. and Htwe N.N. (2019). Application of Electrical Resistivity Imaging and Slope Modeling to the Investigation of the Sliding Geometry of Landslides in Phuket. Geotechnical Engineering. (in waiting for acceptance)

2. Puttiwongrak A. and Htwe N.N. (2019). Prediction of Landslide Geometry and Movement Under Rainfall Condition Using Two-Dimensional Models. (in preparation)